UNIVERSIDADE D
COIMBRA

Ana Filipa Domingues Laranjeiro

ASSESSING THE ROLE OF THE SECRETOME OF BRAIN METASTATIC BREAST CANCER CELLS IN THE PHENOTYPIC SHIFT AND OXIDATIVE RESPONSE OF MICROGLIA

Dissertação no âmbito do Mestrado em Biologia Celular e Molecular, no âmbito do Percurso sem área de Especialização, orientada pela Professora Doutora Célia Maria Freitas Gomes e pela Professora Doutora Emília da Conceição Pedrosa Duarte apresentada ao Departamento de Ciências da Vida da Faculdade de Ciências e Tecnologia da Universidade de Coimbra.

Outubro de 2021

Faculdade de Ciências e Tecnologia da Universidade de Coimbra

Assessing the role of the secretome of brain metastatic breast cancer cells in the phenotypic shift and oxidative response of microglia

Ana Filipa Domingues Laranjeiro

Dissertação no âmbito do Mestrado em Biologia Celular e Molecular, no âmbito do Percurso sem área de Especialização, orientada pela Professora Doutora Célia Maria Freitas Gomes e pela Professora Doutora Emília da Conceição Pedrosa Duarte apresentada ao Departamento de Ciências da Vida da Faculdade de Ciências e Tecnologia da Universidade de Coimbra.

Outubro de 2021

1 2 9 0

UNIVERSIDADE D
COIMBRA

This work was funded by the Portuguese Foundation for Science and Technology (FCT) through the Strategic Project UIDB/04539/2020 and UIDP/04539/2020 (CIBB), by the European Regional Development Fund through the Operational Programme for Competitiveness and Internationalization –COMPETE 2020, and Portuguese national funds via FCT, under projects POCI-01-0145-FEDER-016390: CANCEL STEM.

Agradecimentos

Ao longo do decorrer do ano, até à data, mais importante da minha vida, os agradecimentos devidos são numerosos e profundamente sinceros.

Cabe o primeiro agradecimento à Professora Doutora Célia Gomes. Por me ter recebido no seu grupo e pela orientação durante este ano, que acarretou muitos ensinamentos teóricos e pessoais à cerca do que implica fazer ciência. Acredito plenamente que começar o meu percurso académico sob a sua alçada influenciará positivamente o meu desempenho.

Gostaria também de agradecer à Professora Doutora Emília Duarte por ter aceitado ser minha coorientadora e pela confiança depositada no meu trabalho.

À Professora Doutora Ana Paula Silva agradeço pela supervisão científica no mundo das neurociências e por ter confirmado, de uma forma subtil, que microglia é complicadinha.

Gostaria também de agradecer ao Instituto de Farmacologia e Terapêutica Experimental da Faculdade de Medicina da Universidade de Coimbra e ao iCBR pela oportunidade de desenvolver o meu trabalho.

Quero também agradecer às pessoas que estiveram comigo diariamente "no terreno". Quero agradecer principalmente à Liliana Santos, que me treinou, encorajou, ajudou imenso na otimização de muitos protocolos e em revisões, foi responsável pela cultura das células endoteliais e pela parte animal. Quero também agradecer à Sara Almeida pela supervisão técnica, pelo carinho e pelas mensagens, à Gabriela Ribeiro pela companhia e entreajuda, à Margarida Pereira pela amizade, pelas novidades e por me tirar dúvidas existenciais a más horas, e à Diana Rodrigues, que apareceu já no fim do meu percurso de mestranda, mas de quem gostei logo. À equipa da sala de cultura agradeço a simpatia e o bom ambiente de trabalho. Destas, quero agradecer principalmente à Mariana Magalhães que sempre foi simplesmente incrível comigo e que me encorajou imenso nos dias em que estava mais em baixo. O teu apoio foi fulcral.

Quero também agradecer aos membros dos laboratórios contíguos, nomeadamente ao Ricardo Leitão pela ajuda na otimização de protocolos, à Eliane Sanches pelo super apoio e encorajamento quando andava mais triste com os blots, com a microglia, com tudo. O meu agradecimento vai também para o André Alves, que me

auxiliou quando no fim os blots pareciam ser maiores do que a minha força, e para a simpática e encorajadora Inês Preguiça que me abriu os olhos para a etapa seguinte da minha vida.

Do outro lado do edifício estavam outras pessoas aquém quero também deixar o meu agradecimento: à Mylène Carrascal, à Ana Capitão e à Isabel Ferreira pela simpatia e pela ajuda na interpretação de resultados de RT-qPCR e curva de NO. À Professora Doutora Alexandrina Mendes pelas alíquotas de anticorpos. À Cátia Sousa, super disponível para me ajudar com os blots e com as vias de sinalização um grande obrigada!

Agora, chega a vez de agradecer às pessoas que me permitiram chegar ao ponto de fazer a tese, o mestrado, e muito mais. Ao Professor Doutor João Ramalho um grande obrigada pelo boost de confiança. À Professora Anabela Pinto e à Professora Ana Urbano outro grande obrigada pela experiência laboratorial que me permitiram adquirir. A todo o grupo de Fertilidade do CNS, em particular à Renata e às Inês(es), pela força e boa-disposição.

À professora Maria José pelas longas horas em que me auxiliou com a infausta matemática. Ao professor Luís Oliveira pelos poemas quando mais precisei deles.

À Raquel Pinto, madrinha do coração, de quem sou a cria mais orgulhosa. Ao "avô" Ivo pela pessoa fixe e assertiva que é. À Jessica (Jones): irmã de praxe e companheira para a vida. À marafada Mariana Contreiras pela amizade que quero que dure uma vida. Ao Renato pela amizade e compreensão.

À Bárbara, por uma amizade que leva mais de uma década e a contar. Aos meus amigos do Grupitxo, que sempre compreenderam quando não podia estar ou ficar até tarde por causa da tese e me encorajaram imenso: Eduarda, Andreia, Luís e Gonçalo.

À minha Família da Ponte de Vagos por toda a confiança, carinho e amor com que me acolheram nas suas vidas. Às minhas avós e aos meus primos João e Isabel.

Por último, ao meu núcleo forte, sem o qual já mais tinha chegado onde quer que fosse. Ao meu irmão pelos incentivos. Ao Maurício por passar comigo todo o processo, pela (in)sanidade, e por todo o amor e por toda a boa disposição enquanto trabalhou comigo horas a fio. Ao meu pai que me mandou ser teimosa, sempre me apoiou, confiou e trouxe perspetiva. Por último, à minha mãe que sempre me encorajou e acreditou em mim, esteve presente em todos as crises, todas as dúvidas, todos os bons momentos, me ajudou de todas as maneiras humana e inumanamente possíveis. E à minha irmã, Ana Sílvia, agradeço tudo o que sou e serei.

Sísifo

Recomeça...
Se puderes
Sem angústia
E sem pressa.
E os passos que deres,
Nesse caminho duro
Do futuro
Dá-os em liberdade.
Enquanto não alcances
Não descanses.
De nenhum fruto queiras só metade.

E, nunca saciado,
Vai colhendo ilusões sucessivas no pomar.
Sempre a sonhar e vendo
O logro da aventura.
És homem, não te esqueças!
Só é tua a loucura
Onde, com lucidez, te reconheças...

Miguel Torga

Resumo

Introdução: Os subtipos de cancro da mama triplo negativo (CMTN) e $HER2^+$ apresentam maior incidência de metástases cerebrais. É sabido que os tumores primários preparam o microambiente de órgãos distantes, o chamado nicho pré-metastático (NPM), antes do início da metástase. Presume-se que a microglia, como a principal célula imune inata do cérebro, tenha um papel ativo no processo metastático, mas os mecanismos que lhe estão subjacentes não estão completamente esclarecidos.

Objetivos: Pretendemos explorar a resposta da microglia quando exposta ao secretoma de células de cancro da mama metastático do cérebro (CCMMC), com foco no stress oxidativo, e no papel regulador do zinco extracelular no fenótipo de ativação da microglia. Pretendemos ainda avaliar se a ativação da microglia, induzida por CCMMC pode levar à disfunção de células endoteliais.

Materiais e Métodos: Os meios condicionados (MCs) foram colhidos a partir de células MDA-MB-231 (CMTN) e JIMT-1 ($HER2^+$) e das variantes cerebrais correspondentes. Células da microglia humana (HMC3) foram expostas a esses MCs e testadas quanto à produção de ON pelo ensaio de Griess, expressão de mediadores inflamatórios e marcadores de stress oxidativo por RT-qPCR, produção de espécies reativas de oxigénio intracelulares (iROS) com a sonda H_2DCFDA, taxa de proliferação com o reagente WST-1 e motilidade por um ensaio de *scratch*. A ativação de proteínas quinases ativadas por stress (PQASs) foi avaliada por Western Blot. Experiências de depleção de zinco foram realizadas usando o agente quelante DTPA. A integridade da monocamada de células hCMEC/D3 foi avaliada medindo o fluxo transendotelial da sonda 4kDa-FITC e a Resistência Elétrica Transendotelial (TEER).

Resultados: A exposição da microglia aos MCs das CCMMC leva a um aumento significativo na geração de ON e iROS, bem como a uma maior taxa de proliferação e redução da motilidade, sendo o efeito mais pronunciado alcançado com o MC de células trópicas cerebrais TN. A expressão génica de mediadores inflamatórios e sinalização por PQASs também é induzida, apontando para um fenótipo do tipo M1 sob o efeito da exposição ao secretoma de CCMMC. A produção de ROS não é regulada pela atividade de NOXs, mas sim pela mitocôndria, considerando a regulação de *UCP2*. A depleção de Zn^{2+} extracelular diminuiu a produção de ON e iROS pela microglia e a sua proliferação. Além disso, observou-se um aumento da resposta inflamatória e de stress oxidativo

indicado pela sobreexpressão do gene antioxidante *NRF2*. Observou-se igualmente uma perturbação das propriedades de barreira conferidas pelas células endoteliais quando incubadas com o secretoma de células da microglia ativadas.

Conclusão: A microglia reage ao secretoma de células metastáticas do cancro da mama adquirindo um fenótipo semelhante ao M1, conforme indicado pelo aumento da produção de ON, iROS e pela predominância de citocinas pró-inflamatórias. A quelação de zinco com DTPA reduziu a produção de iROS e geração de ON pela microglia, enquanto exacerbou o ambiente inflamatório com mediadores anti e pró-inflamatórios. Estes resultados destacam a contribuição do Zn^{2+} na indução de uma resposta da microglia. São necessários mais estudos para entender como estes resultados podem estar relacionadas com a formação do NPM.

Palavras-chave: Metástases Cerebrais de Cancro da Mama; Nicho pré-metastático; Microglia, Resposta Oxidativa; Zinco

Abstract

Introduction: The Triple Negative Breast Cancer (TNBC) and $HER2^+$ breast cancer subtypes have a higher incidence of brain metastasis. It is well recognized that primary tumors prepare the microenvironment of distant organs, the so-called premetastatic niche (PMN) before metastasis onset. Microglia, as the major innate immune cells of the brain, are likely to take part in the metastatic process, but the underlying mechanisms are poorly understood.

Aims: We intend to explore the microglial response when exposed to the secretome of brain metastatic breast cancer cells (BCC), with a focus on oxidative stress, and the regulating role of extracellular zinc on microglia activation phenotype. We also aim to evaluate whether BCCs-induced MC activation may lead to endothelial cell dysfunction.

Materials and Methods: Conditioned mediums (CMs) were collected from MDA-MB-231 (TNBC) and JIMT-1 ($HER2^+$) cells and their corresponding brain-tropic variants. Human microglia cells (HMC3) were exposed to these CMs and assayed for NO production by the Griess assay, expression of inflammatory mediators and oxidative stress markers by RT-qPCR, production of intracellular reactive oxygen species (iROS) with the H_2DCFDA probe, proliferation rate with WST-1 reagent, and motility by a scratch assay. Activation of stress-activated protein kinases (SAPKs) was evaluated by Western Blot. Zinc depletion experiments were carried out using the chelating agent DTPA. The hCMEC/D3 monolayer integrity was assessed by measuring the transendothelial flux of the 4kDa-FITC probe and the Transendothelial Electric Resistance (TEER).

Results: The exposure of MCs to the CMs of BC cells leads to a significant increase in NO and iROS generation, as well as a higher proliferation rate and reduced motility, being the most pronounced achieved with the CM from TN brain-tropic cells. Gene expression of inflammatory mediators and SAPKs signaling is also elicited, pointing to an M1-like phenotype under the effect of BCCs secretome exposure. ROS production is not regulated by NOX activity but rather by the mitochondria considering the regulation of *UCP2*. The depletion of extracellular Zn^{2+} impaired the NO and iROS generation by MCs and their proliferation. Conversely, inflammatory signaling was markedly up-regulated and the NRF2 antioxidant gene appears to denote an early state of oxidative distress. The barrier

properties conferred by ECs were disrupted when incubated with the secretome of activated MCs.

Conclusion: MCs react to the secretome of metastatic BCCs by acquiring an M1-like phenotype, as indicated by the increased production of NO, iROS, and the predominance of pro-inflammatory cytokines. Zinc chelation with DTPA reduced the production of iROS and NO generation by MCs while exacerbating the inflammatory environment with anti- and pro-inflammatory mediators. These findings highlight the contribution of Zn^{2+} in eliciting a microglial response. Further studies are required to understand how these findings can be related to the PMN formation.

Keywords: Breast Cancer Brain Metastasis, Pre-metastatic niche, Microglia, Oxidative Response, Zinc

Index

List of Acronyms

ANOVA - One-way Analysis Of Variance

APS - Ammonium Persulfate

ATCC® - American Type Culture Collection

ATP - Adenosine Triphosphate

BBB - Blood-Brain Barrier

BC - Breast Cancer

BCA - Bicinchoninic Acid

BCBM - Breast Cancer Brain Metastasis

BCC - Breast Cancer Cell

BLAST - Basic Local Alignment Search Tool

BMDC - Bone Marrow-Derived Cell

BRCA(x)1 - Breast Cancer gene (x)

BrM - Brain Metastasis

BSA - Bovine Serum Albumin

BTB - Blood-Tumor Barrier

$CaCl_2$ - Calcium Chloride

CCM - Concentrated Conditioned Medium

CD(x) - Cluster of Differentiation (x)

cDNA - complementary DNA

CM - Conditioned Medium

CNS - Central Nervous System

CO_2 - Carbon Dioxide

CSF-1 - Colony-Stimulating Factor-1

Ct - Cycle threshold

CTF - Corrected Total Fluorescence

DAMP - Danger-Associated Molecular Pattern

DCF - 2',7'-Dichlorofluorescein

DMEM - Dulbecco's Modified Eagle's Medium

DNA - Deoxyribonucleic Acid

DPI - Diphenyleneiodonium

DTPA - Diethylenetriamine Pentaacetate

DTT - Dithiothreitol

EC - Endothelial Cell

ECL - Enhanced Chemiluminescence

ECM - Extracellular Matrix

EDTA - Ethylenediamine Tetraacetic Acid

EMEM - Essential Minimum Eagle Medium

ER - Estrogen Receptor

ER^- - Estrogen Receptor negative

ERBB2 - Erythroblastic Leukemia Viral Oncogene Homolog 2

ERK - Extracellular signal-Regulated Kinase

FBS - Fetal Bovine Serum

FITC-Dextran 4 - Fluorescein Isothiocyanate-Dextran 4

GCSF - Granulocyte Colony-Stimulating Factor

GM-CSF - Granulocyte-Macrophage Colony-Stimulating Factor

H_2DCFDA - 2',7'-Dichlorodihydrofluorescein Diacetate

H_2O_2 - Hydrogen Peroxide

H_3PO_4 - Phosphoric acid

HEPES - 4-(2-hydroxyethyl)-1-piperazineethanesulfonic acid

$HER2^-$ - HER2 negative

HER2 - Human Epidermal Growth Factor Receptor 2

$HER2^{+-}$ HER2-enriched

HMC3 - Human Microglia Clone 3

HO-1- Heme Oxygenesase-1

Iba1 - Ionizing calcium-Binding Adapter molecule 1

IL-(x) - Interleukin (x)

iNOS - inducible Nitric Oxide Synthase

iROS - intracellular ROS

JNK - c-Jun N-terminal Kinase

KCl - Potassium Chloride

Keap1 - Kelch-like ECH-associated protein 1

KH_2PO_4 - Potassium dihydrogen Phosphate

LPS – Lipopolysaccharide

MAPK - Mitogen-Activated Protein Kinase

MBC - Metastatic Breast Cancer

MC - Microglia Cell

MDM - Monocyte-Derived Macrophage

$MgCl_2$ - Magnesium Chloride

MMP - Matrix Metalloproteinase

mROS - mitochondrial ROS

Na_3VO_4 - Sodium Orthovanadate

NaCl - Sodium Chloride

NaF - Sodium Fluoride

NaH_2PO_4 - Sodium dihydrogen Phosphate

$NaNO_2$ - Sodium Nitrate

NaOH - Sodium Hydroxide

NFDM - Non-Fat Dry Milk

NF-κB - Nuclear Factor kappa-light-chain-enhancer of activated B cells

NO - Nitric Oxide

NO_2^- - Nitrite

$NO_3^{-\cdot}$ - Peroxynitrite Radical

NOX(x) - NADPH Oxidase (x)

NRF2 - Nuclear factor erythroid 2-related factor 2

$O_2^{\cdot -}$ - Superoxide Radical

$OH^{\cdot}$ - Hydroxyl Radical

PAM50 - Prediction Analysis of Microarray of 50 gene set

PAMP - Pathogen-Associated Molecular Pattern

PBS - Phosphate Buffered Saline

PMN - Pre-Metastatic Niche

PR - Progesterone Receptor

PR^- - Progesterone Receptor negative

PRR - Pattern Recognition Receptor

PVDF - Polyvinylidene Difluoride

RCF - Relative Centrifugal Force

RIPA - Radio Immuno Precipitation Assay

RNA - Ribonucleic Acid

RNS - Reactive Nitrogen Species

ROS - Reactive Oxygen Species

RPM - Revolutions Per Minute

RT-qPCR - Reverse Transcription quantitative real-time Polymerase Chain Reaction

SAPK - Stress-Activated Protein Kinase

SDS - Sodium Dodecyl Sulphate

SEMs - Standard Error of the Means

SLC39A(x) - Solute-linked Carrier 39 (x)

TAM - Tumor-Associated Macrophage

TBS-T - Tris-Buffered Saline with Tween

TEER - Transendothelial Electrical Resistance

TEMED - Tetramethylethylenediamine

TGF-β - Transforming Growth Factor beta

TLR(x) - Toll-Like Receptor (x)

TNBC - Triple Negative Breast Cancer

TNFα - Tumor Necrosis Factor alpha

UCP(x) - Uncoupling Protein (x)

VEGF - Vascular Endothelial Growth Factor

WHO - World Health Organization

WST-1 - 4-[3-(4-iodophenyl)-2-(4-nitrophenyl)-2H-5-tetrazolio-1,3-benzene disulfonate

Zn^{2+} - Zinc

$ZnCl_2$ - Zinc Chloride

List of Figures

List of Tables

Chapter 1 - Introduction

1.1. Breast cancer

According to the World Health Organization (WHO), Breast Cancer (BC) is currently the most prevalent disease worldwide (Figure 1.1). Simultaneously, it is the most common cancer and the 5th most common cause of death from cancer in women [1]. However, it is treatable in approximately 70-80% of patients at an early non-metastatic stage, when the tumor is contained in the breast or has only spread to the axillary lymph nodes [2]. BC is most common after menopause [1], and its incidence is related to the income level of countries. It is registered a higher incidence in high-income regions when compared with lower-income regions (such as middle Africa and eastern Asia, as can be seen in Figure 1.2) [3].

Only 5-10% of BCs have hereditary provenance due to the inheritance of mutations in the breast cancer gene 1 (*BRCA1*) and *BRCA2* [4]. Factors involved in BC occurrence include the use of hormone therapies (estrogen and progestin), obesity, alcohol, physical inactivity, and increased breast tissue density [4]. In western countries, there has been an improvement in long-term survival, due to both medical care improvements and earlier detection rates [1]. BC is also a heterogeneous disease whose survival is significantly correlated with, among others, the histological and molecular subtype, number, and localization of metastases [5].

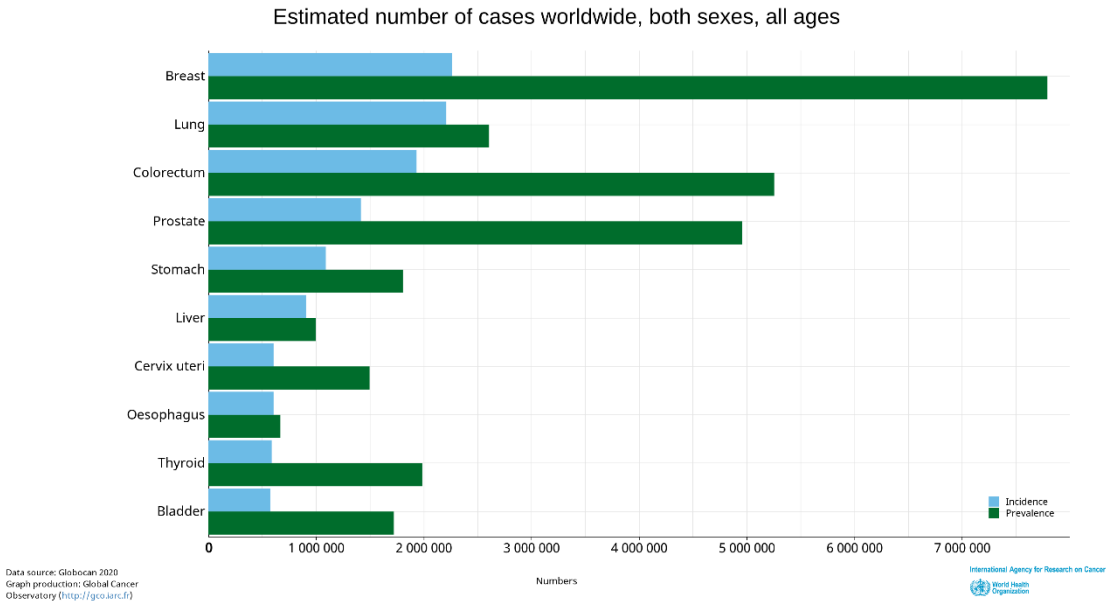

Figure 1. 1 - Estimated number of cancer cases worldwide in 2020 for both sexes and all age groups. Data from [6].

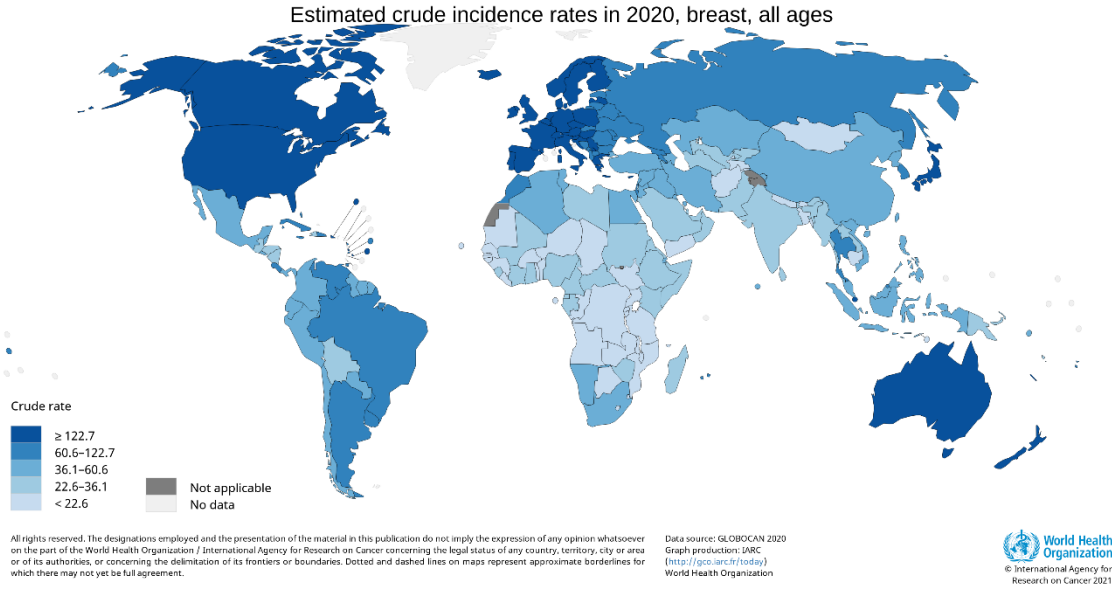

Figure 1. 2 - Heatmap displaying the estimated crude incidence rates of BC in females of all age groups in 2020. Data from [6].

1.2. Classification of breast cancer: types and molecular subtypes

BC is a heterogeneous disease that can be classified according to its delimitation and localization within the breast (e.g. *in situ* ductal carcinoma, invasive tubular carcinoma, etc.) [2,7]. Simultaneously, BC can also be stratified according to molecular markers: it can be positive for the estrogen receptor (ER), for the progesterone receptor (PR), and for the human epidermal growth receptor 2 (HER2), encoded by *ERBB2*, also known as *CD340* or *NEU* [8]. Molecular stratification can further be subclassified by prediction analysis of microarray of a 50 gene set (PAM50) into six molecular subtypes: claudin-low, normal-like, basal-like, HER2-enriched ($HER2^+$), Luminal A, and Luminal B. However, surrogate intrinsic subtypes and clinicians usually encompass the first three phenotypes into a single group: the Triple Negative Breast Cancer (TNBC) subtype [2]. Each molecular subtype has intrinsic characteristics, such as sensitivity to therapy, prognostic and recurrence risk factors, free and overall survival, among several others.

1.2.1. The Triple Negative molecular subtype

The TNBC subtype comprises a heterogeneous group of tumors negative for ER (ER^-), PR (PR^-), and for HER2 ($HER2^-$) receptors that accounts for 10-15% of all BC occurrences [2,9]. Given that no receptor is expressed, TNBC lacks a molecular target for therapy that, in combination with an aggressive clinical behavior, deems it the BC subtype with the worse prognosis associated [10,11]. Also worthy of mention, TNBC patients display an increased risk of central nervous system (CNS) and lung metastases development [11–13].

1.2.2. The HER2$^+$ molecular subtype

HER overexpression is seen in many types of cancer. Statistics point that *HER2* is overexpressed in 13-25% of BCs worldwide [2,14]. Moreover, evidence suggests its amplification is an early event in BC tumorigenesis [15]. This subtype is associated with an aggressive course of the disease, being HER2 overexpression a negative prognostic factor [5]. HER2$^+$ BC can further be subdivided into two types: the non-luminal HER2$^+$ subtype (ER$^-$, PR$^-$ and HER2$^+$), and the HER2$^+$ luminal B (ER$^+$ and/or PR$^+$ and HER2$^+$) [16]. It is also worth mentioning that a known truncated form of HER2 (known as p95^{HER2}) is also present in BC, revealing the HER2$^+$ true diversity within BC [17].

The *HER2* gene (*ERBB2*/*NEU*) located at chromosome 17q12-21 has been shown to play an important role in growth, focal progression, and distant metastases in BC [14]. Its main function is coding for the transmembrane receptor tyrosine kinase known as HER2 [14,15,18]. The amplification of this oncogene is associated with an adverse survival outcome, due to proliferation and invasion of aggressive breast cells [15,19]. Without anti-HER2$^+$ therapy, the median survival for patients is 18 months [5].

HER2 is a well-studied therapeutic target. Besides surgery, radiation therapy, and conventional chemotherapy, HER2$^+$ BC therapies include anti-hormone treatments [14], tyrosine kinase inhibitors (e.g. lapatinib [20]), and monoclonal antibodies, e.g. trastuzumab [20]) or pertuzumab [14,21]. A bispecific antibody [22], HER2-targeted vaccines [23], other pan-HER inhibitors, and drug-antibody conjugates are also being studied [24]. However, historically, these therapies, as for the ones aimed at treating TNBC, are mainly effective at controlling extracranial disease due to the delivery limitations posed by the blood-brain barrier (BBB) and the blood-tumor barrier (BTB) [14,25]. Caveats concerning brain metastasis (BrM) targeted therapy include: 1) heterogenous drug uptake promoted by the BTB, 2) low penetrance rates, 3) subtoxic accumulation of compounds due to the active removal by protein efflux pumps present in the BBB, and the short-lived levels that some drugs display in the brain parenchyma [26].

Since 25% of early HER2$^+$ BC patients still experience disease recurrence after initial anti-HER2 therapy [14] the need for promising therapeutic options that circumvent these issues is paramount. A possible approach is the administration of drugs prior to metastasis onset. This prophylactic approach is currently being tested in a phase I/II trial by the administration of temozolomide to prevent BrM onset and T-DM1 for control of the systemic disease. This “secondary prevention” approach has yielded a BrM-free status in

its first year [27]. This could be interpreted as a beacon reinforcing the need for future studies to also focus on understanding and preventing BrM rather than directing most of the attention to the treatment of an already existing metastasis.

Also important to consider is that an advanced BC, associated with distant metastases, is deemed treatable but incurable with the currently available therapies [2]. Standard treatments for BrM still display high rates of either recurrence or progression, thus limiting survival and quality of life in most patients [26,27]. And even though BC systemic anticancer therapies are becoming ever more effective, BrM incidence is likely to increase due to the longer survival of patients which provides time for BrM to form [28,29]. At this stage, the focus is on prolonging the survival and controlling of patient's symptoms with the lowest toxicity possible to maintain or improve life quality [2,30].

1.3. Metastases and the metastatic cascade – brain metastases as a case study

Metastatic dissemination is very common in BC. It starts as a well-defined (*in situ*, non-invasive) mass of cells that can acquire metastatic (or infiltrating) capacity, thus becoming a Metastatic Breast Cancer (MBC). The process of acquiring invasive capacity occurs through a multistep sequence of events called the metastatic cascade. The metastatic cascade starts with evasion, where cancer cells detach from the primary tumor and enter the systemic circulation (intravasation). If cancer cells survive the migration process (where they might suffer attacks from the immune system, shear stress, and apoptosis), they will adhere to the blood capillaries, where they start invading the new organ (invasion) [16]. Platelets have been shown to guard cancer cells against immune elimination and also promote their arrest at the endothelium, aiding in extravasation and establishment of a secondary lesion [31]. However, even with platelet aid, very few cancer cells get to the stage of infiltrating distant organs. This turns metastization, from a biological point of view, into a very inefficient process [32]. However, metastases are responsible for 90% of BC mortality. The process of distant metastases ends with colonization [16].

The metastatic spread follows a non-random distribution among distant organs, and it has a preference for certain organs/tissues over others, a phenomenon known as tropism or organotropism. Tropism is dependent on the molecular features of cancer cells, cancer cells-tissue interactions, the circulation pattern, and the host organ immune

microenvironment [16]. BC most prevalent organs of secondary lesion are the bones and lungs (60-70% of patients), liver (approx. 30%), and brain (10-20%) [13,16,20,33]. The distinct organs to which BC preferentially metastasize are also determined by the BC molecular subtype (Figure 1.3) [16]. A keystone of BC research is that, among the different subtypes, patients with TN and $HER2^+$ BCs display a higher incidence of BrM (>35%) [26,34].

Some authors point to the evidence that metastasis is a dynamic process of communication between the primary tumor and the secondary tumor site [35,36]. This comes from the refinement of the original view of the Seed and Soil theory for cancer metastases, proposed in 1889 by Paget [37].

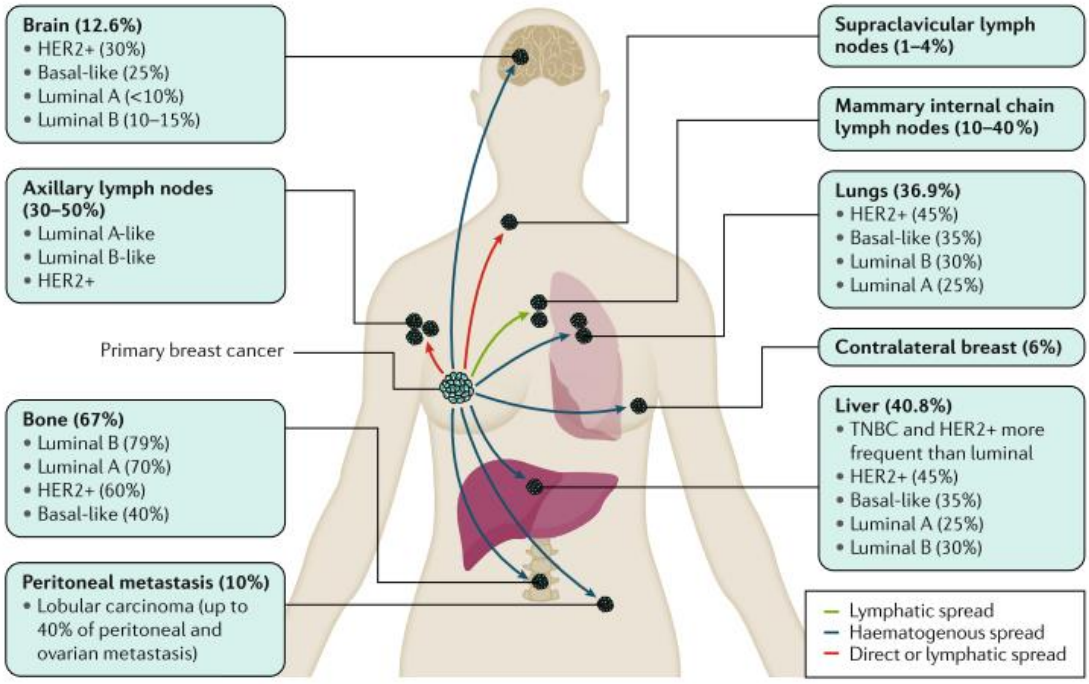

Figure 1. 3 - BC organotropisms and respective probabilities of secondary colonization for each molecular subtype. From [2].

1.3.1. Pre-metastatic niche

As was mentioned, primary tumor cells colonize distant organs to form metastases. However, even before entering blood circulation, tumor cells at the primary site induce profound alterations in the future distant organs through the release of a set of soluble factors and extracellular vesicles [16,38,39], which constitute the cancer secretome. This is termed the pre-metastatic niche (PMN) formation and represents a

crucial step for tumor metastasis [40]. This paracrine communication helps priming the PMN through the activation of resident cells such as fibroblasts or microglia, recruitment of non-resident cells such as bone marrow-derived cells (BMDCs), and remodeling in the extracellular matrix (ECM) [41,42]. These changes turn the local host microenvironment into a pro-tumorigenic milieu that, synchronized with immune deregulation, turns it more permissive to circulating cancer cells successful metastatic homing [38].

Understanding the pathways that lead to PMN formation is an important goal in cancer research, but it remains a challenging task. Despite the fact that patients typically experience metastatic relapse decades after surgical resection of the primary tumor, PMN formation might occur early in tumor development (and may even be induced by surgery), and provide a supportive environment in which tumor cells can settle and remain dormant [16,38]. This issue is often overlooked because the focus is on treating the detectable primary tumor. The difficulty and feasibility of discriminating and getting patient biopsies from a suspected PMN is another challenge. Recent studies have focused on obtaining these tissues in order to follow PMN changes over time and provide new insights into what happens in these complex and sequential processes [38]. Although these are mostly focused on liver and omental biopsies, other tissues, such as the brain parenchyma (where almost 80% of all BrM are identified [16]), require further consideration before biopsy collection. Probably owing to these constraints, brain tissue was not addressed in this initial effort, highlighting the need for alternate study approaches.

1.3.1.1. Pre-metastatic niche formation in the brain

This intriguing and difficult-to-reach organ has two more compelling characteristics when considering it as the future soil for metastases onset. The first is that the brain is regarded to be a relative immunological sanctuary due to the presence of the BBB [43,44]. The BBB is part of the specialized neurovascular unit that regulates brain homeostasis and acts as a physical barrier between blood and the interstitial fluid that bathes the brain parenchyma [45].

Under physiological conditions, the BBB acts as a size-exclusion barrier with extremely low permeability, preventing unwanted entities present in the blood such as

immune and tumor cells as well as pathogens from reaching the brain parenchyma [46,47].

Despite this, it has been demonstrated that the secretome of BC cells causes BBB dysfunction (or vascular leakiness) via vesicular [48] or soluble factors, including zinc-dependent proteases called matrix metalloproteinases (MMPs), cytokines, growth factors such as vascular endothelial growth factor (VEGF) [39,49,50], among many others. This constitutes the initial step in a series of events that occurs through the evolution of PMNs [38], with reeducation of the local tissue-resident cells being the next step.

In addition to BBB dysfunction, other modifications in cellular and noncellular components of the parenchymal brain tissue also occur under the influence of primary tumor cells. Microglia cells (MCs) are one of the examples of brain resident cells that are not passive bystanders and have a well-established and prominent role in brain tumors [51,52]. However, their contribution to the PMN formation is less well documented [53,54]. These are thought to occur mainly through the induction of neuroinflammation at the perivascular niche [55] that, besides aiding in BBB dysfunction, could also act on ECM remodeling and microenvironment reeducation, the subsequent steps in PMN formation. Likewise, neurons have to been shown to change their metabolism due to BC cells secreted factors [56].

The recruitment of non-resident cells, such as BMDCs, also takes place during the PMN formation. So far as we know, no reports regarding the recruitment of non-resident parenchyma cells that could play a role in the PMN formation in the brain were found. Apparently, only resident cells appear to be involved in brain remodeling during the PMN formation. This can be explained because the dysfunction imposed by the BC secretome is not extensive, at least for the case of $HER2^+$ subtypes [57], thus thwarting peripheral immune invasion.

Some specific brain niches referred to as “sleepy niches” can emerge. Those have an adverse environment to metastatic spread, favoring the entry of tumor cells in dormancy for long periods and the appearance of BC metastasis decades after remission [58–61]. Indeed, BrM tend to appear in a late stage of the disease, following lung, liver and/or bone metastasis [16]. Nonetheless, the prevalence of BrM has increased in the past years. It is tough to arise because patients survive longer due to general improvements in the therapies they receive. Some of the risk factors associated with the development of BrM include tumor stage, multiple metastatic sites (>2), large tumor size, and the tumor

subtype, being the $HER2^+$ and TN BCs the ones with higher propensity [13]. In fact, TNBC and $HER2^+$ subtypes display earlier occurrence of BrM and worst survival rates (6-16 months) after diagnosis when compared to luminal BCs [9,13,52]. Surgery has been shown to ameliorate the severe cognitive and physical consequences of BrM and lengthen life expectancy with increased quality but it is viewed as a palliation strategy rather than as an effective cure [62,63].

1.4. Microglia

MCs account for 0.5-16.6% of the total cell population, according to the anatomical brain region [64]. They are auxiliary cells that derive from the yolk sac myeloid progenitors that populate the CNS in an early embryogenic stage [53,65]. By virtue of their myeloid origin and their paramount role in innate immune response, these cells are considered the resident macrophages of the CNS.

In fact, resting MCs survey the brain parenchyma in search of possible disrupters of brain homeostasis, such as small disruptions of the BBB or surplus synapses [66]. These cells are said to present an M0 phenotype, that is characterized by ramified morphology.

However, when MCs find an external body, they become polarized towards a classically activated M1 phenotype, that is characterized by a pro-inflammatory behavior aimed at removing its activator [67]. For this, MCs undergo hypertrophy and shortening of cell processes [68], displaying an amoeboid shape that allows them to engulf cell-damaging entities (such as dead cells, cell debris, and pathogenic microorganisms). In the M1 state, MCs release several bioactive products, including pro-inflammatory cytokines (e.g., tumor necrosis factor α (TNFα), interleukin (IL)-1β), chemokines, proteases, but also reactive oxygen species (ROS) and free radicals to facilitate killing phagocytosed bacteria [69], nitric oxide (NO, by inducible Nitric Oxide Synthase (iNOS)), excitotoxic adenosine triphosphate (ATP) and glutamate [66,70]. Some of the bioactive products mentioned can be used as chemoattractants for other immune cells, further enclosing an effective microbicidal and tumoricidal defense of the host tissue [66,71]. Aside from the cytotoxic role ROS also reinforce the signaling necessary to elicit the M1 phenotype [72].

The classical paradigm of MCs activation also includes an M2 activation state where microglia are characterized by an immunosuppressive and regenerative response

of the brain that is associated with the release of diverse protective factors, such as IL-4, IL-13, fibroblast growth factor, or nerve growth factor [66]. These cells can also display phagocytic activity and tend to accompany long-lasting neurodegeneration situations [66].

Figure 1.4 illustrates the aforementioned microglial activation states that compose the M0/M1/M2 model [71]. It should also be taken into consideration that MCs state is dependent on more than the exogenous activator, such as the pathological environment where the cell is set or the strength of the stimulus. This results in a tremendous diversity of intermediate microglial phenotypes, thus enabling these cells with the specific tools to adequately respond to different conditions [66]. Last, MC polarization can be partially reversible [66] further consolidating their plastic nature.

As part of the innate immune system of the CNS, MCs express several receptors responsible for the detection of damage signals and infections. These are called pattern recognition receptors (PRRs) and one canonical example is the Toll-like receptor (TLR) family that can be activated either by endogenous danger-associated molecular patterns (DAMPs) or by exogenous molecules from external entities, such as bacteria or viruses, pathogen-associated molecular patterns (PAMPs) [54]. A good example of DAMPs constitutes the plethora of proteins secreted by tumor cells. BC cells most depicted DAMPs in the literature include S100s, heat shock proteins, among others [73]. DAMPs induce the activation of signaling pathways in immune cells that lead to the production of pro-inflammatory cytokines and directly increase the aggressive characteristics of tumors through TLRs [73].

Activation of MCs usually occurs after binding of a ligand to the receptors present at the cell membrane. According to the nature of this ligand, different molecular mechanisms are triggered, leading to the production of different bioactive molecules characteristic of each activation phenotype. Figure 1.4 further illustrates these different mechanisms.

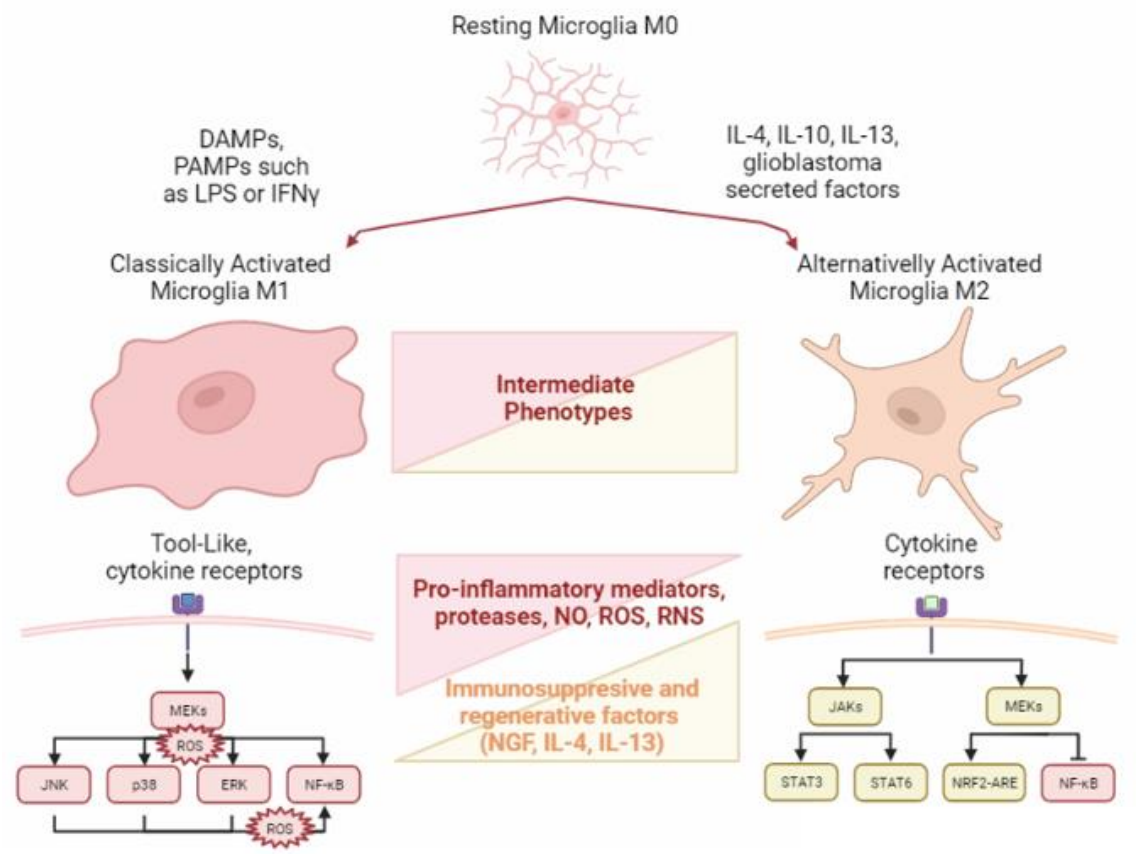

Figure 1. 4 – Microglia activation diagram.

MCs can be classically activated by either M1 or M2 eliciting molecular entities. The classical M1 phenotype entails signaling by pro-inflammatory mediators, such as lipopolysaccharide (LPS) or IFNγ, that bind to Toll-like receptors present at the cell membrane. Signaling through the mitogen-activated protein kinase (MAPK) cascade leads to the phosphorylation of stress-associated kinases such as p38 and c-Jun N-terminal kinase (JNK), extracellular signal-regulated kinase (ERK), and to the phosphorylation of nuclear factors such as NF-κB or STAT1, that bind to the regulatory regions of pro-inflammatory cytokines, growth factors, etc., conducing to the release of a plethora of pro-inflammatory mediators. The classical M2 alternative phenotype entails signaling by an immunosuppressive mediator, such as IL-4, that binds to cytokine receptors. This elicits JAK signaling, STAT3 and STAT6 phosphorylation, as well as inhibition of NF-κB signaling, leading to the expression of specific gene sets associated with immunomodulation, such as *NRF2* [72]. Intermediate phenotypes present a duality of M1 and M2 characteristics with different predominances for either one of the sides of the activation spectrum. This image was made using BioRender 2021.

1.4.1. Microglia in neoplastic diseases

Microglia aberrant activation in brain primary tumors is usually described as being immunosuppressive, M2-like. These cells, together with tumor-associated macrophages (TAMs), are endowed with many tumor-promoting roles such as backing tumor angiogenesis, invasion, matrix remodeling, and generation of a hypoxic niche that promotes immune evasion [52,74]. Microglia and TAMs constitute up to 30-50% of the

tumor mass in gliomas and, for the case of isocitrate dehydrogenase mutant gliomas, MCs are the immune cells that dominate the tumor microenvironment [51]. A good example of how glioma cells modulate MCs phenotype is provided by versican, a glioma-derived proteoglycan. Versican is recognized via TLRs present in MCs and, via the TLR2/p38 MAPK pathway, instigates MCs to produce a metalloprotease that helps re-shaping the brain microenvironment in a pro-tumoral fashion [75]. This is just one of the many examples that show how primary tumor cells can highjack the brain-innate immune system. Other examples regarding how these cells avoid antitumor responses by modulation of MCs phenotypes could have been provided [52,76,77].

Despite what is described in primary brain tumors, the microglial content in growing BrM is largely exceeded by infiltrating leukocytes, monocyte-derived macrophages (MDMs), and T-cells [51]. Nevertheless, microglia still withhold many roles in BrM.

In fact, these cells have been shown to infiltrate the tumor mass creating contacts with carcinoma cells directly after successful extravasation while accumulating in the surrounding gliosis zone [54]. Likewise, a study with living brain slice cultures, a model where peripheral blood-derived macrophages are absent, showed that MCs specifically enhanced the invasion and colonization of the brain by BC cells [78]. Also, a population of MCs, TAMs, and astrocytes was shown to induce a 5-fold increase in breast metastatic cell proliferation while mounting a neuroinflammatory response [79,80]. Last, an interesting study where depletion of the M2 population of macrophages/microglia in the metastatic brain was performed showed that this depletion resulted in a significant reduction of metastasis growth [81]. The primary focus of this study was to reinforce that MCs can display an ambivalent role along with tumorigenic progression but it also evidenced that both MCs and TAMs can subdivide in different M1 and M2 populations at the tumor microenvironment.

One important consideration that should be made is that myeloid cell diversity, particularly their distinct embryological origins and distinct education, has remained defectively or largely unexplored in the field of cancer research [51,82]. In fact, for several years the distinction between infiltrating and resident macrophages of the brain was not properly made, with several articles using markers for both microglia and macrophages (such as F4/80, ionizing calcium-binding adapter molecule 1 (Iba1), CD40, or CD68). This nuance can, in part, be responsible for the heterogenous reported response

to invading cancer cells along with the specificities of each study [80]. Also important to consider is the stage and etiology of the disease.

All the changes mentioned occur because MCs were shown to be re-educated by the many soluble and vesicular factors released from tumor cells. In fact, microglia, due to the presence of phosphatidylserine receptors in their membranes, are cells that are prone to exosome uptake [83,84].

Overall, regardless of the immune context described, MCs always display an important role in the context of BrM that could be exploited in future BC MCs-targeted therapies. Nevertheless, a better understanding of the behavior of these plastic cells has not yet been attained and frustrates this possibility. In fact, a chronological focus on the brain-elicited changes is missing since research has been mainly directed to the changes that occur after metastasis onset. In fact, to the best of our knowledge, only one recent work has focused on the phenotype of MCs, and on how these cells orchestrate changes to the brain vasculature, at an early stage of the metastatic cascade [55]. Hence, more research is necessary to uncover possible vulnerabilities associated with MCs altered functions in BC malignancy.

1.4.1.1. Genesis of microglia-induced neuroinflammation

A local inflammatory microenvironment triggered by the primary tumor is on the basis of the PMN formation with harmful consequences for the brain. This organ is prone to exacerbated inflammation due to modest endogenous antioxidant defense systems, limited capacity for regeneration but also elevated potential for pro-oxidants production, due to the presence of microglia, redox-active transition metals among others [85]. The generation of ROS and nitrogen species (RNS) with pro-oxidant activity can potentially trigger cell death, further promoting neuroinflammation. Apart from being harmful molecules, ROS can also act as second messengers in physiological conditions, and evidence suggests that they can fuel both normal and severe inflammation by activating related signaling pathways [86]. In fact, hydrogen peroxide (H_2O_2) has received particular attention for its role as a second messenger in signaling macrophages transduction pathways [87].

H_2O_2 was shown to modulate the activity of ERK, but also p38 and JNK MAPKs, also known as stress-activated protein kinases (SAPKs), as well as the nuclear factor kappa-light-chain-enhancer of activated B cells (NF-κB), a master regulator of the

inflammatory response [86,88–92]. The activation of MAPKs and NF-κB is intimately associated with inflammatory and tumor-promoting microglial phenotypes [67,74,93].

In fact, studies on mice, human myeloid cells, and mouse macrophages showed that H_2O_2 induced the tyrosine phosphorylation of IκBα, a cytosolic NF-κB inhibitor, and serine phosphorylation of the p65 subunit of NF-κB, promoting its translocation to the nucleus [94]. Once in the nucleus, it regulates the transcription of a plethora of pro-inflammatory cytokines [86,88].

ROS from mitochondrial origin (mROS) have also shown to contribute to MAPK activation and NF-κB translocation. This was demonstrated in murine microglia after pharmacological suppression of mROS which led to a decrease in the activation of the three mentioned MAPKs, reflecting also on NF-κB translocation and on the expression of inflammatory factors [88,95]. Thus, regardless of their origin, a stringent bilateral relationship between iROS and inflammatory activation is present in microglia and macrophages.

1.4.1.2. Reactive oxygen species sources

Irrespective of their origin, ROS are key signaling molecules in mediating inflammatory responses in macrophages. ROS can be produced through enzymatic sources and non-enzymatic sources.

The major source of deliberate ROS production in MCs is the NADPH oxidase (NOX) family group, composed of seven enzymes [86]. NOX enzymes are responsible for the oxidative burst during phagocytosis and are activated in response to DAMPs, making them essential in immune response [86]. *NOX2* and *NOX4* are known to be expressed in MCs. Upon assembly with regulatory subunits, NOX2 is responsible for the production of the superoxide radical ($O_2^{\cdot-}$). Least expressed is the constitutive NOX4 enzyme, responsible for the production of H_2O_2.

Some previous articles argued that MAPKs and NF-κB signaling pathways were potentially modulated by the activity of either NOX enzymes or of the spontaneous reduction of $O_2^{\bullet-}$. However, the specificity of certain NOX pharmacological inhibitors used was later refuted which can be viewed as an opportunity to better understand the relationship between ROS and modulation of the inflammatory response [86]. These included diphenyleneiodonium (DPI), which inhibits mitochondrial respiration, iNOS

and, NF-κB activities [96], but also apocynin, among others. The latter appears to act also as an antioxidant as well, raising the question of whether the decrease in ROS production, observed in some studies, is due to the inhibition of NOX activity or unspecific ROS removal [97]. Also worthy of mention is the fact that intracellular ROS (iROS) generation was not completely abrogated in *NOX* knockout models [98].

In humans, there are 24 enzymes responsible for H_2O_2 production, some of which present at the mitochondria [99,100], but are not considered as major ROS producers.

In fact, the major source of iROS, particularly H_2O_2, occurs in a non-enzymatic manner at the mitochondria. Most iROS come from the mitochondria as byproducts of oxidative phosphorylation. It is estimated that 0.2-2% of the O_2 consumed in the mitochondria is univalent reduced to $O_2^{\bullet-}$, being further converted by superoxide dismutases to H_2O_2 [101]. Notably, mitochondria have mechanisms to maintain mROS in the nontoxic range. The first line of defense against deleterious oxidative stress is mildly uncoupling oxidative phosphorylation from ATP synthesis through the expression of uncoupling proteins (UCPs) [102]. UCP2 is a member of the mitochondrial inner membrane carrier family that is expressed in macrophages [101]. This protein uncouples respiration and has its expression induced under deleterious conditions where ROS or ROS by-products concentrations become pathological, thus creating a negative feedback mechanism for mROS production [101,103]. UCP2 activity has also been proposed to be controlled by covalent modification by glutathione [102,103]. Indeed, studies performed in knockout mouse models demonstrated that UCP2 restricts the production of mROS by decreasing the mitochondrial membrane potential [104], but also controlled p38 and ERK activation as well as inflammatory cytokine expression in macrophages through the activation of ROS-sensitive phosphatases [105–107]. An illustrative scheme is presented in Figure 1.5.

Aside from synthesis, the up-regulation of ROS levels might also occur indirectly as a result of dyshomeostasis of trace elements, such as zinc (Zn^{2+}). This could happen with the help of specific transporters, such as the solute-linked carrier 39 (SLC39A) family of Zn^{2+} importers [108] or metalloenzymes that can alter the amount of loosely bound zinc after reacting with iROS [109]. Throughout the years, Zn^{2+} metabolism has revealed itself to be a conundrum. However scientists have epitomized two main concepts: the first is that Zn^{2+} has predominantly pro-antioxidative functions, and the second is that alterations in zinc status, either deficiency or overload, lead to pro-oxidative

conditions [100,109]. In sum, adverse effects arise when the fine balance of Zn^{2+} metabolism is disturbed.

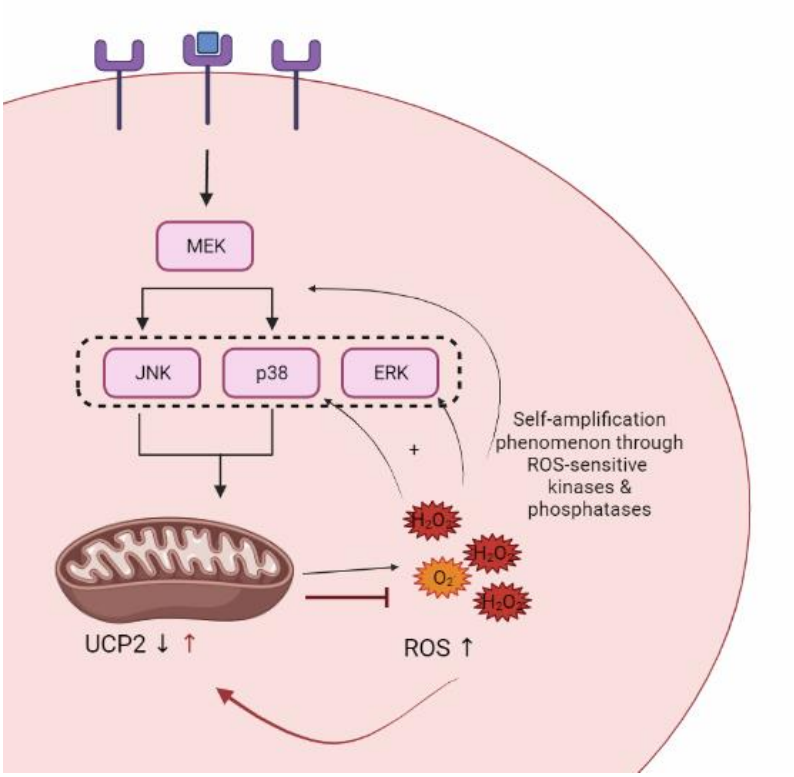

Figure 1. 5 – Illustrative mechanism of UCP2 regulation of mROS.

As proposed by Collins et al., pro-inflammatory stimulus activates the stress-associated protein kinases JNK and p38 which in turn down-regulate the levels of UCP2 in the mitochondrial membrane. This first pro-inflammatory stimulus is further amplificated by the production of mROS that can oxidate several ROS-sensitive phosphatases upstream of the MAPK further leading to increased ROS production. UCP2 levels increase as a protective mechanism before pathological mROS production [72,90,105–107]. This image was made using BioRender 2021.

In fact, research shows that treating macrophages with zinc sulfate or zinc nanoparticles promotes an M1-like phenotype with increased ROS production [110,111]. Simultaneously, several other studies reported that decreasing intracellular Zn^{2+} levels in macrophages decreased their innate inflammatory response through iNOS, p38, ERK, NF-κB. This is due to the fact that Zn^{2+} influx generates increased levels of the second messenger H_2O_2, but is also required to prevent dephosphorylation of p38, MEK1/2, ERK1/2, but also NF-κB [112–115].

Based on the aforementioned, MCs have several complex and dynamic mechanisms for neuroinflammation onset that can mediate both protective and deleterious responses to brain insults. Evidence also suggests that dysregulation of

macrophage metal homeostasis could be involved in the genesis of these processes and, eventually, in the PMN formation.

1.4.1.3 Oxidative stress: a fine balance for effective protection

As was previously mentioned, ROS can have a dual role inside the cell, either as signaling molecules or as cytotoxic entities. Yet, a similar ambivalent role can be attributed to their ensuing consequence, oxidative stress [116], since a physiological level of oxidation promoting entities inside a cell is beneficial to its proper function and can even be coined as oxidative eustress (from the Greek prefix eu- meaning "good"). On the opposing side of the scale, there is the overwhelming of the endogenous antioxidant defense systems by ROS and RNS that leads to oxidative distress. According to the condition, it is sometimes difficult to determine the correct trigger for this self-propelling sequence of events [86]. In fact, glia cells can become overzealous under pathological stimuli, entering into a neuroinflammatory vicious cycle that promotes oxidative distress, and compromises their functions as well as the functions of adjacent cells [86,117].

The fine balance between oxidative eustress and distress seems to be regulated, amidst other things, by the H_2O_2 levels. Physiological H_2O_2 concentrations underlie redox signaling required for homeostatic mechanisms such as cell proliferation or migration, whether higher concentrations lead to adaptive stress responses mediated by master switches such as the nuclear factor E2-related factor 2/Kelch-like ECH-associated protein 1 (NRF2/Keap1) or NF-κB. Supraphysiologic H_2O_2 concentrations lead to damage of biomolecules, referred to as oxidative distress (Figure 1.6).

Adaptive responses mediated by *NRF2* lead to the transcriptional activation of genes with antioxidant properties, such as NADH-quinone oxidoreductase 1 or glutathione-S-transferases, and also to the expression of growth factors, such as VEGF [86,118]. VEGF is associated with angiogenesis, a process that is also dependent on H_2O_2 levels [119]. The transcription of antioxidant entities acts as a brake on microglial inflammation and oxidative distress [86]. Curiously, NRF2 is a zinc-sensitive transcription factor [100], which is in line with the pro-antioxidant function of Zn^{2+} in a range of physiological levels.

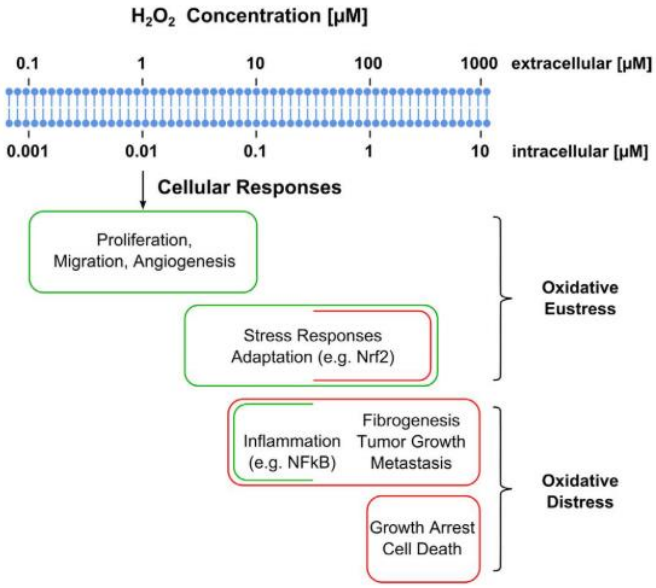

Figure 1. 6 - Predicted ranges of H_2O_2 concentrations and their role in oxidative stress-mediated responses.

The arrow indicates values for normally metabolizing liver cells. Stress and adaptive stress responses occur at higher H_2O_2 concentrations with higher exposure leading to inflammatory response, growth arrest, metastasis, and cell death by various mechanisms. Colors green and red denote predominately beneficial or deleterious responses, respectively. Acute inflammation (as opposed to chronic), is depicted as beneficial. Extracellular and intracellular H_2O_2 concentrations vary with cell type, location, and the activity of enzymatic sinks. Credits to the image to [116].

In sum, NRF2 is highly sensitive to oxidative burst products, including ROS, and upon activation acts to counteract its inducers and the NF-κB-mediated pro-inflammatory response. This maintains the equilibrium between oxidative eustress and oxidative distress, such that under physiological conditions the brain is protected from the onset and progression of neurodegenerative diseases [120]. In fact, in Parkinson's disease mouse models, it was shown that NRF2 deficiency resulted in increased microgliosis with an associated gene expression pattern resembling the M1 phenotype, which is associated with higher neuronal death [121].

1.5. Objectives

Contemporary research is mainly focused on the changes that occur after breast cancer brain metastases (BCBM) but not as much on the early changes that harbor a successful BrM. MCs are depicted as key mediators in glioma progression, but their role on BrM and, especially, on the PMN changes that occur prior to metastasis onset was not the objective of extensive investigation.

Zn^{2+} homeostasis is particularly important for the innate immune system such that dysregulation of its equilibrium is linked to an abnormal inflammatory response. Nonetheless, studies concerning Zn^{2+} dyshomeostasis in MCs were not yet performed in the context of PMN formation.

As to focus on these topics we proposed to explore the changes induced in MCs by the secretome of two highly brain metastatic BC cell lines, with a focus on phenotype and oxidative stress balance. As such, our objectives are:

- To characterize the phenotype that is elicited on the HMC3 microglial cell line by exposure to the TN and $HER2^{+}$ breast cancer cells (BCCs) derived secretomes;
- To understand if extracellular Zn^{2+} influx is a modulator of the microglial phenotype observed under BCCs secretomes exposure;
- To evaluate if the MCs activation induced by the BCCs can influence the barrier properties of the hCMEC/D3 endothelial cell line.

To this end, we hypothesize that the secretomes derived from brain metastatic breast cancer cells (BMBCCs) trigger MCs activation but also that the activation phenotype elicited is regulated by H_2O_2 and Zn^{2+} homeostasis.

Chapther 2 - Materials and Methods

2.1. Cell culture and culture methods

All the procedures concerning cell culture were performed in sterile conditions on a laminar flow chamber. Cells were maintained in an incubator at 37 ^{o}C under a humidified 5% CO_2/95% air atmosphere. Thawing of the different cell lines was done accordingly to the information present on the datasheet of each cell line. After reaching 80% confluency, cells were washed with phosphate-buffered saline (PBS; 8 mM sodium dihydrogen phosphate (NaH_2PO_4, Merck), 3 mM potassium dihydrogen phosphate (KH_2PO_4, Merck), 140 mM sodium chloride (NaCl, Merck), 5 mM potassium chloride (KCl, Merck), pH = 7.4) and dissociated with 0.25% trypsin-ethylenediamine tetraacetic acid (EDTA, Sigma). After centrifugation at 1500 RPM for 5 min, cell viability and number were assessed with a hemocytometer (Superior Marienfeld) using the trypan blue exclusion assay. This method is based on the ability of the dye (0.4% trypan blue, Gibco) to cross only permeable cell membranes, which are typical of non-viable cells. Cells displaying viability equal or superior to 90% were used.

2.1.1. Human Microglia Clone 3 (HMC3) cell line

The Human Microglia Clone 3 (HMC3) cell line (ATCC®CRL-3304) was derived from fetal tissue and is one of the most employed human microglia cell lines throughout literature. HMC3 cells were cultured in Essential Minimum Eagle Medium (EMEM, SIGMA) supplemented with 1% (v/v) L-glutamine (Gibco), 1% (v/v) sodium pyruvate (Gibco), 1% (v/v) penicillin/streptomycin (Gibco), and 10% (v/v) heat-inactivated Fetal Bovine Serum (FBS, Gibco). Cells were grown in 25 and 75 cm^2 culture flasks with dilutions ranging between 1:3 and 1:8. Microglia cells were maintained in culture until passage 30.

2.1.2. MDA-MB-231 cell line

The MDA-MB-231 cell line is a human triple-negative BC cell line. The parental MDA-MB-231 cell line referred to as 231^{P}, and its brain-tropic metastatic variant referred to as 231^{BR}, were cultured in Dulbecco's Modified Eagle's Medium-high glucose (DMEM) supplemented with 1% (v/v) penicillin/streptomycin and 10% (v/v) heat-inactivated FBS. Cells were grown in 25 and 75 cm^2 culture flasks with dilutions ranging

between 1:5 and 1:15. Both cell lines were kindly provided by the laboratory of Dr. Patricia Steeg at the National Cancer Institute.

2.1.3. JIMT-1 cell line

The JIMT-1 cell line is a $HER2^+$ BC cell line of human origin. The parental cells, referred to as JIM^P, and its brain-tropic metastatic variant, referred to as JIM^{BR}, were cultured in DMEM supplemented with 1% (v/v) penicillin/streptomycin and 10% (v/v) heat-inactivated FBS. Cells were grown in 25 and 75 cm^2 culture flasks with dilutions ranging between 1:5 and 1:10. Both cell lines were kindly provided by the laboratory of Dr. Patricia Steeg at the National Cancer Institute.

2.1.4. Human cerebral microvascular endothelial cell line (hCMEC/D3)

The human Cerebral Microvascular Endothelial Cell line (hCMEC/D3), extensively used as a model of the human BBB, was kindly provided by Pierre-Olivier Couraud (Institute Cochin, Universitité Ren Descartes, Paris, France). hCMEC/D3 cells were cultured in EndoGRO basal medium supplemented with 0.2% EndoGRO-LS supplement, 5 ng/mL recombinant human epidermal growth factor, 10 mM L-Glutamine, 1 µg/mL hydrocortisone hemisuccinate, 0.75 U/mL heparin sulfate, 50 µg/mL ascorbic acid, and 5% heat-inactivated FBS. Cells were grown in 25 cm^2 tissue flasks coated with 150 µg/mL collagen type I (R&D Systems, Inc.). hCMEC/D3 cells were maintained in culture until passage 30.

2.1.5. Conditioned medium samples preparation

For conditioned mediums (CM) collection, BC cell lines were seeded at a density of 40 000 $cells.cm^{-2}$ and maintained in culture for 48 h. After this period, the supernatant was harvested and centrifuged at 1 000 RPM for 5 min to remove any cells debris. Part of the cell-free CMs was used for further concentration, by ultracentrifugation in Amicon Ultra-15 10K Centrifugal Filter Devices at 4 000x g, 4° C for 30 min. The protein content in non- and concentrated CMs (CCMs) was determined to ensure that the same amount of protein is used in all experiments. Aliquots of non- and CCMs were stored at -80 °C until use.

2.2. Nitric oxide determination

NO production is an indicator of MC activation. To quantify its production, a Griess assay was performed.

HMC3 cells were seeded at 18 000 cells.cm^{-2} on T25 tissue culture flasks and allowed to adhere overnight. After 6 and 24 h stimulus, 100 µL aliquots of media were mixed with 100 µL of Griess reagent (1% sulfanilamide in 5% phosphoric acid (H_3PO_4) and 0.1% naphthylethlyenediamene) and then incubated for 30 min at room temperature in the dark. Then, absorbance was read at 540 nm and 620 nm (reference wavelength) in a Synergy™ HT plate reader. NO concentration was determined using a standard curve of sodium nitrate ($NaNO_2$). Data were normalized to the control condition after baseline subtraction.

2.3. Reverse Transcription quantitative Real-Time Polymerase Chain Reaction

Gene expression was evaluated by reverse transcription-quantitative real-time polymerase chain reaction (RT-qPCR).

2.3.1. RNA extraction and cDNA synthesis

HMC3 cells were plated at a density of 18 000 cells.cm^{-2} on T25 tissue culture flasks and allowed to adhere overnight. After a 24 h incubation period, cells were washed with PBS and detached with trypsin-EDTA. A centrifugation step at 1500 RPM for 5 min at 4 °C ensured cell pelleting. The pellets obtained were washed with PBS and centrifuged again at 1500 RPM for 5 min at 4 °C. The last washing step was performed, and the cell pellet was centrifuged at 6000 relative centrifugal force (RCF) for 5 min at 4 °C to prepare cells for total RNA extraction with the NZY Total RNA Isolation kit (NZYTech).

At the cell hood, after cleaning with 70% ethanol and RNase AWAY (Molecular BioProducts™) the cell pellets were lysed, and total RNA was retrieved in 40 µL of Molecular Biology Grade-Water in compliance with the manufacturer instructions.

RNA quantification and quality assessments were done using the NanoDrop® ND-1000 Spectrophotometer. RNA was used in cDNA synthesis when the values for the absorption ratios 260/280 and 260/230 were ~1.8 and ~2.0, respectively.

Prior to complementary DNA (cDNA) synthesis with the NZY First-Strand cDNA Synthesis Kit (NZYTech), the cell hood was again cleansed with 70% ethanol and RNase

AWAY. This kit has a combination of oligo(dT) primers, which display mRNA specificity, and of random hexamers that are a good choice when synthesizing a large pool of cDNA. This combination increases sensitivity and hence, data quality.

The procedure for cDNA synthesis was performed according to manufacturer instructions. Briefly, 2 μg of RNA are combined with Molecular Biology Grade-Water, NZYRT 2× Master Mix (containing the primers, dNTPs, optimized reverse transcriptase buffer, and $MgCl_2$), and with the NZYRT Enzyme Mix (containing both the reverse transcriptase and a ribonuclease inhibitor). The cDNA synthesis was performed in a C1000^{TM} Thermal Cycler BIO-RAD apparatus that was set as follows: initial incubation at 25 ºC for 10min, followed by incubation at 50 ºC for 30min for reverse transcription and 85 ºC for 5 min for heat inactivation, followed by rapid cooling to 4 ºC.

Afterward, RNase H was added to the mix and incubated for 20 min at 37 °C to ensure that the final cDNA product is free from the RNA template in cDNA:RNA hybrids. cDNA samples were diluted 10 times in Molecular Biology Grade-Water and stored at -20 °C for RT-qPCR.

2.3.2. Real-Time quantitative PCR

A Primer-BLAST search was performed to evaluate primer specificity and self-complementarity values of already validated and published primer sequences. The final selected primers used in RT-qPCR experiments were synthesized by Eurofins Genomics and are listed in Table 2.1.

Each RT-qPCR mix contained the target cDNA, forward and reverse primers at 3.5 μM each, and the Xpert Fast SYBR (uni) (GRISP) mix. For each experiment, a CFX Connect Real-time PCR Detection System (BioRad) was used with the following protocol: initial denaturation step at 95 °C for 3 min, followed by 40 cycles of 30 s at 95 °C, 20 s at 55 °C to allow primer annealing, 20 s at 72 °C for DNA extension and a final elongation cycle also at 72 °C for 10 min. After, a melting curve analysis (increments from 55 to 95 °C at 0.5 °C/10 s rate) was done to evaluate the specificity of each pair of primers. All RT-qPCR conditions were assayed in duplicate.

Screening for reliable reference genes was done with the help of the RefFinder tool [122]. The threshold cycle (Ct) was obtained from duplicate samples and yielded a score for each reference gene. Genes with a score near one were used as reference genes. Relative gene expression was evaluated with the ΔΔCt method as follows:

$$\Delta Ct_{Gene\ of\ Interest} = Ct_{Average\ of\ Gene\ of\ Interest} - Ct_{Geometric\ Average\ of\ Reference\ Genes}$$

$$\Delta\Delta Ct = \Delta Ct_{Gene\ of\ Interest} - \Delta Ct_{Average\ of\ Control}$$

$$Relative\ Gene\ Expression = 2^{-\Delta\Delta Ct}$$

Table 2. 1 - Primer sequences used for RT-qPCR analysis.

	Gene	Primer sequence	Reference
Oxidative stress	UCP2	F:5'-GGCTGGAGGTGGTCGGAGATAC-3'	[123]
		R:5'-CAGCACAGTTGACAATGGCATTACG-3'	
	NOX2	F:5'-CCCTTTGGTACAGCCAGTGAAGAT-3'	[124]
		R: 5'-CAATCCCGGCTCCCACTAACATCA-3'	
	NOX2	F:5'-AAATGGTGGCATGGATGATT-3'	[125]
		R:5'-GGGATTGGGCATTCCTTTAT-3'	
	NOX4	F:5'-AACCGAACCAGCTCTCAGAA-3'	
		R:5'-CCCAAATGTTGCTTTGGTTT-3'	
	NRF2	F:5'-CAATGAGGTTTCTTCGGCTACG-3'	[126]
		R:5'-AAGACTGGGCTCTCGATGTG-3'	
Inflammatory mediators	IL-1β	F:5'-GCT TGG TGA TGT CTG GTC-3'	[127]
		R:5'-GCT GTA GAG TGG GCT TAT C-3'	
	TNFα	F:5'-CAGGTCCTCTTCAAGGGCCAA-3'	[128]
		R:5'-GGGGCTCTTGATGGCAGAGA-3'	
	VEGFA	F:5'-GCCTCCGAAACCATGAACTTT-3'	[129]
		R:5'-CTTGGCATGTTGGAGGTAGAG-3'	
	IL-6	F:5'-TCTGGATTCAATGAGGAGACTTG-3'	[127]
		R:5'-TCACTACTCTCAAATCTGTTCTGG-3'	
	IL-10	F:5'-GGCACCCAGTCTGAGAACAG-3'	[130]
		R:5'-ACTCTGCTGAAGGCATCTCG-3'	
	TGF-β	F:5'-CAGTCACCATAGCAACACTC-3'	[131]
		R:5'-CCTGGCCTGAACTACTATCT-3'	
RGs	18S	F:5'-GAAGATATGCTCATGTGGTGTTG-3'	
		R:5'-CTTGTACTGGCGTGGATTCTG-3'	
	TBP	F:5'-CTGGCCCATAGTGATCTTTGC-3'	[132]
		R:5'-TCAATTCCTTGGGTTATCTTCACA-3'	

Note – F: Forward; R: Reverse; RG: Reference Gene.

2.4. Reactive oxygen species detection assay

Aside from their role in cell signaling, ROS act as indicators of the activation state of immune cells while also being a major component of their killing response. The 2',7'-dichlorodihydrofluorescein diacetate (H_2DCFDA, Thermo Fisher) probe is a versatile indicator of oxidative stress. This cell-permeant molecule is useful for the detection of

H_2O_2, the hydroxyl radical ($OH^{-\cdot}$), or peroxynitrite ($NO_3^{-\cdot}$). After diffusion through the cell membrane, the probe is hydrolyzed by intracellular esterases and can now be oxidized into the highly fluorescent 2',7'-dichlorofluorescein (DCF) form, as indicated.

$$H_2DCFDA \xrightarrow{Deesterification} DCFH \xrightarrow{Oxidation\ by\ H_2O_2\ or\ free\ radicals} DCF$$

To detect ROS production, cells were seeded at 28 000 cells.cm^{-2} and let adhere overnight on opaque Corning® 96 well plates. Stimuli were added the following day and allowed to act for 24 h. At the end of the incubation period, culture mediums were removed, and the wells were washed with PBS. After, 100 µL of KREBS buffer [142 mM NaCl, 4 mM KCl, 1 mM magnesium chloride ($MgCl_2$, Sigma-Aldrich), 1 mM calcium chloride ($CaCl_2$), 10 mM glucose (Merck), 10 mM 4-(2-hydroxyethyl)-1-piperazineethanesulfonic acid (HEPES); pH 7.4] containing 5 µM of the H_2DCFDA probe were added in the dark to each well and incubated at 37 °C for 2 h. Fluorescence values were measured after 2 h of incubation in a Synergy^{TM} HT plate reader at 485/20 nm excitation, 528/20 nm emission, sensitivity 100. Each condition was assayed in triplicate in each independent experiment.

2.5. Viability assay

Following fluorescence detection by the H_2DCFDA probe viability was determined using a colorimetric resazurin reduction assay. Resazurin (5 µM, Sigma) was added to each well, and absorbance at 570 and 600 nm (reference wavelength) were red after a 4-h incubation period in a Synergy^{TM} HT plate reader. Experimental conditions assayed for the ROS detection assay viability are the same as the viability assay and are as follows:

- DMEM (control)
- DMEM + 100 ng/mL LPS (positive control, Sigma-Aldrich)
- H_2O_2 100 µM (positive control, Sigma-Aldrich)
- CM 231^{P}, CM 231^{BR}
- CM JIM^{P}, CM JIM^{BR}
- DMEM + 5, 10, 25, 40, 50 µM zinc chloride ($ZnCl_2$, Sigma-Aldrich)

- DMEM + 5, 10, 25, 50 µM DTPA (Alfa Aesar)
- CM $231^{P,BR}$ + 5, 10, 25, 50 µM DTPA
- CM JIM^{BR} + 5, 10, 25, 50 µM DTPA

2.6. Scratch wound-healing assay

HMC3 cells were seeded in 24-well plates (OrangeScientific) at a density of 35.000 cells.cm^{-2} and allowed to adhere overnight. On the following day, the stimuli were added and allowed to act for 24 h. After that, a scratch was performed with a 200 µL pipette tip along the confluent cell monolayer. The wells were washed twice with PBS to remove cell debris and replenished with stimuli-containing fresh medium. Four to five representative images were taken from each well at different time points: 0, 8, 10, and 24 h. Images were captured in an inverted microscope at a magnification of 10x with the Motic Images Plus 3.0 software. The wound areas were measured with the Fiji software and were normalized to their respective initial wound-healing area.
The different stimuli:

- DMEM (control)
- DMEM + 100 ng/mL LPS (positive control)
- DMEM + CCM $231^{P, BR}$
- DMEM + CCM JIM^{BR}

2.7. Proliferation evaluation assay

Microgliosis is characterized by an increase in the number of activated MCs. To assess if the BCC secretome stimulates the proliferation of MCs, the cell proliferation reagent 4-[3-(4-iodophenyl)-2-(4-nitrophenyl)-2H-5-tetrazolio]-1,3-benzene disulfonate (WST-1, Roche) assay was employed. This sensitive colorimetric test correlates absorbance with the number of metabolic active cells. The WST-1 salt is cleaved into the soluble formazan by the glycolytic production of NAD(P)H in viable cells.

MCs cells were seeded in 96-well plates (OrangeScientific) at a density of 6000 cells.cm^{-2} and allowed to attach overnight. Next day, the CCMs were added to each well and the cells were maintained in the incubator for 24, 48, and 72 h. After each incubation period, the WST-1 reagent was added to each well. After 2 h of incubation, the plate was

agitated in an orbital shaker for 1 min to dissolve formazan crystals and the absorbance was read at a wavelength of 450 nm and 630 nm (reference filter) in a Synergy^{TM} HT plate reader. A WST-1 assay was performed at time-zero before adding the stimuli to estimate the absorbance of the starting number of cells.

Absorbance values for each time point were normalized to the corresponding values measured at time-zero and expressed as a percentage.

2.8. Western Blotting

2.8.1. Preparation of cellular extracts

HMC3 cells were seeded at 18 000 cells.cm^{-2} in T25 culture flasks and allowed to adhere overnight. On the following day, the culture medium was replaced by the CMs. After 24 h of incubation, the cells were washed and scraped in cold PBS. The resulting cell suspension was centrifuged at 1500 RPM, 4 ^{o}C for 10 min. The supernatant was removed, and the pellet was slowly resuspended in Radio Immuno Precipitation Assay (RIPA) Buffer [150 mM NaCl, 1% (v/v) Triton X-100 (Sigma), 0.5% (v/v) sodium deoxycholate (Sigma), 0.1% (w/v) sodium dodecyl sulphate (SDS, BioRad), 50 mM Tris (pH 8.0, Sigma), and 2 mM EDTA (Sigma)] for cell lysis. The RIPA buffer was also supplemented with a cocktail of phosphate (Roche) and protease inhibitors (Roche), 1 mM dithiothreitol (DTT, Sigma-Aldrich), 1 mM sodium fluoride (NaF, Sigma-Aldrich), and 2 mM sodium orthovanadate (Na_3VO_4, Sigma-Aldrich). After an incubation period of 30 min at 4 ^{o}C, the cell suspensions were sonicated with three to five-second pulses at 40 MHz in an ultrasound device (Vibra Cell Sonics and Materials Inc.) while dipped on ice.

2.8.2. Protein quantification

Total protein quantification was performed using the bicinchoninic acid (BCA, Sigma Life Sciences) colorimetric assay coupled to a Bovine Serum Albumin (BSA, Sigma Life Science) standard curve. This method is based on the formation of complexes between proteins and copper ions that can be detected between 540 nm and 590 nm. The reduction of Cu^{2+} to Cu^{+} is proportional to the amount of protein present in the solution. Both testing samples and BSA proteins standards were incubated with a mixing BCA

reagent and copper (II) sulfate solution (Sigma-Aldrich) for 30 min. A standard curve was made, and protein concentration was calculated after an absorbance reading at 570 nm.

Protein samples were denatured with a denaturing solution containing 0.25 M Tris (pH 6.8), 4% (w/v) SDS, 200 mM DTT, 20% (v/v) glycerol, bromophenol blue (Sigma-Aldrich), and type I water. The protein lysates were heated at 95 °C for 10 min in a 1 to 3 ratio of denaturing solution and stored at -20 °C prior to gel electrophoresis.

2.8.3. Gel electrophoresis and electrotransferance

Proteins were separated based on their molecular size by sodium dodecyl sulfate gel electrophoresis (SDS-PAGE). SDS-polyacrylamide gels of 12% were prepared [30% acrylamide/bisacrylamide solution (ACRYL/BISTM 29:1, VWR Life Sciences), 20% (w/v) SDS, 10% (w/v) ammonium persulfate [APS, AMRESCO], tetramethylethylenediamine (TEMED, Sigma-Aldrich)]. Forty to 50 µg of protein were loaded into the SDS-polyacrylamide gels along with a protein marker (GRS Protein Marker MultiColour). Electrophoresis were carried out in a Mini-PROTEAN Tetra System (Biorad) at 100 V for 10 min and at 140 V for approximately 1h30 min in buffer solution containing 100 mM Tris-HCl, 100 mM bicine (Sigma-Aldrich), and 0.1% (w/v) SDS.

After electrophoresis, proteins were transferred into a polyvinylidene difluoride (PVDF, GE Healthcare) membrane previously activated in 100% methanol (VWRTM International). The cassette assembly was dipped in electrotransference buffer [12.5 mM Tris-HCl (pH 8.0-8.5), 96 mM glycine (Sigma-Aldrich), and 20% (v/v) methanol)] and electrotransference was performed at a constant current of 0.3 A for 2 h at 4 °C in the Mini-PROTEAN Tetra System.

Following electrotransference, the PVDF membranes were blocked in a solution that prevented non-specific interactions between the proteins present in the membrane and the antibodies used. This blocking solution contained either 5% (w/v) BSA or 5% (w/v) non-fat dry milk (NFDM) in a Tris-Buffered Saline with Tween (TBS-T, made of

20 mM Tris (pH 7.6), 137 mM NaCl, 0.1% (v/v) Tween 20 (VWR™ International), for 1 h at room temperature, with soft agitation, according to the antibody specifications.

After blocking, the membranes were probed overnight at 4 ºC with the primary antibodies according to the conditions indicated in Table 2.2.

Table 2. 2 - Primary antibodies used in western blotting and respective conditions.

Antibody	MW (kDa)	Dilution and Incubation Solution	Company
Phospho-p44/42 (ERK1/2) (Thr202/Tyr204)	42, 44	1:2000 in 5% BSA	Cell Signalling Tecnhology
p44/42 (ERK1/2)		1:1000 in 1% NFDM	
Phospho-P38 MAPK (Thr180/Tyr182)	43	1:1000 in 5% BSA	
p38 MAPK		1:1000 in 1% NFDM	
Phospho-SAPK/JNK (Thr183/Tyr185)	46, 54	1:1000 in 5% BSA	
Anti-JNK/SAPK1		1:1000 in 1% NFDM	Upstate®
Anti-NF-kB p65 (phospho S276)	65	1:1000 in 5% BSA	Abcam
NF-kB p65		1:1000 in 1% NFDM	
β-actin	45	1:1000 in 1% NFDM	Cell Signalling Tecnhology

Note – MW: Molecular Weight; BSA: Bovine Serum Albumin; NFDM: Non-Fat Dry Milk.

After incubation, membranes were washed in TBS-T three times for 10 min per wash and then incubated with the respective secondary antibody for 1 h at room temperature. Secondary antibodies [Immuno-Star™ Goat Anti-Rabbit HRP Conjugate (BioRad) or Immuno-Star™ Goat Anti-Mouse HRP Conjugate (Biorad)] were diluted in the respective blocking solution at 1:10 000. Membranes were then washed in the same way and incubated with an Enhanced Chemiluminescence (ECL) reagent (Clarity Western ECL Substrate, BioRad) and revealed using the ImageQuant LAS500 apparatus.

After the revelation, membranes were washed twice in TBS-T for 15 min, followed by a wash in Molecular Biology Grade-Water for 5 min and then stripped in 0.02 M sodium hydroxide (NaOH, Merck). After repeating the washing step in Molecular Biology Grade-Water, membranes were blocked. Lastly, quantification of band intensity was done using the Fiji software [133].

2.9. Evaluation of the integrity of the ECs monolayer

MCs are a key component of the neurovascular unit. However, once stimulated, they can unwittingly compromise endothelial cell cohesion, thus affecting the integrity of the BBB. To evaluate whether microglia stimulated with the BCC secretome induce alterations in the endothelial cells (ECs) barrier properties, we measured the permeability and the Transendothelial electrical resistance (TEER) of ECs after exposure to MC-derived secretome previously stimulated with the CMs of BCCs.

For that, MCs were plated at a density of 20 000 cells.cm^{-2} and allowed to adhere overnight, and then stimulated with CCM from the triple-negative 231 (parental and brain tropic) and from the HER2^{+} brain tropic JIM-1 cells. The medium was collected after a 24 h-stimulus for subsequent studies with ECs.

2.9.1. Endothelial transwell permeability assay

hCMEC/D3 cells were plated at a density of 17 000 cells.cm^{-2} in 12-well plate transwell inserts (12 mm diameter and 0.4 µm pore size, Corning) coated with 150 µg/mL of collagen type I (R&D Systems, Inc.). Cells were maintained for 7 days for endothelial monolayer formation. After that, the culture medium was replaced by the CMs derived from MCs for 24 h. ECs exposed to the fresh DMEM culture medium were used as a control.

Then, 1 mg/mL of the 4 kDa fluorescein isothiocyanate-dextran (FITC-Dextran 4, Sigma) probe was added to the apical side of each transwell insert. Samples (50 µL) were collected from the lower compartment and replaced by culture medium at 20 min intervals for 180 min. Fluorescence was measured on a Synergy^{TM} HT plate reader and plotted against time. Permeability values were determined from the linear slope changes without and after exposure to the CMs.

2.9.2. Transendothelial electrical resistance measurement

The TEER of the hCMEC/D3 monolayers was measured using an Epithelial Volt/Ohm (TEER) Meter (World Precision Instruments) coupled to an STX-2 electrode. The TEER readings of cell-free inserts were subtracted from the values obtained with cells. Only EC monolayers with a TEER above 50 Ω.cm^2 after subtracting the TEER of empty inserts were used in subsequent experiments. The TEER measurements were

performed before and at 24 h after incubation with the CMs. Results were expressed as a percentage (%) of the control condition.

2.10. Immunohistochemistry

To assess MCs activation after BCC secretome stimulus, the Iba1 marker was stained *ex vivo*. Summarily, swiss nu/nu mice were intra-peritoneally injected with CCM obtained from 231^{P} and 231^{BR} cells for 15 days. After mouse sacrifice and brain collection, slices of the prefrontal cortex were obtained and prepared for Iba1 staining. Herein, all steps were done at room temperature unless stated otherwise. After cryosection, the tissue was rinsed two times with PBS. Then followed a permeabilization step with 0.20% (v/v) Triton X-100 for 20 min and incubation with 3% (w/v) BSA for 1 h. After, Anti-Iba1 (Wako Chemical Pure Industries Ltd.) was diluted 1:200 in a solution composed of 10% (w/v) BSA and 90% of 0.25% (v/v) Triton X-100 and incubated overnight in a wet atmosphere at 4 ^{o}C. On the following day, the primary antibody solution was aspirated, and the coverslip was washed two times with PBS for 10 min before secondary antibody incubation. After, Hoechst 33342 (1:1000, Sigma-Aldrich) and anti-rabbit (GE Healthcare) 1:200 were diluted in a solution composed of 10% (w/v) BSA and 90% of 0.25% (v/v) Triton X-100 and incubated for 1 h in the dark. After washing two times with PBS the coverslips are assembled in Dako fluorescence medium (Dako North America Inc.).

Images were blindly captured using a Zeiss Axio Observer Z1 inverted microscope (Carl Zeiss, Thornwood, New York). For quantification, the totality of the area in each photograph was considered and, to subtract background fluorescence, three different zones without staining (black) were selected. The formula to obtain the corrected total fluorescence (CTF) can be found below [134]. Results were expressed as the mean fluorescence intensity (arbitrary units) of five brain slices obtained from one animal for each experimental group.

$$\mathrm{CTF} = (\text{integrated intensity}) - (\text{area of picture} \times \text{mean background})$$

2.11. Statistical analysis

Data are expressed as means ± standard error of the means (SEMs). The "n" stands for the total number of experiments obtained from independent cell cultures. Significance was set at the level of $P<0.05$. Graphical artwork and statistical analysis were computed using GraphPad Prism Software version 7.4. (GraphPad Software, San Diego, CA).

Chapter 3 - Results and Discussion

3.1. Microglia increase the production of NO and up-regulate the expression of inflammatory mediators following exposure to the secretome derived from BCCs

The production of NO is considered an indicator of the classical M1 activation phenotype of MCs [135]. Based on that, we measured the concentrations of nitrite (NO_2^-), which is an inert major metabolite of NO, in the cell-free supernatants collected from MCs, using the Griess assay. This assay relies on a diazotization reaction that was originally described by Griess in 1879 and measures NO indirectly as NO_2^- levels.

This experiment was performed after 6 and 24 h incubation of MCs with the CMs of two BC cell lines representative of the triple-negative (231) and $HER2^+$ (JIM) BC subtypes, including both parental (CM 231^P and CM JIM^P) and corresponding brain tropic derivates (CM 231^{BR} and CM JIM^{BR}). The CMs derived from BC cells were collected after being cultured for 48 h. Fresh DMEM culture medium was used as a control to assess the basal NO production by MCs.

As depicted in Figure 3.1 and Table 3.1, exposure to the CMs of BCCs induced a significant increase in the production of NO_2^- by MCs as compared to the control condition. This effect was observed with the CMs of all BC cell lines and increased progressively with the exposure time, being more pronounced with the CM of the brain-tropic variant of TNBC cells (CM 231^{BR}). Indeed, when compared to untreated controls CM 231^{BR} caused a 14- and a 23-fold increase in NO_2^- production at 6, and 24 h, respectively.

Regarding the $HER2^+$ subtype, although significant, the increase in the NO_2^- levels were not so pronounced as compared with those induced by the triple-negative subtype. Moreover, the NO_2^- levels were quite similar between the parental and its brain tropic variant, both at 6 h and 24 h post-incubation, contrary to what was seen with the TNBC cell line variants.

Microglia exposed to LPS (100 ng/mL) for 6 or 24 h induced a smaller increase in the production of NO_2^- when compared to control (data not shown), suggesting that LPS *per se* is not enough to stimulate the production of NO in this human microglial cell line. Evidence reviewed elsewhere has pointed that the passage number is something to equate when using this particular cell line [125,131], but also that one particular feature of HMC3 cells is their weak expression of TLR4 [136], the key receptor involved in LPS recognition. We believe this could explain the unresponsiveness to the LPS stimulus.

Nonetheless, the HMC3 has been extensively employed in many studies concerning both cancer research and neurosciences, as it is deemed a fit MC model.

These findings show that the TNBC subtype, specifically, the brain tropic variant, secretes important soluble and/or vesicular factors that promote the activation of MCs through NO generation.

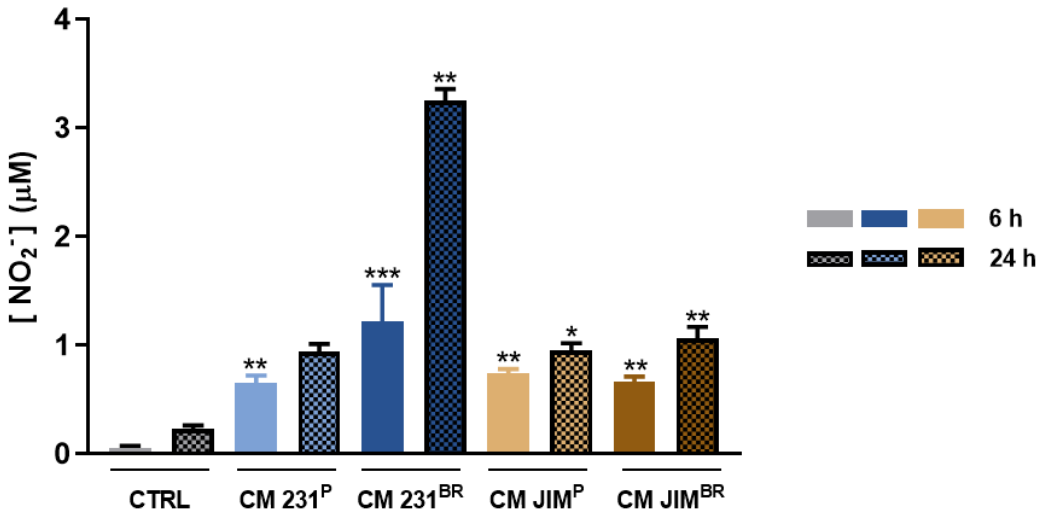

Figure 3. 1 - Comparison of nitrite production and accumulation by MCs after exposure to different BCC secretomes for 6 and 24 h.

MCs were treated with BC-derived secretomes for 6 and 24 h. Nitrite concentrations were calculated by interpolation of the absorbance of each sample in a standard curve of sodium nitrite. Data are expressed as means ± SEMs (n = 3-4), *P<0.05, **P<0.01, and ***P<0.001 when compared to the respective control (either 6 or 24 h) using the Kruskal-Wallis test followed by Dunn's multiple comparations test.

Table 3. 1 - Nitrite production (µM) by MCs after exposure to different BCC secretomes for 6 and 24 h.

	CTRL	CM 231^{P}	CM 231^{BR}	CM JIM^{P}	CM JIM^{BR}
6 h	0.05 ± 0.02	0.66 ± 0.07**	1.22 ± 0.34***	0.74 ± 0.04**	0.66 ± 0.05**
24 h	0.23 ± 0.03	0.94 ± 0.07	3.25 ± 0.09**	0.95 ± 0.07*	1.06 ± 0.10**

Data are expressed as means ± SEMs (n = 3-4), *P<0.05, **P<0.01, and ***P<0.001 when compared to the respective control (either 6 or 24 h) using the Kruskal-Wallis test followed by Dunn's multiple comparations test.

Another hallmark of reactive microglia is the release of pro-and anti-inflammatory mediators as part of its defensive role. Herein, we analyzed the expression of some cytokines and of *VEGFA* by RT-qPCR in MCs after being exposed to the CMs collected

from the different BCCs variants for 24 h. The relative changes in gene expression were evaluated by the $2^{-\Delta\Delta Ct}$ method. Overall, there was a trend towards up-regulation of pro-inflammatory mediators in MCs exposed to CMs of BCs, as depicted in Figure 3.2.

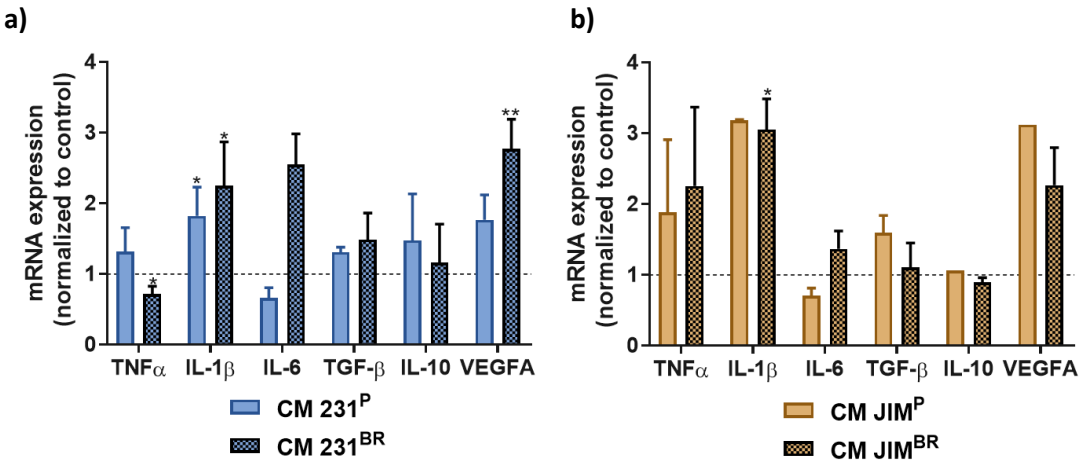

Figure 3. 2 - Gene expression of inflammatory mediators in MCs exposed to the secretome derived from the **a)** parental (CM 231^{P}) and brain-tropic (CM 231^{BR}) triple-negative cell line and **b)** parental (CM JIM^{P}) and brain-tropic (CM JIM^{BR}) $HER2^{+}$ BC cells.

HMC3 cells were incubated for 24 h with the CMs derived from the BCCs. Gene expression levels ($2^{-\Delta\Delta Ct}$) of inflammatory mediators were evaluated by RT-qPCR and normalized to the untreated control. Data are expressed as means ± SEMs (n= 3-4 for **a)** and n=1-3 for **b)**), *P<0.05, and **P<0.01 when compared to the untreated control using the Kruskal-Wallis test followed by Dunn's multiple comparations test.

In the case of MCs treated with the CM of TNBC cells, the most pronounced increases were observed in the expression of *IL-1β*, *IL-6*, and *VEGFA*. Also, an incremental tendency was observed with the CM of its brain tropic variant. Regarding the $HER2^{+}$ subtype, the most pronounced induced increases were in *TNF-α*, *IL-1β*, and *VEGFA* expression, both for the parental and for brain tropic variants. None of the CMs induced increases in the anti-inflammatory cytokines *IL-10* or transforming growth factor-β (*TGF-β*) in MCs, which are more associated with an M2-like phenotype.

Once again, no major differences were observed between the parental and brain tropic variant of the $HER2^{+}$ subtype, regarding the induced expression pattern of inflammatory mediators.

In sum, this first set of results suggests that MCs acquired an M1-like activation phenotype when exposed to the BCC secretomes, devoided from tumor cells. These findings demonstrate the reactivity of microglia in response to the biomolecules produced

and released by breast tumor cells, suggesting its involvement in the preparation of the PMN before the arrival of tumor cells to the brain parenchyma.

In brain tumors, e.g. glioblastoma, microglia acquire a tumor-promoting M2 phenotype. A study by Yong et al. showed that M2 microglia can be rescued in the presence of iNOS positive regulation, reflecting a phenotype similar to the one presented by MCs derived from non-glioma patients. This resulted in a higher production of cytotoxic NO that was correlated with the reduction of tumor size [137] but under biological settings, it could also imply off-target death. NO is a weapon of nonspecific immune defense that can have deleterious effects on neurons [138]. The NO levels observed in our study could be preceding the initiation of the self-propelling M1-associated phenomenon known as reactive microgliosis [139] since the brain would start to be populated by cellular debris that support M1 activation. This could be at the base of early neuroinflammation aimed at reshaping the natural immunosuppressive landscape of the brain.

The results from the restricted panel of inflammatory mediators evaluated directed us towards the presentation of an anti-tumor M1 microglial phenotype under the effect of the secretome of both TN and $HER2^+$ cells. However, further studies including a broader panel would be required to confirm this hypothesis.

Looking at the panel in question, we can see that *TNFα* gene expression in MCs appears to differ according to the BC subtype from which the secretome was collected. Faden and colleagues had previously associated both TNFα and NO production to the self-propagating cycle responsible for prolonged microglial activation and neuroinflammation [140]. It is interesting to see that, at least for the $HER2^+$ subtypes, both NO production and TNFα expression suggest a possible early stage of reactive microgliosis.

Unlike *TNFα*, the cytokine *IL-1β* displays the same gene expression pattern regardless of the BC subtype, with systematically up-regulated expression. This is noteworthy since this inflammatory cytokine is paramount for the onset of neuroinflammation. In fact, *IL-1β* induces the expression of *TNFα*, and *VEGFA* [141] but could also be at the root of excessive oxidative stress and neuronal damage when its expression is severely dysregulated [142]. It is also worth noting that while NO production, *TNFα* and *IL-1β* expression are all well-established M1 markers, their expression does not have to be controlled synchronously [87,140].

IL-6 also displays the same behavior in both BC subtypes. Nevertheless, its up-regulation is more pronounced for MCs conditioned with the secretome of brain-tropic triple-negative cells. This marked *IL-6* up-regulation could be beneficial since it stimulates host defense, mainly through the stimulation of acute-phase responses, immune reactions, and hematopoiesis [67]. Nonetheless, this prototypic cytokine displays pleiotropic roles on many immune and nonimmune cells that can have antagonizing effects. In fact, it can also suppress tumor immune surveillance. Interestingly, in the presence of glioblastoma-derived factors, M2 MCs also up-regulate the expression of this cytokine leading to endothelial cell dysfunction [77]. Since the secretome of the brain-tropic TNBC cell line induces the most notorious up-regulation of *IL-1β*, *IL-6*, and NO production, it is reasonable to assume this is the cell line variant wherein MCs activation is most prominent.

It appears that an inflammatory microenvironment is being favored over the immunosuppressive observed in gliomas, where both *TGF-β* and *IL-10* are up-regulated in tumor-infiltrated MCs [81]. This mechanism is said to promote angiogenesis, matrix deposition, and exogenous immune paralysis, thus creating a stable environment hospitable for tumor growth [143]. However, we cannot dismiss the possibility that after continuous exposure to the secretome of BCCs, microglia change their phenotype to provide a more permissive milieu for metastatic colonization.

VEGFA is a principle angiogenic growth factor that contributes to the outgrowth of BrM [16] and is associated with disruption of endothelial integrity, inducing BBB dysfunction. We have observed that *VEGFA* was consistently up-regulated across all treatments. Notably, *VEGFA* expression is significantly up-regulated in MCs in the presence of the secretome derived from the brain-tropic TNBC variant similar to what occurs in the secretome of this cell line [144]. Eliciting microglial *VEGFA* expression could potentiate VEGFA levels in the brain and could help explain the significantly shorter mean survival of mice that were injected with the brain-tropic cell line compared to the parental cell line [144]. VEGFA was also deemed to be an important pro-permeability factor in studies conducted with endothelial hCMEC/D3 cells and glioma shed vesicles [145], thus pointing to a possible conserved role in glioma, BrM, and in the weakening of the BBB during PMN formation.

In sum, both the $HER2^+$ BCCs-derived secretomes were able to activate MCs to an M1-like phenotype, although the brain-tropic TN subtype was the one that elicited the

most pronounced effects. NO production and expression of inflammatory mediators do not show marked differences between the two $HER2^+$ cell line variants. In the future, protein expression could be evaluated to further confirm gene expression results.

3.2. The secretome of BC brain-tropic cells promotes the generation of iROS by MCs

The production of ROS is another indicator of the classical M1 activation phenotype of MCs. Therefore, we analyzed the production of ROS by HMC3 cells upon 24 h incubation with the different BCC secretomes. Treatment with 100 ng/mL LPS and 100 µM H_2O_2 were used as positive controls. The results were normalized to the untreated DMEM control and can be seen in Figure 3.3.

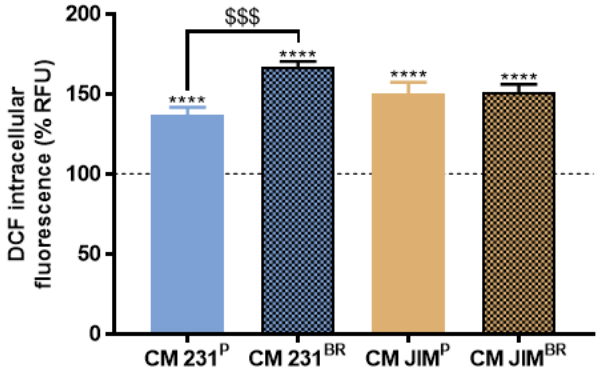

Figure 3. 3 – BCC secretomes increase intracellular ROS production by MCs.

HMC3 cells were exposed to the CMs derived from the BCCs for 24 h. Afterward, cells were incubated for 2 h in Krebs solution containing 5 µM of the cell-permeant H_2DCFDA probe. The DCF intensity is directly proportional to the amount of intracellular ROS generated. Each condition was assayed in triplicate. The values obtained were measured at ex/em 485/528 nm, normalized to the untreated control, and are presented as percentages of the control. Results are expressed as means ± SEMs (n>5). α = 0.05 ****P<0.0001 as compared to untreated control cells. $^{\$\$\$}$P<0.001 as compared to MCs exposed to CM 231^P using the non-parametric Kruskal-Wallis test followed by Dunn's multiple comparisons test.

As depicted in Figure 3.3, exposure of MCs to the four CMs derived from the BCCs induced significant increases in the production of iROS as compared to the untreated control condition (P<0.0001). Once again, even though this effect was detected with the CMs of all BC cell lines, the most marked increase was observed with the CM 231^{BR}. In fact, the increase in iROS production induced by CM 231^{BR} is demarked from its parental counter-part CM 231^P (167 % ± 3.38 % vs. 136.8 % ± 5.04 %, P<0.001, respectively). As to the $HER2^+$ subtype, the increases seen in iROS in MCs after exposure

to CM JIM^{P} and CM JIM^{BR} were very similar (150.5 % ± 6.96 % and 151.5 % ± 4.59 %, respectively) and less pronounced than the one induced by CM 231^{BR}.

Once again, 100 ng/mL LPS alone had no effect on MCs regarding ROS production, since there was no increase in DCF fluorescence (106.9 % ± 9.54 %, data not shown). Incubation with 100 µM H_2O_2 stimulates ROS generation as indicated by the substantial increase in fluorescence compared to control (475.6 % ± 26.82 %, data not shown).

After DCF fluorescence readings, MCs were incubated with resazurin for 4 h to access cell viability in response to the stimuli with secretomes derived from the BCCs. The reduction of resazurin yields resorufin and is proportional to the fraction of live cells. No significant differences were observed in cell viability between the untreated control and treated cells with the secretomes, further demonstrating that MCs were not compromised by the experimental conditions. As such, the differences in ROS production are not a consequence of impaired cell viability.

Being the mitochondria and NOX enzymes the main sources of cellular ROS, we analyzed the expression levels of the mitochondrial ROS regulator *UCP2* and of the *NOX2* and *NOX4* isoforms, as well as the expression of the master regulator of redox homeostasis *NRF2* by RT-qPCR. Results were normalized to the untreated controls and can be found in Figure 3.4.

Surprisingly, no detectable levels of *NOX2* were found in MCs under control or secretome-treated conditions. The mean Ct values were consistently above 35 for two different primer sequences. The *NOX4* mRNA showed a reduction in secretome-treated microglia, achieving significance with CM 231^{BR} and CM JIM^{P} (0.72 ± 0.05, and 0.59 ± 0.07, respectively) as compared to the untreated control.

The mRNA levels of *UCP2* showed a slight decrease in MCs treated with both the CM 231^{P}, and CM JIM^{P} BCCs variants (0.88 ± 0.21, and 0.82 ± 0.02, respectively), and an increasing bias with both CM 231^{BR}, and CM JIM^{BR} exposure (1.17 ± 0.28, and 1.33 ± 0.31, respectively). The levels of the transcription factor *NRF2*, activated upon overwhelming of the oxidative stress balance, remained unchanged across all treatments.

As was previously stated, one of the *ex libris* of M1-activated MCs is the generation of ROS [146], which contributes to host defense but, if exacerbated, can also lead to neuroinflammation and neurodegeneration [72]. Our results suggest that the amount of iROS produced is still within a physiological range, as the two oxidative

eustress markers, *NRF2* expression and resazurin oxidation levels are unchanged in the presence of these stimuli.

However, it is well known that iROS have a central role in the control of cellular functions as they act as modulators of proinflammatory processes in MCs [72,94,147]. We presume that the rise in iROS plays a physiological regulating role in MCs because no evident signs of oxidative stress were detected.

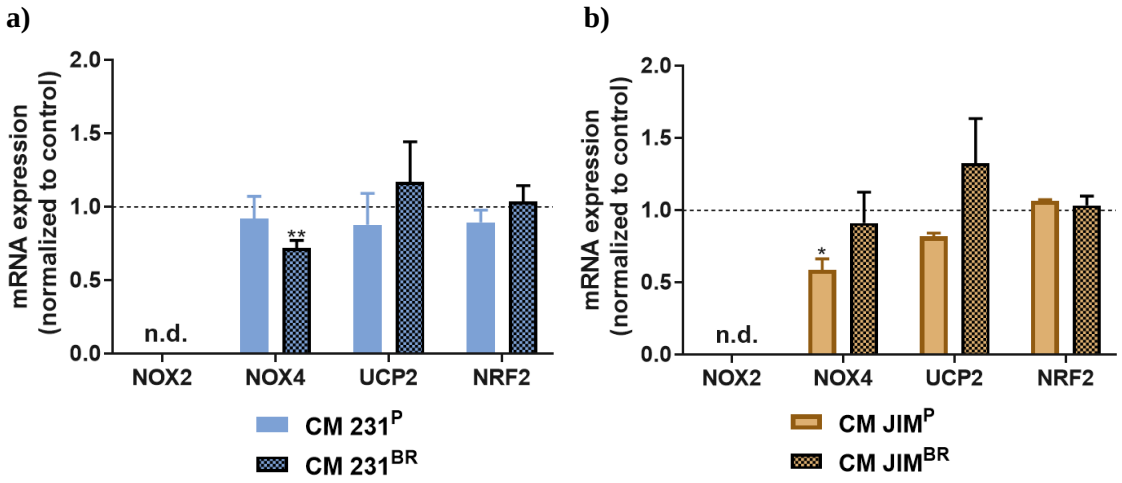

Figure 3. 4 – Relative mRNA expression of oxidative stress-related genes in MCs after exposure to the secretome of **a)** TNBC and of **b)** the HER2^{+} BC subtypes.

HMC3 cells were incubated with the BCC-derived CMs for 24 h. Gene expression levels ($2^{-\Delta\Delta Ct}$) of oxidative stress-related genes were evaluated by RT-qPCR and normalized to the untreated control. Results are expressed as means ± SEMs (n=3-4). $\alpha = 0.05$ *P<0.05, and **P<0.01 as compared to untreated control cells using the non-parametric Kruskal-Wallis test followed by Dunn's multiple comparisons test. n.d. – not detected.

Indeed, the increased up-regulation of iROS and of genes associated with an M1 phenotype is consistent with what was previously reported with the mouse microglial cell line SIM-A9 treated with CMs derived from 231^{BR} cells [148], further corroborating our findings. Also, a study by Chen et al. examining the effect of glioblastoma-secreted factors on mouse MCs also shows similarity to our findings. They exposed BV2 mouse microglial to the CM of three different glioma cell lines and found a significant increase in peroxide production without compromising cellular viability.

Interestingly, they have also linked peroxide production to both NO production and activation of ERK and JNK signaling, since both NO production and MAPK phosphorylation were decreased in the presence of two different antioxidants [147]. This favors our hypothesis that BCCs induce changes in MCs through the modulation of inflammatory pathways by iROS such as H_2O_2.

In fact, both our study and the one performed by Chen et al. employed the H_2DCFDA probe for measuring intracellular levels of ROS, which is oxidized mainly by H_2O_2, being recognized by some as a specific H_2O_2 sensor [149]. Reasons for favoring H_2O_2 as a pivotal ROS include the fact that this is the most stable ROS [100], the end product of SODs, and it has good membrane permeability, reinforcing its cytotoxic functions [101].

The work by Chen et al. also shows that MCs contributions through both the up-regulation of RNS, ROS, and MAPKs activation were associated with an enhanced migration capacity of glioma cells. This supports the notion that both distant and near tumors secrete factors with the capability of modulating MCs behavior into a pro-tumoral phenotype in a seemingly similar manner. The aggravation of ROS and inflammatory mediators production in microglia exposed to the secretome from brain-tropic TNBC cells when compared with the secretome from parental cells could thus be attributed to a better fitting of these cells to the glioblastoma characteristics, as the brain-tropic variant is obtained after several rounds of brain-colonization and as inherent genomic changes when compared to the parental cell line [150].

As for the source of the ROS, results are not as straightforward to interpret. We thought that the up-regulation of ROS observed with the oxidation of the H_2DCFDA probe would be attributed to the NOX family, known inducers of ROS in microglia following activation of PRRs by DAMPs signaling [86]. Yet, RT-qPCR results show that *NOX2* is not present in HMC3 cells and *NOX4* expression is down-regulated following treatment with the secretomes derived from the BCCs. We have used two different primer sequences to try to analyze the expression levels of *NOX2* in MCs without success (Cq>35). Nevertheless, similar reports with the HMC3 cell line are present in the literature [125]. In fact, since NOX2 is deemed the most highly expressed NOX in both human and murine microglia the validity of this cell line as a model for MCs has been further questioned [86]. As a consequence of NOX2 absence, NOX4 has been identified as the key regulator of ROS production in HMC3 cells [125]. However, since *NOX4* expression is also down-regulated, the increase in iROS observed cannot be attributed to either one of these enzymes.

To determine if the production of iROS was of mitochondrial origin, we measured the levels of the *UCP2* gene. In the presence of brain-tropic CMs, *UCP2* levels were slightly up-regulated, indicating that, at least in part, some of the ROS produced could

have been of mitochondrial origin, and *UCP2* could have been up-regulated to further stop their synthesis. In fact, overexpression of *UCP2* in RAW264 cells has led to the reduction of mROS [104] as UCP2 induces proton leak that decreases ROS emission from the mitochondria [101]. However, the down-regulation observed with both the parental counterparts undoubtedly implies that there could be mitochondrial involvement in ROS production in MCs stimulated with both secretomes, as *UCP2* down-regulation acts as a brake that is switched to allow mROS production [105]. These seemingly contradictory mechanisms work because *UCP2* regulation is thought to occur as a negative feedback loop [101]. The mechanism can be seen in Figure 1.5. Interestingly, *UCP2* down-regulation is mediated via JNK and p38 pathways activation, and both ERK and p38 kinases are activated by mROS [105,151]. As a result, UCP2 regulates and is regulated by MAPK regulation and the reason we detected an up-regulation with CM 231^{BR} and CM JIM^{BR} and down-regulation with CM 231^{P} and CM JIM^{P} could just be a result of the time frame upon which we perform the RNA extraction and of the level of ROS present. Notwithstanding, the increase in iROS observed in MCs conditioned by both brain-tropic derived-secretomes could still have unknown origins that at the time of this work we could not fully explain.

Since the results obtained so far revealed no significant differences between the parental and brain tropic variant of the $HER2^{+}$ JIM BC cell line, in the subsequent studies, we only used the brain tropic variant of this cell line.

3.3. Microglia activated by the BCCs secretomes display concomitant SAPKs and NF-κB activation

Our panel of pro-inflammatory mediators, as well as the increase in iROS generation, prompted us to analyze the activation status of SAPKs and NF-κB signaling pathways in MCs primed with BCCs secretomes. In fact, *UCP2* expression levels were also directing us in this way. As such, we analyzed the protein expression of the total and phosphorylated forms of p38 and JNK, as well as of the nuclear transcription factor NF-κB, at 6 and 24 h after stimuli by Western Blot. Fresh DMEM culture medium was used as a control to assess the basal expression of these proteins in MCs. The results obtained can be seen in Figure 3.5.

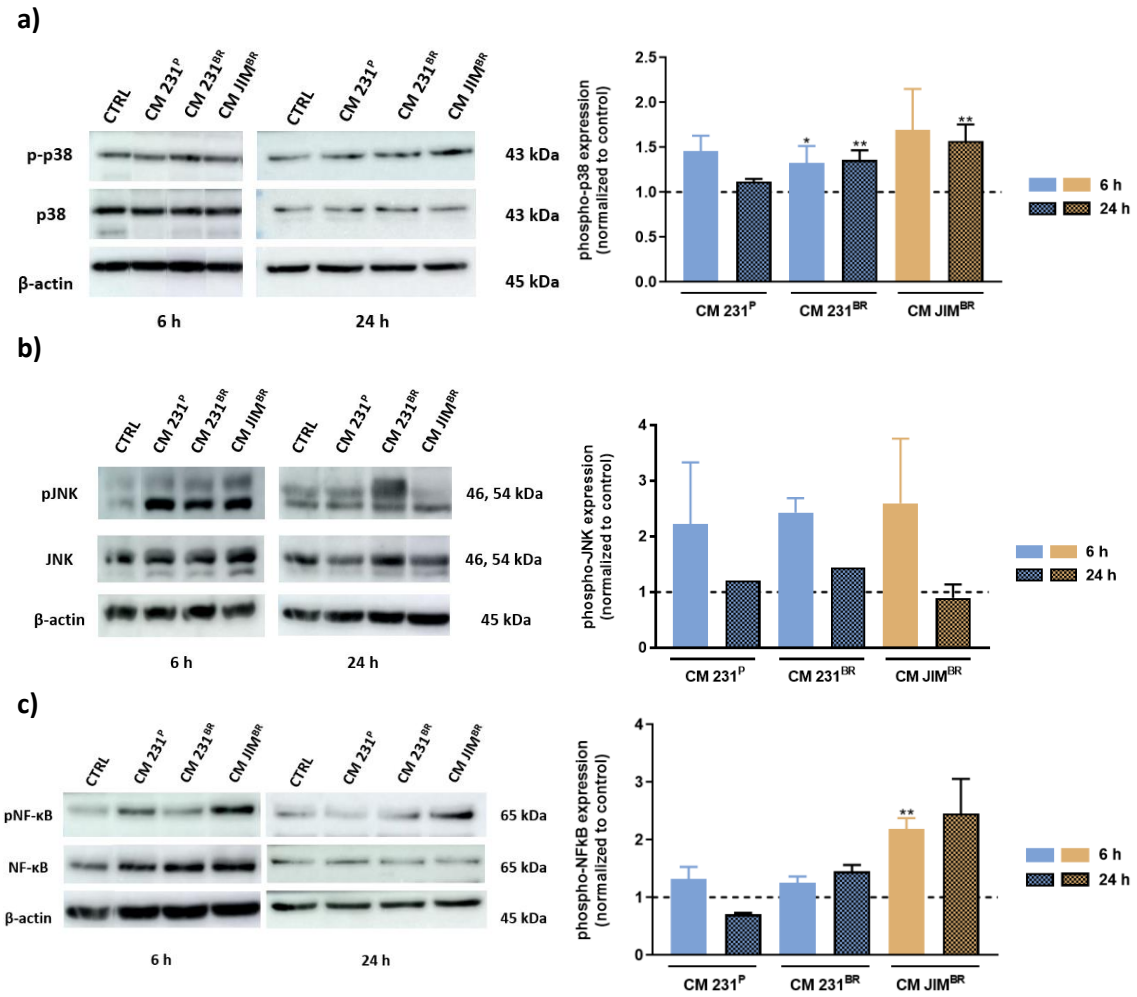

Figure 3. 5 – Protein expression of phosphorylated and total forms of **a)** p38, **b)** JNK and **c)** NF-κB by Western blot analysis in MCs treated with the secretome of BCCs.

Quantitative analysis of p-p38, pJNK, and pNF-κB expression after 6 and 24-h incubation with the parental and brain-tropic secretomes of the TNBC cell line (CM 231^{P} and CM 231^{BR}), and with the brain-tropic secretome of the HER2^{+} BC cell line (CM JIM^{BR}). Representative WB images of the analyzed proteins are shown on the left. All values were normalized to the expression of the total form of the protein and then normalized to their respective untreated control. Results are expressed as means ± SEMs (n=3 for p-p38 and pNF-κB expression at 6 and 24 h, and n=2 and 1 pJNK expression at 6 and 24 h, respectively). α = 0.05 *P<0.05, and **P<0.01 as compared to untreated control cells using the non-parametric Kruskal-Wallis test followed by Dunn's multiple comparisons test.

There is a trend towards the up-regulation of the phosphorylated forms of the SAPKs and NF-κB proteins in MCs exposed to the secretome of both triple-negative and HER2^{+} cells compared to untreated cells. Nonetheless, MCs activated by the secretome of the brain-tropic HER2^{+} cells appear to display the most pronounced p38 and NF-κB pathway activation.

Figure 3.5 a) reveals that MCs exposed to CM 231^{P} appear to decrease p38 activation over time (1.46 ± 0.17 and 1.12 ± 0.03, respectively) whereas MCs exposed to the brain-tropic secretome display a rather constant reliance on p38 signaling from 6 to 24 h (1.32 ± 0.19 and 1.36 ± 0.11, respectively). The microglia that were conditioned by the secretome of the brain-tropic $HER2^{+}$ cell line (JIM^{BR}) also seem to display stabilized p38 signaling at both time points (1.69 ± 0.48 vs. 1.57 ± 0.18 at 6 and 24 h, respectively).

It appears that the different stimuli induce a ubiquitous activation of JNK at 6 h, decreasing the phosphorylation of this SAPK to basal levels at 24 h. No differences were observed between the effects mediated by the different BCC secretomes.

Activation of the NF-κB transcription factor is more pronounced in MCs-activated by the secretome of the brain-tropic $HER2^{+}$ cell line than in MCs-activated by the secretome of both TNBC cell line variants. Except for MCs exposed for 24 h to the CMs derived from the parental TNBC cells, it appears that NF-κB signaling is stably up-regulated by the secretomes of TNBC cells. Also, both brain tropic-cell lines appear to elicit an increment on the activation of this transcription factor from 6 to 24 h conditioning (1.26 ± 0.10 vs. 1.45 ± 0.11 for CM 231^{BR}, respectively and 2.18 ± 0.19 vs. ± 2.46 ± 0.60 for CM JIM^{BR}, respectively).

Overall, we observe a trend in the activation of the p38 and NF-κB inflammatory pathways in MCs that were activated by the BCCs secretomes. This activation mostly supports our results from the NO and expression of inflammatory mediators, as increased phosphorylation of the p38 and NF-κB is linked to the classical activation phenotype of MCs. Nonetheless, protein expression results do not show a pronounced activation trend of inflammatory pathways in MCs exposed to the secretome derived from brain-tropic TNBC cells when compared to other stimuli.

Even though based on preliminary studies, we have observed a tendential decrease in the activation of the JNK pathway with time. These results could corroborate our hypothesis that the different BCCs secretomes do not elicit oxidative distress in MCs, as the initial up-regulation observed at 6 h for all treatments is resumed to basal levels at 24 h. In fact, prolonged JNK overexpression is associated with cell death [152–154].

We had previously hypothesized that the up-regulation of iROS observed, particularly H_2O_2, could be at the base of the M1-like activation phenotype observed due to SAPKs and NF-κB activation. Even though the trend in iROS production does not follow a similar pattern to the activation of pro-inflammatory signaling, we observe an

increased activation of both SAPKs and NF-κB activity that, based on previous studies, cannot be dissociated from this phenomenon and further corroborates the M1-like activation phenotype proposed [72]. Nonetheless, future studies employing ROS scavengers, such as catalase, and the evaluation of the phosphorylation levels of NF-κB at serine 529 [94], could undoubtedly mark an axis between the BCC's secreted factors and an H_2O_2-dependent M1-like inflammatory phenotype. Simultaneously, evaluation of the activation of M2 transcription factors, such as STAT3 and STAT6, and different M1 transcription factors, such as STAT1, CREB, or ATF-2, could further validate the M1-like phenotype acquired by MCs stimulated by the different BCCs-derived secretomes.

A study by Wang et al. conducted with mice bearing xenografted human BCs has shown that cancer-secreted vesicles induce a pro-inflammatory phenotype in distant macrophages present at the axillary lymph nodes. The uptake of those vesicles led to the activation of the TLR2 which resulted in NF-κB translocation, and secretion of pro-inflammatory cytokines such as TNFα and IL-6, but also granulocyte colony-stimulating factor (GCSF), and CCL2 [74]. Results from this study present some parallels with our own results and can imply that similarly to what is seen in macrophages from the axillary lymph node, MCs at the brain can also be activated in the absence of tumors cells. As a consequence, the inflammation elicited could be at the root of the profound remodeling required for PMN formation.

3.4. BCCs secretome stimulate MCs proliferation and reduce their motility

We also analyzed whether inflammatory processes and microglia activation induced by the BCCs secretomes stimulated the proliferation of microglia.

For this, MCs were treated with the CCMs from the different BCCs for a total of 72 h, and proliferation was evaluated at 24 h intervals by using the WST-1 reagent. Cleavage of the WST-1 salt can be used as a proliferation indicator as the end product formazan is proportional to the number of healthy cells. Similar to the other experiments, fresh DMEM culture medium was used as a control to assess the basal proliferation of MCs. The results obtained are present in Figure 3.6 and Table 3.2 accompanied by the expression levels of both pERK and ERK proteins after 24 h stimuli. Aside from being directly involved in the pro-inflammatory response, pERK overexpression is also linked to proliferation [155].

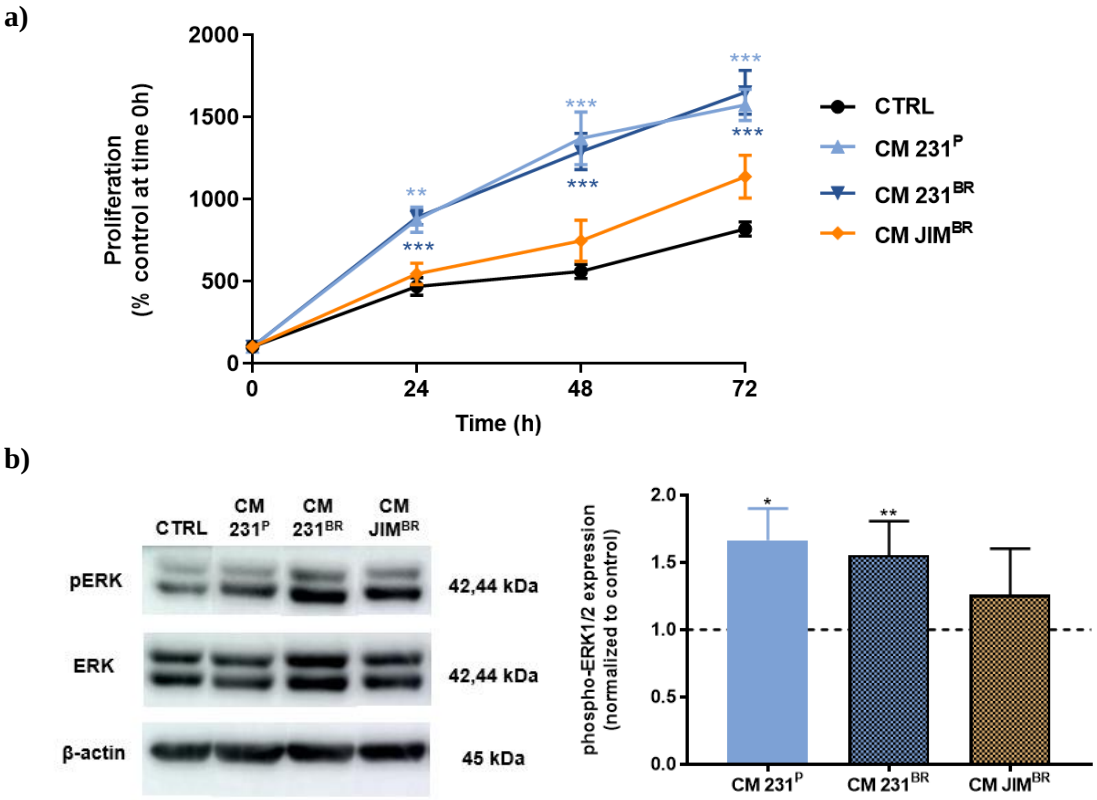

Figure 3. 6 - Effects of TNBC and HER2$^+$ secretomes in the proliferation rate of MCs. **a)** MCs proliferation after 24, 48, and 72 h conditioning with CCMs from parental and brain-tropic TNBC and brain-tropic HER2$^+$ cells and **b)** representative Western Blot images of pERK, ERK, and β-actin expression after 24-h incubation with CMs and respective pERK quantification.

a) Cell proliferation was evaluated using the WST-1 assay. Each condition was assayed in triplicate. Values were normalized to untreated control cells measured at 0 h. Data are expressed as means with ± SEMs, n=3-4. **P<0.005, and ***P<0.001 when compared to the untreated control using a one-way ANOVA test followed by the non-parametric Kruskal-Wallis test. **b)** Representative Western Blot images of pERK, ERK, and β-actin expression after 24-h incubation with CMs. All values were normalized to total ERK. Results are shown as means ± SEMs, n=3. *P<0.05, and **P<0.01 when compared to the untreated control using a one-way ANOVA test followed by the non-parametric Kruskal-Wallis test.

Table 3. 2 - MCs proliferation (%) in the presence of TNBC and HER2$^+$ secretomes.

	CTRL	CM 231^P	CM 231^{BR}	CM JIM^{BR}
0 h	100 ± 3.97	100 ± 3.97	100 ± 3.97	100 ± 3.97
24 h	469.9 ± 54.32	875.4 ± 76.29**	889.1 ± 43.61***	545.8 ± 64.84
48 h	561.3 ± 43.98	1370 ± 161.10***	1292 ± 110.40***	747.1 ± 124.7
72 h	819.4 ± 42.90	1574 ± 94.50***	1651 ± 133.10***	1138 ± 130.6

Results are shown as means ± SEMs, n=3. **P<0.005, and ***P<0.001 when compared to the untreated control using a one-way ANOVA test followed by the non-parametric Kruskal-Wallis test.

As shown in Figure 3.6 and Table 3.2, MCs proliferation was enhanced in the presence of the three BCCs-derived secretomes. The most pronounced effects observed

are seen just 24 h of conditioning with the CM 231^{BR} when the number of MCs nearly doubles with respect to the untreated control. This tendency is maintained with both CM 231^{P} and CM 231^{BR} in subsequent times. The secretome of JIM^{BR} cells also stimulates the proliferation of MCs, but to a lesser extent.

The expression of pERK is up-regulated in all the tested experimental conditions. Both CM 231^{P} and CM 231^{BR} induced a similar and significant increase in the phosphorylated form of this kinase when compared to its basal expression (1.67 ± 0.26 and 1.55 ± 0.25, respectively). The expression of pERK is modestly enhanced (1.26 ± 0.34) in response to CM JIM^{BR}, which is consistent with the results obtained with the WST-1 proliferation assay.

It is well known that the secretome of cancer cells contains many factors capable of activating cellular pathways involved in cell cycle control [156]. Although it had been previously seen that glioblastoma-derived factors were able to potentiate microglial proliferation and ERK phosphorylation [147,157] information regarding MCs proliferation under the influence of secreted factors by metastatic brain cancer cells is scarce. Nonetheless, we report that MCs proliferation is significantly up-regulated in the presence of TNBC-secreted factors and only mildly increased in the presence of $HER2^{+}$-secreted factors. Possible explanations could be the differential content of the secreted factors by the two BC subtypes, regarding immune-stimulatory cytokines, such as granulocyte-macrophage colony-stimulating factor (GM-CSF) or colony-stimulating factor (CSF)-1 [147]. In fact, a comparative study between the MDA-MB-231 and the SKBR-3 cell line ($HER2^{+}$) revealed that the TNBC cell line secreted more CSF-1 than the other cell lines present in the study [158]. Even though both TN and $HER2^{+}$ BC subtypes are highly aggressive, they have distinct molecular signatures that could explain the different effects were observed in MCs.

The role of iROS in the activation of MAPKs, such as ERK, is well recognized [140,147]. In fact, H_2O_2 has already been linked to MCs proliferation in rats [89]. However, the NOX family was identified as the source of ROS pinpointed at the time. Nonetheless, there are also reports of mROS activating this pathway [90,105–107] and our results concerning *UCP2* mRNA expression favor that hypothesis. Nonetheless, the proliferation observed could be mediated by different immunomodulatory cytokine patterns expressed in the BCC secretomes. This mechanism could be the trigger for iROS production, inducing microglial proliferation in response to the BCC secretomes.

We also evaluated whether the activation status of microglia influences their migratory ability. A scratch-wound healing assay was performed after a 24 h incubation of MCs with the secretomes derived from the BCCs. Images were collected at time 0 immediately after performing the scratch and at 8 h and 24 h. Wounding area values were normalized to the area of the first time-point for each experimental condition. Results are presented in Figure 3.7.

No differences in MC motility were observed between groups at 8 h after scratching. The differences in motile behavior were only evident at 24 h-post-scratch. At this time point, MCs treated with either CM 231^{P} or CM 231^{BR} showed a significant decrease in motility when compared to untreated control MCs. The effects mediated by CM JIM^{BR} were not significantly different from what was observed under control conditions.

The positive control, 100 ng/mL LPS, did not affect MCs motility. Previous studies have shown that LPS-treated MCs are relatively immobile, while M2-MCs display increased migration and branching [159,160]. Our *in vitro* results show that MCs do not acquire increased motility upon BCC's stimuli, and this is in line with the aforementioned M1 proposed phenotype. Interestingly, a study by Canoll et al. noted that glioma cells induce a migratory phenotype in the MCs present at the infiltrative margins of the tumor [161]. As was previously mentioned, the predominant microglial activation phenotype in gliomas is the M2, thus advocating that the differences observed in MCs motility exposed solely to the tumor cells-free BCCs secretomes can reflect the early stage in the metastatic process that we were trying to mimic.

Nonetheless, the motility of MCs stimulated by the brain-tropic TNBC secretome was found to be significantly reduced. Looking at the data in Figure 3.4, we can see a decrease in the *NOX4* mRNA expression in MCs upon exposure to the same stimulus. A work by Asmis et al. found that NOX4, due to its localization, is required for actin dynamics and hence to stress response, since it affects monocyte adhesion and migration abilities [121,162]. Thus, *NOX4* down-regulation may possibly contribute to the reduced motility observed with MCs. Future works aimed at quantifying integrin expression levels in MCs could help corroborate this hypothesis [163].

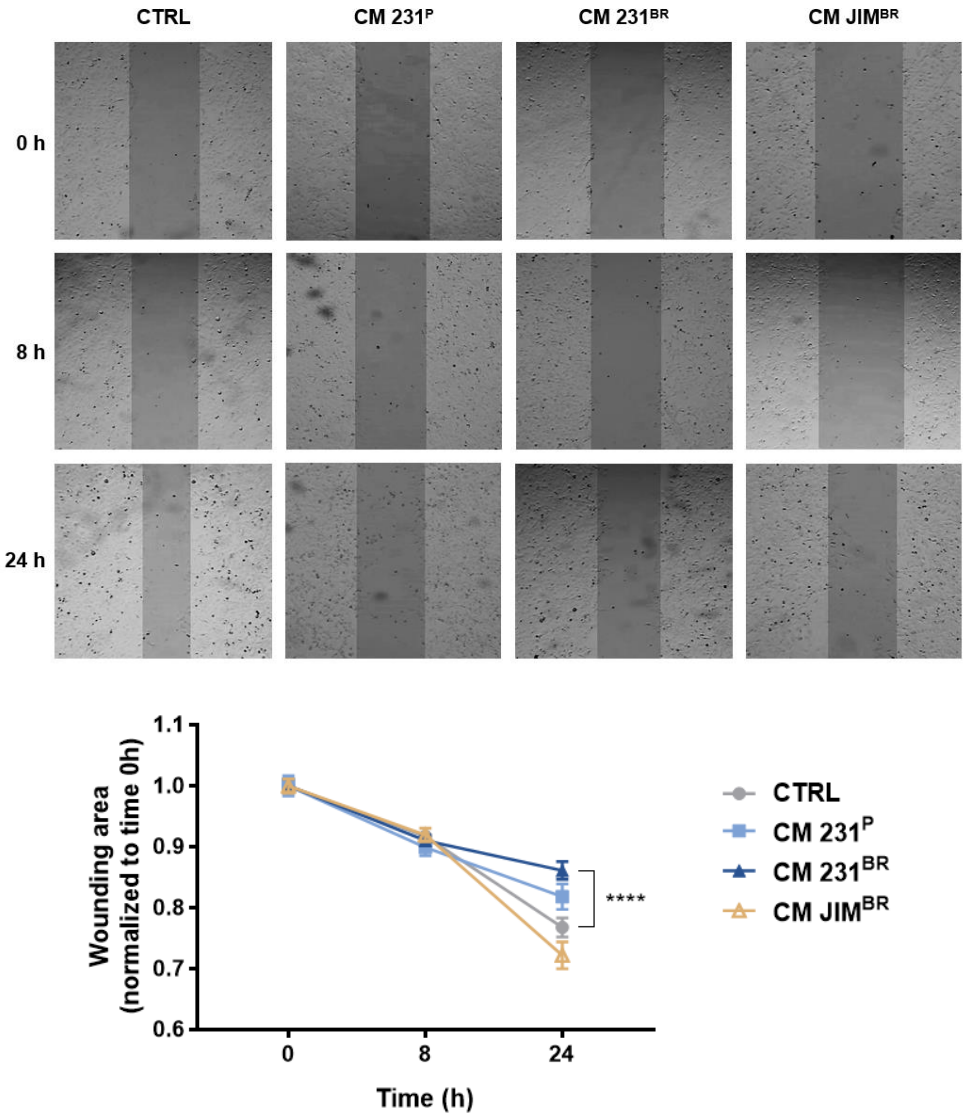

Figure 3. 7 - MCs decrease their motile capacity after exposure to the BCCs secretome as evaluated by a wound-healing assay.

MCs formed a confluent monolayer and were then treated for 24 h with CCMs from three different BC cell lines. A scratch was performed and the areas were recorded in images that were later analyzed using the Fiji software. Representative images are found in the upper part of this figure where the gray area represents the wounding area. Data are normalized to the initial wound area of each condition and are expressed as means with ± SEMs, n=3-4. ****P<0.0001 when compared to the untreated control using a one-way ANOVA test followed by Holm-Sidak's multiple comparisons test.

3.5. Zn^{2+} homeostasis influences microglia phenotype

The secretomes of both TN and $HER2^{+}$ BC subtypes activate MCs towards an M1-like phenotype. This M1 phenotype was characterized by NO and ROS production, up-regulation of pro-inflammatory mediators and concomitant activation of inflammatory

signaling pathways, stimulation of microglial proliferation, and decreased motility. The most pronounced M1 features were seen in MCs exposed to the secretome from triple-negative BCCs.

Our findings demonstrate that the iROS generated by the CMs are not detrimental to the MCs and may even act as modulators of the inflammatory signaling that underlies the M1-like phenotype. We hypothesized that Zn^{2+} is linked to the features elicited by the CMs on microglia since this metal is a critical regulator of iROS production and macrophage activity. As was previously mentioned, either deficiency or overload of the tightly-controlled Zn^{2+} metal influences redox homeostasis and signaling, leading to pro-oxidative conditions [100,109].

Extracellular Zn^{2+} has been deemed an essential trigger of iROS generation that is at the base of MCs priming towards an inflammatory phenotype [114,115,164,165]. MCs display Zn^{2+} importers at the cell membrane and Zn^{2+} uptake via the SLC39A family was characterized as the first step in zinc-triggered MCs activation [166]. However, as Zn^{2+} homeostasis can also be modulated by the activity of zinc transporters and metallothioneins, this effect does not have to be evoked solely by an increased extracellular Zn^{2+} concentration.

The concentration of Zn^{2+} is typically decreased in the serum of BC patients. [167,168]. Even though some studies report different findings [169] these could be attributed to the different stages of the disease. Nonetheless, the intracellular levels of free zinc required for the regulation of Zn^{2+} homeostasis are in the femtomolar range [170]. If MCs were deprived of Zn^{2+}, the presence of low zinc levels would activate oxidative stress sensors, such as NRF2 [100,109], which is the opposite of what we observed in MCs primed by the BCC secretomes. As a result, the Zn^{2+} concentration in the BCC secretomes, along with several other factors, may be driving a dysregulation in the Zn^{2+} metabolism of MCs, potentially rewiring these cells into a pro-inflammatory phenotype.

Considering this hypothesis, we conducted a set of experiments in which we evaluated the impact of extracellular Zn^{2+} on microglial activation. Afterward, we performed another set of experiments with CMs in the presence of diethylenetriaminepentaacetic acid (DTPA) to reduce the extracellular Zn^{2+} availability considering this might reflect in a decreased Zn^{2+} influx. DTPA is a metal complexing compound that, at physiological pH, shows a 20-fold higher selectivity for Zn^{2+} compared

with EDTA [171]. DTPA also displays an even lower affinity for Ca^{2+} and monovalent ions such as P^{+} and Na^{+} [171]. Thus, we expected that decreasing extracellular Zn^{2+} availability would rescue the phenotype of MCs to some extent.

3.5.1 Zn^{2+} contributes to ROS generation by BCC's activated-MCs

To see whether Zn^{2+} plays a modulatory role in microglial activation in the context of BCC secretome-mediated PMN formation, we first had to access if the HMC3 cell line was responsive to this metal. To accomplish this, we measured iROS production by MCs under exposure to increasing $ZnCl_2$ concentrations (5-50 μM) during a 24 h period. Results were normalized to the untreated control and are presented in Figure 3.8.

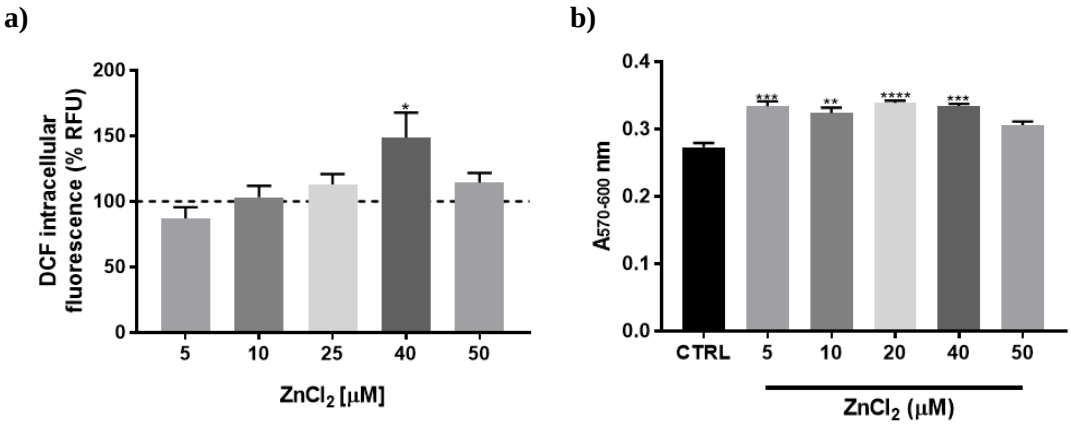

Figure 3. 8 - Effect of $ZnCl_2$ on microglial **a)** iROS production and **b)** viability.

Quantitative analysis of iROS production and viability upon incubation with different $ZnCl_2$ concentrations ranging from 5 to 50 μM. All values were normalized to the untreated control. Results are expressed as means ± SEMs (n=3). α = 0.05 *P<0.05, **P<0.01, ***P<0.001, and ****P<0.0001 as compared to untreated control cells using the non-parametric Kruskal-Wallis test followed by Dunn's multiple comparisons test.

A progressive increase in iROS production was observed, reaching a maximum with the addition of 40 μM $ZnCl_2$ to the culture medium, as shown in Figure 3.8 a). At this $ZnCl_2$ concentration, the generation of iROS increased by 50% as compared to the untreated control. Moreover, none of the tested $ZnCl_2$ concentrations were toxic to HMC3 cells. On the contrary, it was noticed a slight increase in the viability of HMC3 cells. Concentrations spanning 5 to 40 μM $ZnCl_2$ increased the metabolic activity, as indicated by the resazurin assay.

To further evaluate if the Zn^{2+} content in the secretome plays an active role in the generation of iROS, we investigated whether extracellular Zn^{2+} chelation with DTPA may prevent iROS generation during the 24-h BCCs conditioning of MCs. Different

concentrations of DTPA ranging from 5 to 50 μM were tested. In this range of concentrations, there were no cytotoxic effects nor effects on basal iROS generation by MCs under resting conditions (Figure 3.9 a, b).

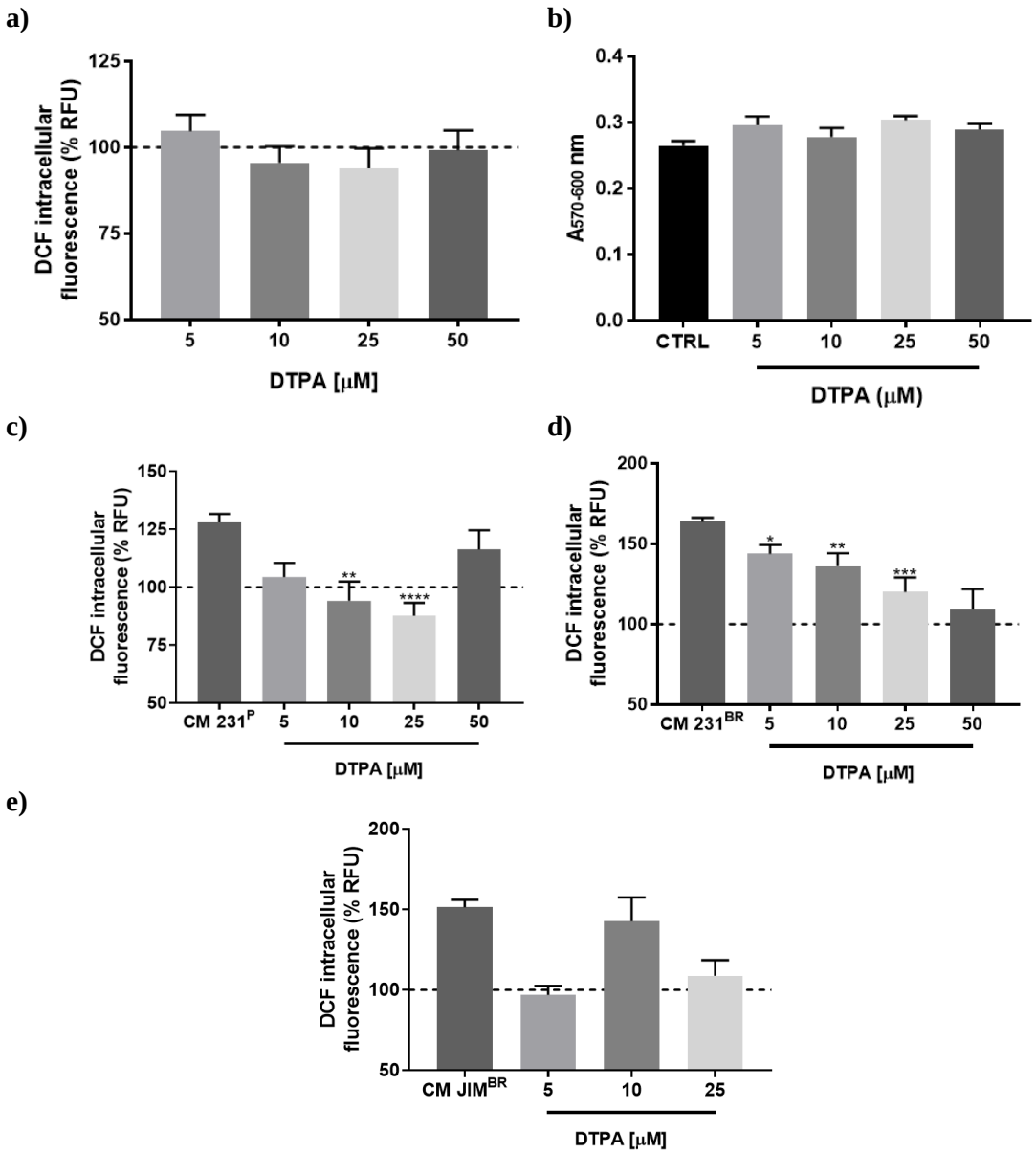

Figure 3. 9 - Effect of different DTPA concentrations on microglial **a)** iROS production and **b)** viability under extracellular Zn^{2+} chelation, and extracellular Zn^{2+} chelation plus exposure to the **c)** CM 231^{P}, **d)** CM 231^{BR}, and **e)** CM JIM^{BR}.

Quantitative analysis of iROS production and viability upon extracellular Zn^{2+} chelation in presence of DTPA concentrations ranging from 5 to 50 μM after 24 h stimulus. All values were normalized to the untreated control. Results are expressed as means ± SEMs (n>5 for the condition representing the secretome-treated cells, n=3 for cells treated with the secretomes with DTPA, except for cells exposed to CM JIM^{BR} and DTPA where n=1). $\alpha = 0.05$ *P<0.05, **P<0.01, ***P<0.001, and ****P<0.0001 as compared to secretome-treated cells using the non-parametric Kruskal-Wallis test followed by Dunn's multiple comparisons test.

Afterward, we evaluated the effects of extracellular Zn^{2+} chelation with DTPA in iROS production by MCs exposed to CMs derived from the different BCCs. Figure 3.9 c) shows iROS production in conditioned MCs with CM 231^{P} in the presence of the previously evaluated DTPA concentrations. With 5 µM DTPA it was observed a decrease in iROS production close to the basal levels. The maximum effect was observed with 25 µM DTPA, where iROS production decreased to values below what is observed under basal settings (87.75 ± 5.56, P<0.0001).

A similar study was performed in MCs treated with CM 231^{BR}. In this case, despite having observed a progressive decrease in iROS generation with the increased DTPA concentrations, only with 50 µM DTPA did the iROS return to the basal levels (Figure 3.9 d). The effects of DTPA on the CM JIM^{BR}-induced iROS production are displayed in Figure 3.9 e). As it can be seen, 5 and 25 µM DTPA decrease the iROS observed in the presence of CM JIM^{BR} to the untreated control values registered. Exposure of MCs to CM JIM^{BR} with 10 µM DTPA induced only a small decrease of the iROS production as compared to the production elicited by CM JIM^{BR}.

Overall, MCs react to $ZnCl_2$ and Zn^{2+} chelation from the secretomes of the different BC cells with marked changes in iROS production. Forty µM $ZnCl_2$ elicits an increase in the amount of ROS detected that is similar to what was observed under the influence of CM 231^{BR}, thus reinforcing the relevance of Zn^{2+} in iROS production. Zinc uptake in MCs is thought to occur through SLC39A1, culminating in the polarization of these cells towards an M1 phenotype [114]. iROS derived from Zn^{2+} uptake have been shown to induce oxidative stress that stimulates the activation of the NF-κB pathway [114,115].

Another interesting finding was the effect of Zn^{2+} chelation in the BCCs-derived secretomes, which allows us to infer the contribution of extracellular Zn^{2+} in the priming of MCs. We have observed a tendency for a decrease in iROS production under simultaneous Zn^{2+} chelation and BCCs-secretome conditioning. We hoped to see if the decrease in iROS would also reflect on other M1 features of MCs since H_2O_2 is associated with the activation of M1 SAPKs and NF-κB signaling and is also produced in Zn^{2+}-deficient cells [92].

The lack of total abrogation of iROS production at the higher concentration of DTPA tested could be due to flux from intracellular Zn^{2+} pools, further promoting ROS

generation [172]. As was mentioned, there is tight intracellular Zn^{2+} regulation for the maintenance of cellular homeostasis.

Cell viability was not significantly affected in the presence of the different CMs with DTPA (data not shown), demonstrating that these combined stimuli did not elicit cellular distress. Nonetheless, the consistency of the data obtained with incubation of the different CMs with 25 µM DTPA prompted us to elaborate on the effects of decreasing extracellular Zn^{2+} bioavailability with BCCs-secretome activation of MCs.

3.5.2. Zn^{2+} depletion decreases the NO production but not the expression of inflammatory mediators in MCs stimulated by the brain-tropic derived BCC secretomes

Following that, we evaluated whether extracellular Zn^{2+} chelation had an effect on NO production by MCs. To assess that, MCs were incubated with secretomes of the two brain-tropic cell lines, 231^{BR} and JIM^{BR} with and without 25 µM DTPA. The production of NO_2^- was measured at 6 and 24 h after treatments. Results are presented in Figure 3.10.

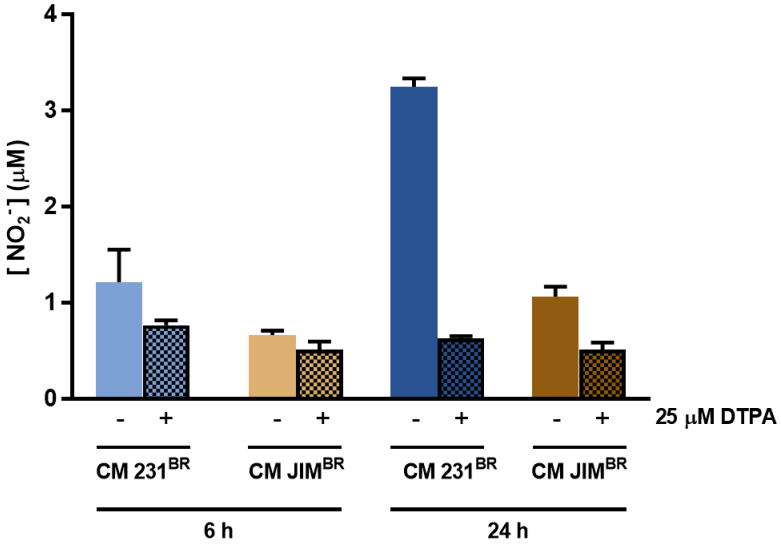

Figure 3. 10 - Effects of Zn^{2+} chelation in nitrite production by MCs exposed to brain-tropic BCCs secretome.

MCs were incubated with the secretomes of the two brain-tropic cell lines, 231^{BR} and JIM^{BR} with and without 25 µM DTPA, for 6 and 24 h. Nitrite concentrations were calculated by interpolation of the absorbance of each sample in a standard curve of sodium nitrite. Data are expressed as means ± SEMs (n = 1-4).

Extracellular Zn^{2+} chelation decreased the production of NO_2^- by MCs conditioned with CM 231^{BR} and CM JIM^{BR}, as depicted in Figure 3.10. This reduction was noticeable after 6 h of co-incubation, but it was more pronounced at 24 h. Accordingly, this effect was more pronounced in MCs stimulated by the brain tropic TNBC cell line, whose NO_2^- production levels were less than a fifth of what was reported without Zn^{2+} chelation. This effect is less noticeable for MCs conditioned with CM JIM^{BR} plus 25 µM DTPA, as their NO_2^- production drops to half of that observed without DTPA. Addition of 25 µM DTPA to control cells (fresh DMEM) did not elicit any changes in NO_2^- production (data not shown). Thus, we observe that extracellular Zn^{2+} plays an important role in the production of NO during MCs priming by the brain-tropic secretomes of the TN and $HER2^+$ BC cell lines.

Additionally, we measured the mRNA expression of the panel of inflammatory mediators and oxidative stress-related genes previously presented in section 3.1, in MCs exposed to the secretome of the two brain tropic cell lines in the presence of 25 µM DTPA. Results are presented in Figure 3.11 and Figure 3.12.

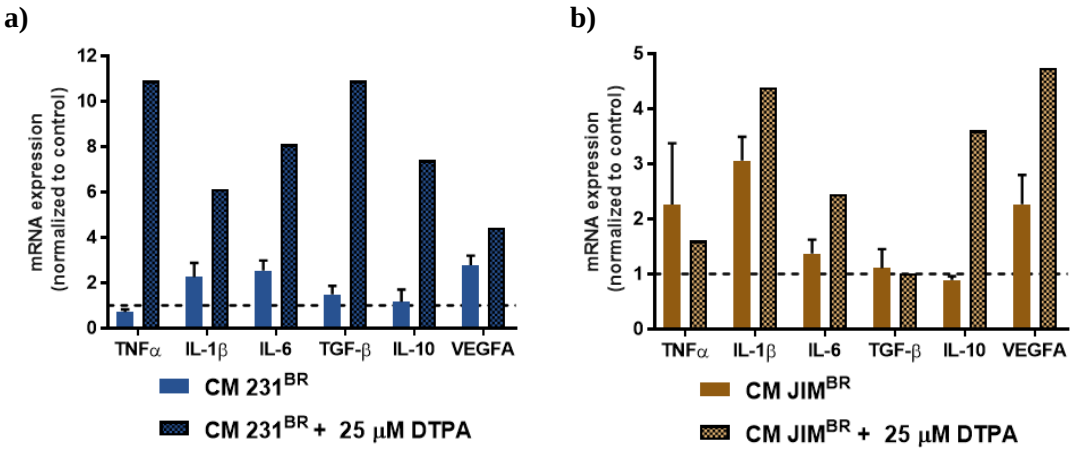

Figure 3. 11 - Gene expression of inflammatory mediators in MCs exposed to the secretome derived from CM 231^{BR} and CM JIM^{BR} with and without 25 µM DTPA.

HMC3 cells were incubated with the CMs with and without 25 µM DTPA for 24 h. Gene expression levels ($2^{-\Delta\Delta Ct}$) of inflammatory mediators were evaluated by RT-qPCR and normalized to the untreated control. Data are expressed as means ± SEMs (n=1-4).

Exposure of MCs to either CM 231^{BR} or CM JIM^{BR} with chelation of extracellular Zn^{2+} by 25 µM of DTPA increases the mRNA expression levels of almost all the inflammatory mediators evaluated. In fact, the expression of both pro-and anti-inflammatory cytokines, as well as *VEGFA*, are increased by extracellular Zn^{2+} chelation.

However, one exception is made for *TGF-β* expression in MCs exposed to CM JIM^{BR} with DTPA, where gene amplification was not enhanced. Microglial exposure to 25 µM DTPA has no effects on the mRNA expression levels of the genes analyzed (data not shown).

The most pronounced effects of extracellular Zn^{2+} chelation were observed in MCs treated with the CM 231^{BR}, where *TNFα* and the two anti-inflammatory cytokines, *TGF-β* and *IL-10*, are up-regulated almost ten and eight times compared to the effect of CM 231^{BR} alone. The chelation of Zn^{2+} in the CM JIM^{BR} induced similar effects, although less pronounced, except for the expression of *TNF-α* and *TGF-β* that appeared to remain unchanged.

Based on the panel of inflammatory mediators obtained, the depletion of extracellular Zn^{2+} by DTPA in the secretome of the brain-tropic TNBC cell line elicits an intermediary microglial activation phenotype, characterized by an increased expression of both pro- anti-inflammatory mediators. Similarly, although to a smaller extent, this effect appears to also be elicited when extracellular Zn^{2+} is chelated concomitant to exposure to brain-tropic HER2^{+} secretome.

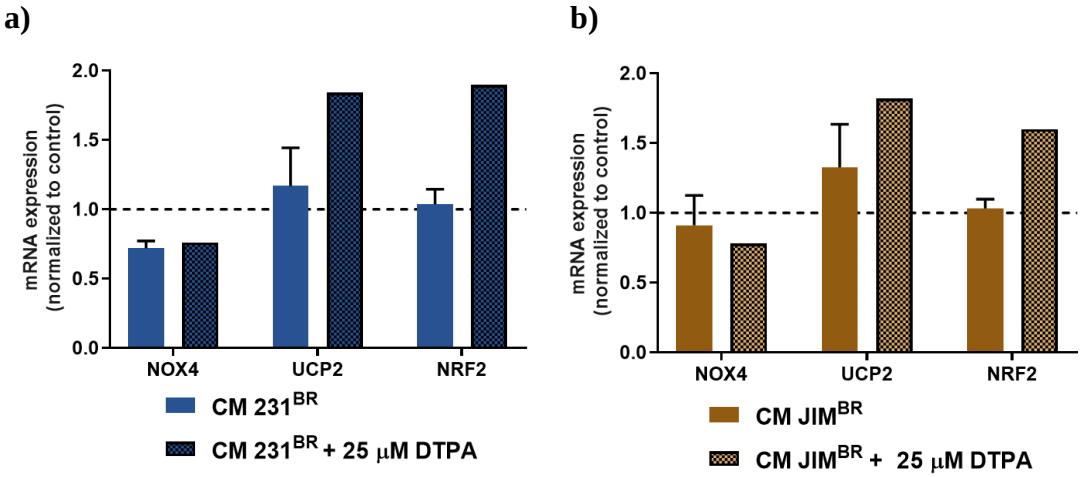

Figure 3. 12 - Gene expression of oxidative stress-related genes in MCs exposed to the secretome derived from CM 231^{BR}, and CM JIM^{BR} with and without 25 µM DTPA.

HMC3 cells were incubated with the CMs with and without 25 µM DTPA for 24 h. Gene expression levels ($2^{-\Delta\Delta Ct}$) of oxidative stress-related genes were evaluated by RT-qPCR, and normalized to the untreated control. Data are expressed as means ± SEMs (n=1-4).

We have also evaluated the mRNA expression levels of *NOX4*, *UCP2*, and *NRF2* to check if these oxidative stress-related genes revealed a shift in iROS origin and to clarify if extracellular Zn^{2+} chelation was inducing an oxidative imbalance in MCs. Figure

3.12 shows that *NOX4* mRNA expression remained unchanged while an increment in *UCP2* mRNA expression was observed with CM exposure and Zn^{2+} depletion. Howbeit what was observed with a resazurin assay, *NRF2* expression was up-regulated by Zn^{2+} chelation concomitant to BCCs-conditioning.

Overall, the results obtained under extracellular Zn^{2+} chelation were different from what had been foreseen. Even though we saw a decrease in the ROS and NO production of MCs that were activated by the BCCs-derived secretomes the expression of both pro and anti-inflammatory mediators evaluated by RT-qPCR was up-regulated.

The decline seen in both NO and ROS can be explained by the activation of the NRF2 pathway. As was mentioned, NRF2 is an oxidative sensor that elicits the activation of several antioxidant genes, such as heme oxygenase-1 (HO-1) under oxidative distress. As such, NRF2 activation could have been elicited to abrogate the production of both NO and ROS. Similar results were obtained in RAW cells, where induction of *HO-1*, a NRF2 downstream effector, led to decreased iNOS and NO levels after TNBC conditioning [173].

Even though extracellular Zn^{2+} chelation by 25 µM DTPA reduced the amount of iROS generated by MCs, this treatment appeared to elicit a pronounced reliance on mROS that also appear to be causing oxidative distress. The increase seen in the mitochondrial *UCP2* gene expression in CM 231^{BR} and CM JIM^{BR} with Zn^{2+} chelation denotes that there could have been uncoupling at the mitochondria. Further studies tracking intracellular zinc pools could further elucidate if Zn^{2+} could be effluxed from this organelle under mild Zn^{2+} deficiency, leading to a possible collapse of the mitochondrial membrane potential [172,174]. The low levels of *NOX4* expression also point that the iROS observed were not of enzymatic origin.

Our results also evidence that the increased expression levels of the inflammatory mediators could be mediated by extracellular Zn^{2+} depletion, which could, in turn, elicit Zn^{2+} internal efflux, which also affects iROS production. In fact, Zn^{2+} influx during the exposure of microglia to the BCC secretomes could be necessary to sustain its activation. A study by Saito et al. showed that MC priming with extracellular Zn^{2+} before LPS stimulus elicited a more pronounced M1 phenotype [115], pointing that this metal has a predominant role in eliciting ROS production and subsequent NF-κB signaling. Nonetheless, it appears that an artificial extracellular Zn^{2+} depletion also induces a similar result, as we saw the up-regulation of pro-inflammatory mediators after exposure to the

BCC secretomes. If extracellular Zn^{2+} influx is partially abrogated, a state of Zn^{2+} deficiency, which promotes inflammatory cytokine release, can be elicited [109]. In fact, exacerbated Zn^{2+} deficiency was shown to decrease the M2 features of both T lymphocytes and macrophages and to promote inflammation [175].

This aggravation of some of the M1 features when extracellular Zn^{2+} is chelated at the time of BCCs-priming of MCs further notes that Zn^{2+} plays a key role in MCs-induced inflammation and that further studies of the homeostasis of this metal in the context of BCBM could reveal a profound modulatory effect of the activation of these cells prior to cancer onset.

3.5.3 Depletion of extracellular Zn^{2+} activates inflammatory signaling pathways

The stress-related and inflammatory gene expression patterns of MCs exposed to the brain-tropic CMs supported an inflammatory-mediated response. The protein expression analysis of the phosphorylated forms of p38, and NF-κB in MCs exposed to the BCC secretomes with and without 25 μM DTPA also showed alterations in these pathways (Figure 3.13).

Although preliminary, these data suggest that zinc-depleted BCC secretomes induce an activation of the p38 signaling pathway, as indicated by the increased p38 phosphorylation mainly at 24 h. This effect was more pronounced with the secretome of brain-tropic $HER2^{+}$ cells in both time points.

Contrarily to what was observed for the p38 pathway, NF-κB signaling is activated only with TNBC-derived secretomes. In fact, MCs conditioned with both Zn^{2+}-depleted TNBC-derived secretomes increase their reliance on NF-κB signaling when compared to CM exposure under normal Zn^{2+} levels. MCs conditioned with CM 231^{P} also up-regulate NF-κB expression from 6 to 24 h.

The partial depletion of Zn^{2+} in the CM JIM^{BR} induced an almost two-fold decrease of NF-κB activation at both time points. This could point to a p38 signaling co-option in the presence of diminished Zn^{2+} influx at the time of $HER2^{+}$ BCCs-conditioning.

Apparently, TNBC-activated MCs appear to be more sensitive to extracellular Zn^{2+} levels in the regulation of their inflammatory signaling pathways. It has previously been shown that p38 and NF-κB can be activated by iROS either in conditions of

intracellular Zn^{2+} abundance but also in Zn^{2+} deficiency [100,109,115], and both the parental and brain tropic TNBC cell lines showed a more pronounced iROS reduction and up-regulation of the expression of inflammatory mediators under extracellular Zn^{2+} chelation.

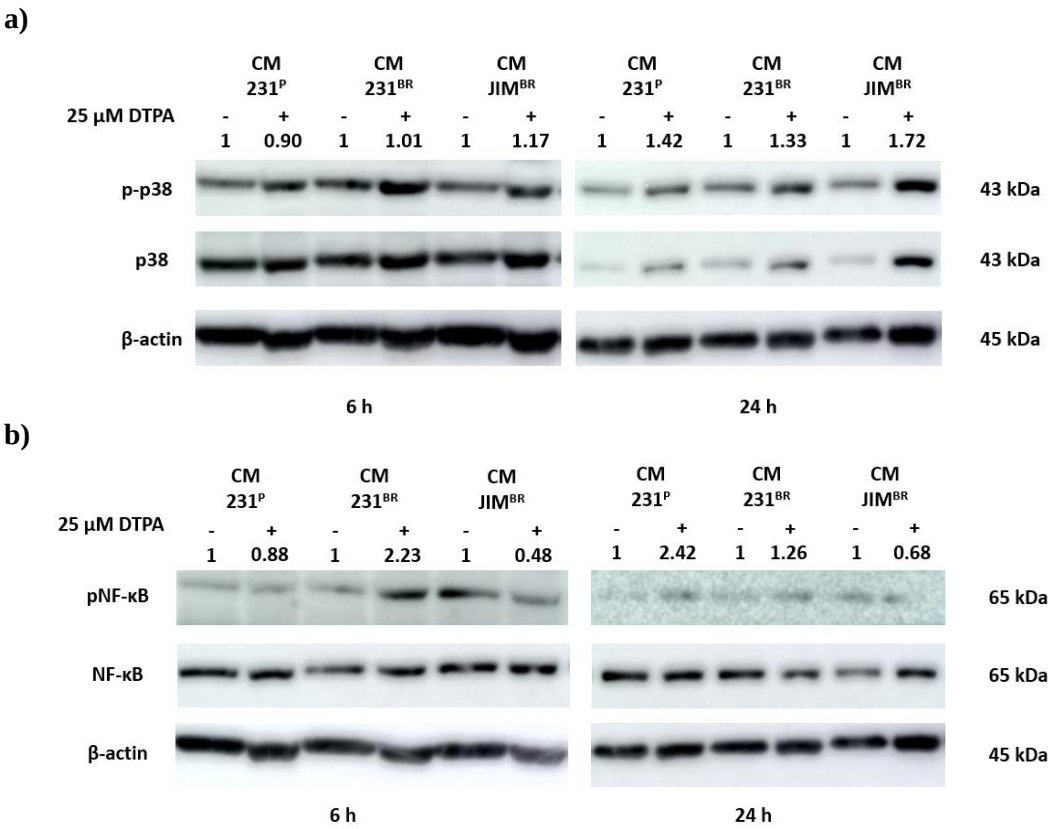

Figure 3. 13 - Effect of extracellular Zn^{2+} chelation on the microglial expression levels of **a)** p-p38 and **b)** pNF-κB after 6 and 24 h exposure to the secretome of BCCs.

Quantitative analysis of p-p38, and pNF-κB expression after a 6 and 24-h incubation with the parental and brain-tropic secretomes of the TNBC cell line (CM 231^{P} and CM 231^{BR}), and with the brain-tropic secretome of the $HER2^{+}$ BC cell line (CM JIM^{BR}) with and without 25 µM DTPA. Representative WB images of the analyzed proteins are shown. All values were normalized to the expression of the total form of the protein, normalized to their respective untreated control, and then to the respective values obtained in the absence of 25 µM DTPA (n=1).

3.5.4. Extracellular Zn^{2+} chelation decreases MC proliferation

We also evaluated if Zn^{2+} depletion in the BCC secretomes could modulate the proliferation of MCs. Therefore, we evaluated MC proliferation under the effect of BCCs-conditioning with and without 25 µM DTPA for a 48 and 72 h period using the WST-1 assay. We have also evaluated the expression levels of the phosphorylated form of the

ERK protein for 6 and 24 h under the same stimuli. Both results were normalized to the respective conditioning without extracellular Zn^{2+} chelation and can be seen in Figure 3.14, Table 3.3, and Figure 3.15.

As shown in Figure 3.14 and Table 3.3, there was a trend towards a decrease in the proliferation of MCs under Zn^{2+} depletion, further suggesting that MCs might rely in part on Zn^{2+} for their mitogenic processes. Twenty-five µM DTPA has no effect on MC proliferation since only a marginal decrease was observed at 72 h (data not shown).

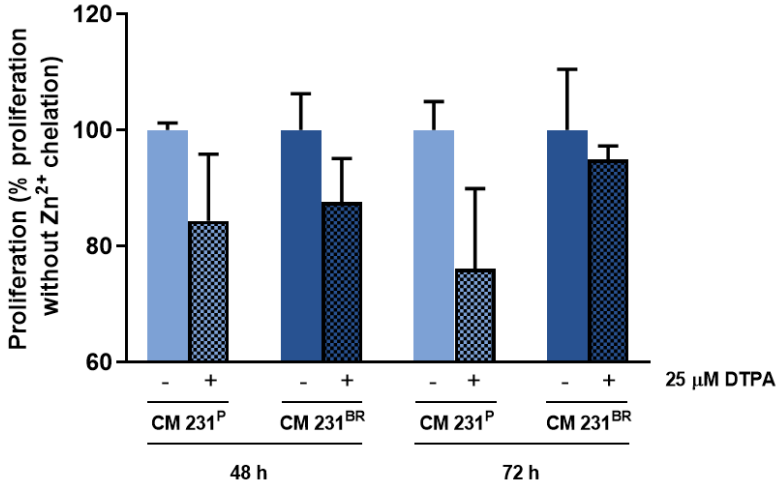

Figure 3. 14 - Effect of extracellular Zn^{2+} chelation on the BCCs-induced MC proliferation.

MCs were incubated with the parental and brain-tropic secretomes of the two TNBC cell line variants 231^{P} and 231^{BR} with and without 25 µM DTPA. Proliferation was evaluated with the WST-1 assay after 48 and 72 h stimulus. Each condition was assayed in triplicate. All values were normalized to the condition of 25 µM DTPA absence. Results are expressed as means ± SEMs (n=1).

Table 3.3 - Effect of extracellular Zn^{2+} chelation on the BCCs-induced MCs proliferation (%).

	CM 231^{P}		**CM 231^{BR}**	
25 µM DTPA	-	+	-	+
48 h	100 ± 1.23	84.36 ± 11.53	100 ± 6.29	87.62 ± 7.52
72 h	100 ± 4.93	76.09 ± 13.82	100 ± 10.47	94.94 ± 2.33

Results are expressed as means ± SEMs (n=1).

Analysis of ERK signaling showed a decrease in the phosphorylation of this MAPK under Zn^{2+} depletion. In fact, Zn^{2+}-chelation induced a decrease in ERK phosphorylated levels compared to what was observed in the presence of the BCCs secretomes. Attenuation of ERK signaling becomes even more pronounced when comparing pERK expression at 6 and 24 h for both treatments with the CMs of both brain-

tropic cell lines. A study by Oteiza et al. also found that Zn^{2+} deficiency leads to a decrease in the phosphorylation of the ERK pathway [92]. Interestingly, Oteiza and colleagues postulated that this decrease was independent of H_2O_2 activities as a second messenger and could, instead, be a direct consequence of Zn^{2+} being a requirement for cell growth.

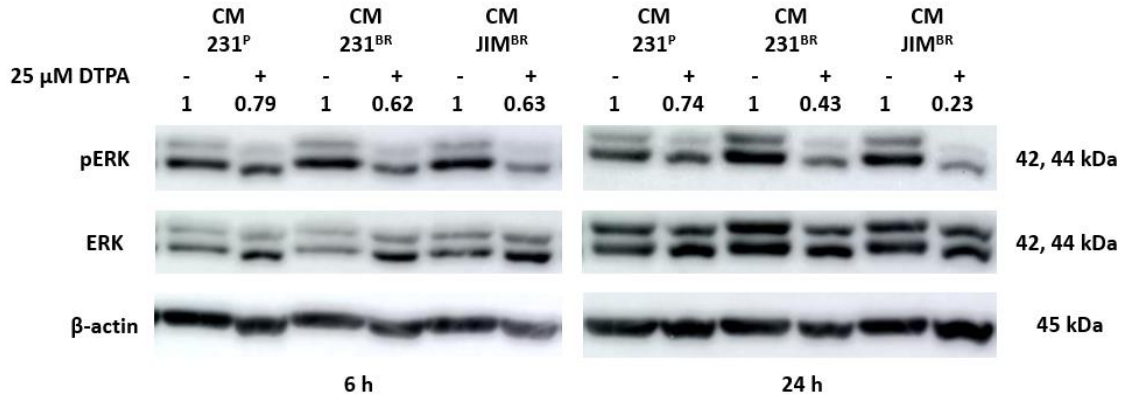

Figure 3. 15 - Effect of extracellular Zn^{2+} chelation on the microglial expression levels of p-ERK following 6 and 24 h exposure to the secretome of BCCs.

Quantitative analysis of p-ERK expression after a 6 and 24-h incubation with the parental and brain-tropic secretomes of the TNBC cell line (CM 231^{P} and CM 231^{BR}), and with the brain-tropic secretome of the $HER2^{+}$ BC cell line (CM JIM^{BR}) plus 25 µM DTPA. Representative WB images of the analyzed proteins are shown. All values were normalized to the expression of the total form of the protein, normalized to their respective untreated control, and then to the respective values obtained in the absence of 25 µM DTPA (n=1).

Overall, we had hypothesized that depletion of the extracellular bioavailable Zn^{2+} pool would decrease the influx rate of this metal in MCs, which could then be associated with the M1-like microglial phenotype shift seen under exposure to the BCC secretomes. In fact, Zn^{2+} depletion decreased NO, iROS, and microglial proliferation, but some of the M1-like features, such as inflammatory signaling and subsequent up-regulation of inflammatory mediators were up-regulated. This supports the idea that unbalanced Zn^{2+} metabolism, on either end of the scale, can lead to pro-oxidant cellular features. This is of particular importance because, although the serum of BC patients is not particularly rich in Zn^{2+}, the brain is one of the organs that store the most Zn^{2+}. In fact, Zn^{2+} is predominantly present at the synaptic boutons of the hippocampus and cerebral cortex neurons [166] and, under severe pathophysiological conditions such as ischaemia, there is a massive release of Zn^{2+} from these neuronal subsets [111], that has been associated

to iROS generation and to the M1 microglial phenotype [166]. This mechanism is possibly elicited under BCCs' remodeling of the brain.

Likewise, a secretome analysis has shown that the secretome of murine TNBC cells displays an increment in the levels of a Zn^{2+} importer, SLC39A10, when compared to a $HER2^{+}$ murine cell line [170]. A different study found SLC39A10 in the exosomes of highly metastatic murine BC cell lines [176]. This Zn^{2+} importer has been shown to modulate macrophage survival under pro-inflammatory stimuli, as it regulated inflammatory cytokines and p53 levels during immune response [177]. The preliminar results from our study concerning Zn^{2+} chelation could be envisaged as a way of counteracting the effects mediated by this importer and can be interpreted as eliciting a more aggressive M1 phenotype that, if it was to be sustained in time could, in fact, lead to overwhelming of the NRF2 antioxidant effect and negatively affect MCs survival. In the future, we also aim to quantify Zn^{2+} levels at the different BCC secretomes to improve our experimental design.

3.6. MCs exposed to the secretome of BCCs contribute to BBB dysfunction *in vitro*

The onset of brain metastasis requires the extravasation of tumor cells across the BBB and colonization into the brain parenchyma. The BBB is composed of a tight EC monolayer that, under normal conditions, limits the passage of tumor cells. Tumor cells are known to compromise the integrity of BBB through the release of specific factors for metastatic progression. With this in mind, we tested whether activated microglia could compromise the integrity of the EC monolayer using brain microvascular hCMEC/D3 ECs. These specialized cells form a monolayer and are currently used as an *in vitro* model of the BBB. Endothelial monolayer integrity was assessed by measuring the TEER, which is an indicator of the integrity of the intercellular junctions between adjacent ECs, and the transendothelial flux of a low molecular weight dextran (4 kDa), which quantifies the paracellular permeability across the cell monolayer.

This analysis was performed after 24 h incubation with the secretome of MCs pretreated with the CCMs of two BC cell lines representative of the parental and brain tropic triple-negative MDA-MB-231 (CM 231^{P} and CM ^{BR}), and brain tropic $HER2^{+}$ JIMT-1 (CM JIM^{BR}) cells for 24 h. Figure 3.16 shows the results from TEER measurements and permeability assays.

As depicted in Figure 3.16 a) there is a decrease in the TEER values of the hCMEC/D3 cell monolayer after exposure to the CMs collected from the BCCs-activated-microglia. Of particular note is the decrease in the TEER value of the hCMEC/D3 cell monolayer after CM 231^{BR} exposure when compared to the untreated control (63.82 % ± 0.66 %). The same was observed in the permeability assays to the 4-kDa FITC dextran as depicted in Figure 3.16 b), which showed increased permeability only in the presence of the CM 231^{BR} as compared to control (1.31 ± 0.04).

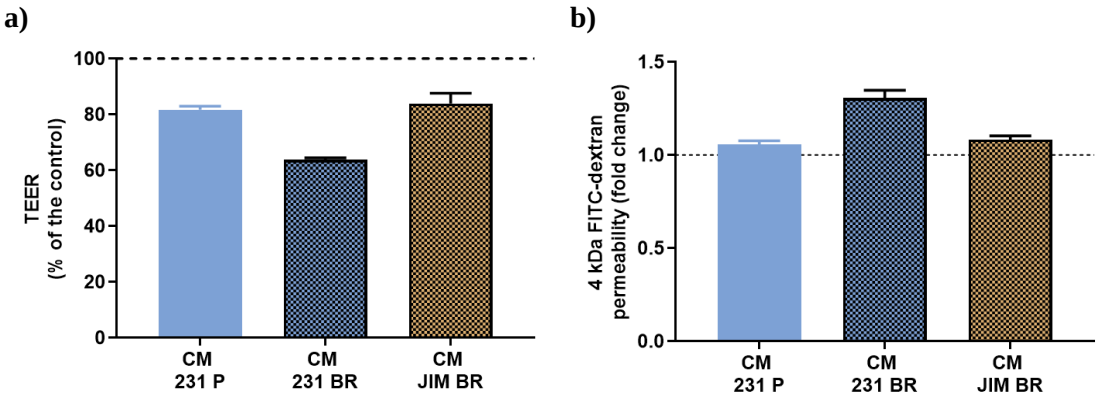

Figure 3. 16 - Effect of microglia cells-conditioned mediums on endothelial cells monolayer integrity. The secretome from MCs that had been previously activated by the different breast cancer cell's secretome change the **a)** TEER and **b)** the 4 kDa FITC permeability values of the endothelial cell monolayer.

Results are shown as means ± SEMs compared with the untreated control cells, n=1.

It is worth noting that CM 231^{P} and CM JIM^{BR} reduced the TEER values of the hCMEC/D3 cell monolayer (81.71 % ± 1.22 %, and 83.97 % ± 3.68 %, respectively), despite the fact that the 4 kDa FITC dextran permeability remain unchanged.

Usually, a decrease in TEER values is explained by an increase in paracellular permeability to ions. As such, if a smaller probe, such as fluoresceine (375 Da), had been used, we could have seen the expected increases in the paracellular ion flux of hCMEC/D3 cells after exposure to the CMs collected from the BCCs-activated-microglia. Nonetheless, it was previously described that the $HER2^{+}$ BC subtype is not strongly correlated with changes in vascular permeability [178,179].

Taken together, these data provide evidence for the contribution of activated microglia to EC monolayer dysfunction, mainly when activated by the brain tropic variant.

MCs contribute to the loss of integrity of the BBB which can be attributed to the secretion of inflammatory cytokines such as IL-1β, TNFα, IL-6, and of the angiogenic growth factor VEGFA [141]. In fact, the paracellular permeability of ECs was shown to increase in the presence of glioma cells and was correlated to the presence of chemokines and cytokines, one of which being IL-6 [180]. A different study has also shown that the cross-talk between glioma and microglia cells led to a synergistic production of IL-6 that was also implicated in the process of endothelial dysfunction [77]. Data from section 3.1 showed that the secretome that induced the biggest up-regulation of IL-6 on MCs was the one collected from CM 231^{BR} which is in accordance with the information retrieved from both TEER and 4 kDa permeability assays.

VEGFA originating from 231^{BR} cells was previously shown to be correlated with the increased vascular permeability of these cells [181,182]. Expression of this growth factor by activated MCs prior to cancer arrival might promote an earlier impairment of endothelial adherence junctions thus promoting faster transmigration of these cells to the brain parenchyma. In future works, evaluation of the secretion patterns of metalloproteinases by the BCCs-activated MCs would also help to explain their effect on endothelial cell monolayer disfunction.

BBB permeability to small molecules is a common feature of many inflammatory diseases and is at the base of metastatic brain colonization. Literature has shown us that the M1-like microglial phenotype observed under BCCs influence can be connected to the BBB increased permeability due to the secretion of the aforementioned soluble factors. These mechanisms of vascular hyperpermeability can help cancer transmigration through the vascular wall, improving the success rate of BrM.

3.7. Immunostaining of microglia in the prefrontal cortex of mice conditioned with the secretome of brain tropic-TNBC cells

A very preliminary study was carried out in swiss nu/nu mice, to see if there is *in vivo* any reactivity of microglia when exposed to the secretome of BC cells. For that, swiss nu/nu mice were pre-treated with CM of the TNBC cell's secretome 231^{P} and 231^{BR} for 15 days. With this approach, we intend to mimic the existence of a primary tumor in mice. Prefrontal cortex slices were prepared and stained with Iba1, which is an actin-bundling protein that allows the membrane ruffling that occurs during MCs activation.

Images were obtained using a Zeiss Axio Observer Z1 inverted microscope (Carl Zeiss, Thornwood, New York). After background fluorescence correction, Iba1 immunofluorescence values were obtained and then normalized to the number of cells present in each image. Representative images of each condition and the respective fluorescence quantification can be seen in Figure 3.17.

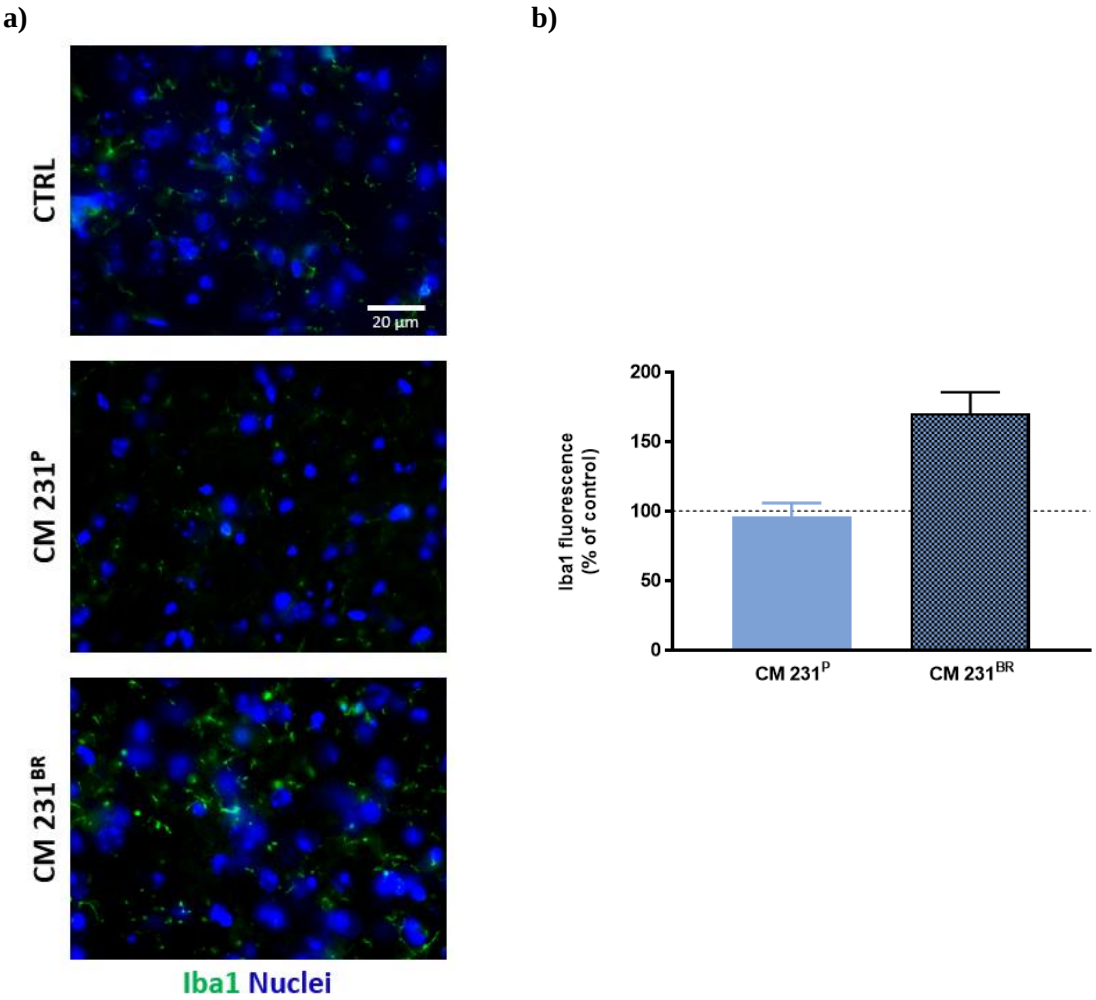

Figure 3. 17 - Iba1 expression increases in mouse prefrontal cortex following exposure to the secretome of brain-tropic TNBC cells.

a) Representative images and **b)** quantification of Iba1 (green) immunoreactivity in 20 µm brain slices under different experimental conditions as follow: untreated control (CTRL), CM 231^{P}, and CM 231^{BR} treatments. Nuclei were stained with Hoechst 33342 (blue). N = 1 for CTRL, and n=2 for CM 231^{P}, and CM 231^{BR}. Scale bar 20 µm (63x magnification).

Comparison of Iba1 immunofluorescence staining showed an increase in the fluorescence intensity in the prefrontal cortex of the animals treated with the CM of the brain tropic cells compared to the untreated control (170.5 % ± 15.04 %), indicating a

reactive response of microglia to the CM 231^{BR} treatment. However, we cannot conclude whether the higher fluorescence staining we observed is related to microglia activation [28] or due to an increased density of microglia cells in this brain region. As already mentioned these are very preliminary data, and future studies with a more detailed assessment of microglia morphological analysis are required to conclude about the proper role of microglia during the PMN formation.

Chapter 4 - Conclusions

Our preliminary results point that MCs are activated by the BCCs-secreted factors towards an M1-like phenotype. This phenotype is characterized by the secretion of NO, up-regulation of inflammatory mediators such as *IL-1β*, *IL-6*, *TNFα*, and *VEGFA*, but also increased proliferation, decreased motility, and iROS production. The increase observed in iROS could not be attributed to NOX activity. Nonetheless, *UCP2* fluctuations hint at a possible mitochondrial origin. There was also a propensity towards a more pronounced M1 microglial phenotype under the effect of the secretome of the brain-tropic variant of the TNBC cell line, eliciting enhancement of all the aforementioned features.

We did not exclude that the observed up-regulation of iROS could be targeted to the outside of the cell, but we knew that iROS, particularly H_2O_2, are associated with the modulation of MAPKs and NF-κB activity, possibly eliciting this inflammatory response. As such, we asked what could be at the basis of this response and hypothesized, among other factors, that Zn^{2+} influx could be a key player. Zinc homeostasis has revealed itself to be especially important in the regulation of the innate immune response of microglia. Evidence in the literature points that the secretome of TNBC cells is enriched in the Zn^{2+} importer SLC39A10 and, as such, we assumed that there could be up-regulation of Zn^{2+} influx that could, in turn, be mediating the pronounced response of MCs conditioned with the secretome of brain-tropic TNBC cells.

Under decreased Zn^{2+} influx, we have observed impairment in NO and ROS production, which was in accordance with our hypothesis. However, we have observed a pronounced up-regulation of the inflammatory signaling mediated by both the p38 and NF-κB pathways, leading to the up-regulation of the aforementioned inflammatory mediators, as well as *NRF2* overexpression, implying oxidative distress onset.

Thus, our results point that Zn^{2+} influx could be acting as a brake for severe microglial activation and consequent neuroinflammation under the effect of BC-secreted factors. Somewhat paradoxically, the levels of a redox inert ion, such as Zn^{2+}, appear to play a prominent role in the redox down-regulation of MCs inflammatory pathways under BCCs-activation. This leads to a collective of changes that deem MCs phenotype mildly amenable and that could allow a more facilitated invasion and growth of metastatic cancer cells as neuroinflammation could be kept tightly regulated by constant Zn^{2+} levels in MCs. Nevertheless, the mildly M1 phenotype reported after BCC secretome conditioning was still able to induce dysfunction on the barrier properties of the hCMEC/D3

monolayer, advocating for our interpretation of the M1-phenotype elicited in an environment depleted of BC cells. Overall, we report a shift towards an M1-like phenotype that is elicited by the different BCC secretomes *in vitro*, differing from what is usually observed when metastases or gliomas are present.

Iba1 fluorescence *ex vivo* also upholds our hypothesis of premature PMN formation, as MCs from the prefrontal cortex display enhanced activation after TNBC cell's secretome conditioning.

In sum, we have gathered evidence pointing that BC-secreted factors can modulate MCs phenotype towards an M1-like activation status very early and from a distance. Nonetheless, further studies are issued to better unravel the extent of microglial action in the brain microenvironment at the time of PMN formation.

Chapter 5 - Bibliography

1. WCRF International, W.C.R.F.I. for C.R. Diet, nutrition, physical activity and breast cancer. *Contin. Updat. Proj.* **2018**, 124, doi:10.1007/s12082-007-0105-4.
2. Harbeck, N.; Cortes, J.; Gnant, M.; Houssami, N.; Poortmans, P.; Ruddy, K.; Tsang, J.; Cardoso, F. Breast cancer. **2019**, *5*, doi:10.1038/s41572-019-0111-2.
3. Ginsburg, O.; Bray, F.; Coleman, M.P.; Vanderpuye, V.; Eniu, A.; Kotha, S.R.; Sarker, M.; Huong, T.T. Health , equity , and women ' s cancers 1 The global burden of women ' s cancers : a grand challenge in. *Lancet* **2016**, *6736*, 7–20, doi:10.1016/S0140-6736(16)31392-7.
4. Majeed, W.; Aslam, B.; Javed, I.; Khaliq, T.; Muhammad, F.; Ali, A.; Raza, A. Breast cancer: Major risk factors and recent developments in treatment. *Asian Pacific J. Cancer Prev.* **2014**, *15*, 3353–3358, doi:10.7314/APJCP.2014.15.8.3353.
5. Weide, R.; Feiten, S.; Friesenhahn, V.; Heymanns, J.; Kleboth, K.; Thomalla, J.; van Roye, C.; Köppler, H. Metastatic breast cancer: prolongation of survival in routine care is restricted to hormone-receptor- and Her2-positive tumors. *J. Korean Phys. Soc.* **2014**, *3*, 1–8, doi:10.1186/2193-1801-3-535.
6. WHO International Agency for Research on Cancer Available online: https://gco.iarc.fr/today/online-analysis-multi-bars?v=2018&mode=cancer&mode_population=countries&population=900&populations=900&key=total&sex=0&cancer=39&type=0&statistic=5&prevalence=0&population_group=0&ages_group%5B%5D=0&ages_group%5B%5D=17&nb_items (accessed on Jul 7, 2021).
7. Sinn, H.P.; Kreipe, H. A brief overview of the WHO classification of breast tumors, 4th edition, focusing on issues and updates from the 3rd edition. *Breast Care* **2013**, *8*, 149–154, doi:10.1159/000350774.
8. Yeo, S.K.; Guan, J.L. Breast Cancer: Multiple Subtypes within a Tumor? *Trends in Cancer* **2017**, *3*, 753–760, doi:10.1016/j.trecan.2017.09.001.
9. Heitz, F.; Harter, P.; Lueck, H.J.; Fissler-Eckhoff, A.; Lorenz-Salehi, F.; Scheil-Bertram, S.; Traut, A.; Bois, A. du Triple-negative and HER2-overexpressing breast cancers exhibit an elevated risk and an earlier occurrence of cerebral metastases. *Eur. J. Cancer* **2009**, *45*, 2792–2798, doi:10.1016/j.ejca.2009.06.027.
10. Stovgaard, E.S.; Nielsen, D.; Hogdall, E.; Balslev, E. Triple negative breast cancer–prognostic role of immune-related factors: a systematic review. *Acta Oncol. (Madr).* **2018**, *57*, 74–82, doi:10.1080/0284186X.2017.1400180.
11. Buonomo, O.C.; Caredda, E.; Portarena, I.; Vanni, G.; Orlandi, A.; Bagni, C.; Petrella, G.; Palombi, L.; Orsaria, P. New insights into the metastatic behavior after breast cancer surgery, according to well-established clinicopathological variables and molecular subtypes. *PLoS One* **2017**, *12*, 1–17, doi:10.1371/journal.pone.0184680.
12. Kumar, P.; Aggarwal, R. An overview of triple-negative breast cancer. *Arch. Gynecol. Obstet.* **2015**, *293*, 247–269, doi:10.1007/s00404-015-3859-y.
13. Carvalho, R.; Paredes, J.; Ribeiro, A.S. Impact of breast cancer cells´ secretome on the brain metastatic niche remodeling. *Semin. Cancer Biol.* **2019**, 0–1, doi:10.1016/j.semcancer.2019.10.011.
14. Wang, J.; Xu, B. Targeted therapeutic options and future perspectives for her2-positive breast cancer. *Signal Transduct. Target. Ther.* **2019**, *4*,

doi:10.1038/s41392-019-0069-2.
15. Iqbal, N.; Iqbal, N. Human Epidermal Growth Factor Receptor 2 (HER2) in Cancers: Overexpression and Therapeutic Implications. *Mol. Biol. Int.* **2014**, *2014*, 1–9, doi:10.1155/2014/852748.
16. Chen, W.; Hoffmann, A.D.; Liu, H.; Liu, X. Organotropism: new insights into molecular mechanisms of breast cancer metastasis. *npj Precis. Oncol.* **2018**, *2*, doi:10.1038/s41698-018-0047-0.
17. Molina, M.A.; Sáez, R.; Ramsey, E.E.; Garcia-Barchino, M.J.; Rojo, F.; Evans, A.J.; Albanell, J.; Keenan, E.J.; Lluch, A.; García-Conde, J.; et al. NH2-terminal truncated HER-2 protein but not full-length receptor is associated with nodal metastasis in human breast cancer. *Clin. Cancer Res.* **2002**, *8*, 347–353.
18. Beser, A.R.; Tuzlali, S.; Guzey, D.; Dolek Guler, S.; Hacihanefioglu, S.; Dalay, N. HER-2, TOP2A and chromosome 17 alterations in breast cancer. *Pathol. Oncol. Res.* **2007**, *13*, 180–185, doi:10.1007/BF02893497.
19. Di Fiore, P.P.; Pierce, J.H.; Kraus, M.H.; Segatto, O.; King, C.R.; Aaronson, S.A. ErbB-2 is a potent oncogene when overexpressed in NIH/3T3 cells. *Science (80-.).* **1987**, *237*, 178–182, doi:10.1126/science.2885917.
20. Palmieri, D.; Bronder, J.L.; Herring, J.M.; Yoneda, T.; Weil, R.J.; Stark, A.M.; Kurek, R.; Vega-Valle, E.; Feigenbaum, L.; Halverson, D.; et al. Her-2 overexpression increases the metastatic outgrowth of breast cancer cells in the brain. *Cancer Res.* **2007**, *67*, 4190–4198, doi:10.1158/0008-5472.CAN-06-3316.
21. Alanazi, I.O.; Khan, Z. Understanding EGFR Signaling in Breast Cancer and Breast Cancer Stem Cells : Overexpression and Therapeutic Implications. *Asian Pacific J. Cancer Prev.* **2016**, *17*, (2):445-53.
22. Simone Diermeier-Daucher, Olaf Ortmann, Stefan Buchholz, G.B. Trifunctional antibody ertumaxomab: Non- immunological effects on Her2 receptor activity and downstream signaling. *MAbs* **2012**, *4*, 614–622, doi:10.4161/mabs.21003.
23. Costa, R.; Sharpe, S.; Helenowski, I.; Shaw, C. A brief report of toxicity end points of HER2 vaccines for the treatment of patients with HER2 + breast cancer. *Dove Med. Press J. Drug Des. Dev. Ther.* **2019**, 309–316.
24. Nakada, T.; Sugihara, K.; Jikoh, T.; Abe, Y.; Agatsuma, T. Drug Discovery: Recent Progress and the Future The Latest Research and Development into the Antibody – Drug for HER2 Cancer Therapy. *Chem. Pharm. Bull.* **2019**, *67*, 173–185, doi:10.1248/cpb.c18-00744.
25. Jae Sik Kim and In Ah Kim Evolving treatment strategies of brain metastases from breast cancer: current status and future direction. *Ther. Adv. Med. Oncol.* **2020**, *12*, 1–21, doi:10.1177/https.
26. Zimmer, A.S.; Van Swearingen, A.E.D.; Anders, C.K. HER2-positive breast cancer brain metastasis: A new and exciting landscape. *Cancer Rep.* **2020**, 1–15, doi:10.1002/cnr2.1274.
27. Zimmer, A.S.; Steinberg, S.M.; Smart, D.D.; Gilbert, M.R.; Armstrong, T.S.; Burton, E.; Houston, N.; Biassou, N.; Gril, B.; Brastianos, P.K.; et al. Temozolomide in secondary prevention of HER2-positive breast cancer brain metastases. *Futur. Oncol.* **2020**, *16*, 899–909, doi:10.2217/fon-2020-0094.
28. Steeg, P.S. The blood–tumour barrier in cancer biology and therapy. *Nat. Rev. Clin. Oncol.* **2021**, *0123456789*, doi:10.1038/s41571-021-00529-6.

29. Mills, M.N.; Figura, N.B.; Arrington, J.A.; Yu, H.H.M.; Etame, A.B.; Vogelbaum, M.A.; Soliman, H.; Czerniecki, B.J.; Forsyth, P.A.; Han, H.S.; et al. Management of brain metastases in breast cancer: a review of current practices and emerging treatments. *Breast Cancer Res. Treat.* **2020**, doi:10.1007/s10549-020-05552-2.
30. Oura, S.; Mori, M.; Makimoto, S. A Case of Solitary Lung Metastasis of Breast Cancer Successfully Treated with Stereotactic Body Radiotherapy after Chemotherapy. *Case Rep. Oncol.* **2020**, *13*, 398–402, doi:10.1159/000506733.
31. Gay, L.J.; Felding-Habermann, B. Contribution of platelets to tumour metastasis. *Nat. Rev. Cancer* **2011**, *11*, 123–134, doi:10.1038/nrc3004.
32. Mhatre V. Ho, Ji-Ann Lee, and K.C.M. Serpins Promote Cancer Cell Survival and Vascular Cooption in Brain Metastasis. *Bone* **2012**, *23*, 1–7, doi:10.1038/jid.2014.371.
33. Gennari, A.; Conte, P.F.; Rosso, R.; Orlandini, C.; Bruzzi, P. Survival of metastatic breast carcinoma patients over a 20-year period: A retrospective analysis based on individual patient data from six consecutive studies. *Cancer* **2005**, *104*, 1742–1750, doi:10.1002/cncr.21359.
34. Tanaka, Y.; Hirata, M.; Shinonome, S.; Torii, M.; Nezasa, K.I.; Tanaka, H. Distribution analysis of epertinib in brain metastasis of HER2-positive breast cancer by imaging mass spectrometry and prospect for antitumor activity. *Sci. Rep.* **2018**, *8*, 1–12, doi:10.1038/s41598-017-18702-2.
35. Comen, E.; Norton, L.; Massagué, J. Clinical implications of cancer self-seeding. *Nat. Rev. Clin. Oncol.* **2011**, *8*, 369–377, doi:10.1038/nrclinonc.2011.64.
36. Pienta, K.J.; Robertson, B.A.; Coffey, D.S.; Taichman, R.S. The cancer diaspora: Metastasis beyond the seed and soil hypothesis. *Clin. Cancer Res.* **2013**, *19*, 5849–5855, doi:10.1158/1078-0432.CCR-13-2158.
37. Paget, S. Distribution of secondary growths in cancer of the breast. *Lancet* **1889**, *7*, 91–93, doi:10.1007/s12307-014-0163-5.
38. Peinado, H.; Zhang, H.; Matei, I.R.; Costa-Silva, B.; Hoshino, A.; Rodrigues, G.; Psaila, B.; Kaplan, R.N.; Bromberg, J.F.; Kang, Y.; et al. Pre-metastatic niches: Organ-specific homes for metastases. *Nat. Rev. Cancer* **2017**, *17*, 302–317, doi:10.1038/nrc.2017.6.
39. Carvalho, R.; Paredes, J.; Ribeiro, A.S. Impact of breast cancer cells´ secretome on the brain metastatic niche remodeling. *Semin. Cancer Biol.* **2019**, *60*, 294–301, doi:10.1016/j.semcancer.2019.10.011.
40. Hoshino, A.; Costa-Silva, B.; Shen, T.L.; Rodrigues, G.; Hashimoto, A.; Tesic Mark, M.; Molina, H.; Kohsaka, S.; Di Giannatale, A.; Ceder, S.; et al. Tumour exosome integrins determine organotropic metastasis. *Nature* **2015**, *527*, 329–335, doi:10.1038/nature15756.
41. Grivennikov, S.I.; Greten, F.R.; Karin, M. Immunity, Inflammation, and Cancer. *Cell* **2010**, *140*, 883–899, doi:10.1016/j.cell.2010.01.025.
42. Hanahan, D.; Coussens, L.M. Accessories to the Crime: Functions of Cells Recruited to the Tumor Microenvironment. *Cancer Cell* **2012**, *21*, 309–322, doi:10.1016/j.ccr.2012.02.022.
43. Arvanitis, C.D.; Ferraro, G.B.; Jain, R.K. The blood–brain barrier and blood–tumour barrier in brain tumours and metastases. *Nat. Rev. Cancer* **2019**, *20*, 26–41, doi:10.1038/s41568-019-0205-x.

44. Schulz, M.; Salamero-Boix, A.; Niesel, K.; Alekseeva, T.; Sevenich, L. Microenvironmental Regulation of Tumor Progression and Therapeutic Response in Brain Metastasis. *Front. Immunol.* **2019**, *10*, 1713, doi:10.3389/fimmu.2019.01713.
45. Louveau, A.; Harris, T.H.; Kipnis, J. Revisiting the concept of CNS immune privilege. *Trends Immunol.* **2016**, *36*, 569–577, doi:10.1016/j.it.2015.08.006.Revisiting.
46. Taylor, P.; Lampson, L.A. Monoclonal antibodies in neuro-oncology. *MAbs* **2011**, *3*, 153–160, doi:10.4161/mabs.3.2.14239.
47. Winkler, F. The brain metastatic niche. *J. Mol. Med.* **2015**, *93*, 1213–1220, doi:10.1007/s00109-015-1357-0.
48. Zhou, W.; Fong, M.Y.; Min, Y.; Somlo, G.; Liu, L.; Palomares, M.R.; Yu, Y.; Chow, A.; O'Connor, S.T.F.; Chin, A.R.; et al. Cancer-Secreted miR-105 destroys vascular endothelial barriers to promote metastasis. *Cancer Cell* **2014**, *25*, 501–515, doi:10.1016/j.ccr.2014.03.007.
49. Lee, B.C.; Lee, T.H.; Avraham, S.; Avraham, H.K. Involvement of the chemokine receptor CXCR4 and its ligand stromal cell-derived factor 1α in breast cancer cell migration through human brain microvascular endothelial cells. *Mol. Cancer Res.* **2004**, *2*, 327–338.
50. Avraham, H.K.; Jiang, S.; Fu, Y.; Nakshatri, H.; Ovadia, H.; Avraham, S. Angiopoietin-2 mediates blood-brain barrier impairment and colonization of triple-negative breast cancer cells in brain. *J. Pathol.* **2014**, *232*, 369–381, doi:10.1002/path.4304.
51. Kloosterman, D.J.; Akkari, L. Mapping the Uncharted Territories of Human Brain Malignancies. *Cell* **2020**, *181*, 1454–1457, doi:10.1016/j.cell.2020.06.003.
52. You, H.; Baluszek, S.; Kaminska, B. Immune Microenvironment of Brain Metastases — Are Microglia and Other Brain Macrophages Little Helpers ? **2019**, *10*, 1–12, doi:10.3389/fimmu.2019.01941.
53. You, H.; Baluszek, S.; Kaminska, B. Supportive roles of brain macrophages in CNS metastases and assessment of new approaches targeting their functions. *Theranostics* **2020**, *10*, 2949–2964, doi:10.7150/thno.40783.
54. Chuang, H.N.; van Rossum, D.; Sieger, D.; Siam, L.; Klemm, F.; Bleckmann, A.; Bayerlová, M.; Farhat, K.; Scheffel, J.; Schulz, M.; et al. Carcinoma cells misuse the host tissue damage response to invade the brain. *Glia* **2013**, *61*, 1331–1346, doi:10.1002/glia.22518.
55. Rodrigues, G.; Hoshino, A.; Kenific, C.M.; Matei, I.R.; Steiner, L.; Freitas, D.; Kim, H.S.; Oxley, P.R.; Scandariato, I.; Casanova-Salas, I.; et al. Tumour exosomal CEMIP protein promotes cancer cell colonization in brain metastasis. *Nat. Cell Biol.* **2019**, *21*, 1403–1412, doi:10.1038/s41556-019-0404-4.
56. Fong, M.Y.; Zhou, W.; Liu, L.; Alontaga, A.Y.; Chandra, M.; Ashby, J.; Chow, A.; O'Connor, S.T.F.; Li, S.; Chin, A.R.; et al. Breast cancer-secreted miR-122 reprograms glucose metabolism in pre-metastatic niche to promote metastasis. *Nat. Cell Biol.* **2015**, *17*, 183–194, doi:10.1038/ncb3094.Breast.
57. Yonemori, K.; Tsuta, K.; Ono, M.; Shimizu, C.; Hirakawa, A.; Hasegawa, T.; Hatanaka, Y.; Narita, Y.; Shibui, S.; Fujiwara, Y. Disruption of the blood brain barrier by brain metastases of triple-negative and basal-type breast cancer but not HER2/neu-positive breast cancer. *Cancer* **2010**, *116*, 302–308,

doi:10.1002/cncr.24735.

58. Ghajar, C.M.; Peinado, H.; Mori, H.; Matei, I.R.; Evason, K.J.; Brazier, H.; Almeida, D.; Koller, A.; Hajjar, K.A.; Stainier, D.Y.R.; et al. The perivascular niche regulates breast tumour dormancy. *Nat. Cell Biol.* **2013**, *15*, 807–817, doi:10.1038/ncb2767.
59. Karrison, T.G.; Donald, J.; Meier, P. Dormancy of Mammary Carcinoma After Mastectomy. *J Natl Cancer Inst.* **1999**, *91*, 1–6, doi:10.1093/jnci/91.1.80.
60. Bos, P.D.; Zhang, X.H.F.; Nadal, C.; Shu, W.; Gomis, R.R.; Nguyen, D.X.; Minn, A.J.; Van De Vijver, M.J.; Gerald, W.L.; Foekens, J.A.; et al. Genes that mediate breast cancer metastasis to the brain. *Nature* **2009**, *459*, 1005–1009, doi:10.1038/nature08021.
61. Witzel, I.; Oliveira-Ferrer, L.; Pantel, K.; Müller, V.; Wikman, H. Breast cancer brain metastases: Biology and new clinical perspectives. *Breast Cancer Res.* **2016**, *18*, 1–9, doi:10.1186/s13058-015-0665-1.
62. Weil, R.J.; Palmieri, D.C.; Bronder, J.L.; Stark, A.M.; Steeg, P.S. Breast Cancer Metastasis to the Central Nervous System. *Am. J. Pathol.* **2005**, *167*, 913–920, doi:10.1016/S0002-9440(10)61180-7.
63. Takahashi, H.; Isogawa, M. Management of breast cancer brain metastases. *Chinese Clin. Oncol.* **2018**, *7*, 1–7, doi:10.21037/cco.2018.05.06.
64. Bachiller, S.; Jiménez-Ferrer, I.; Paulus, A.; Yang, Y.; Swanberg, M.; Deierborg, T.; Boza-Serrano, A. Microglia in neurological diseases: A road map to brain-disease dependent-inflammatory response. *Front. Cell. Neurosci.* **2018**, *12*, 1–17, doi:10.3389/fncel.2018.00488.
65. Van Eldik, L.J.; Carrillo, M.C.; Cole, P.E.; Feuerbach, D.; Greenberg, B.D.; Hendrix, J.A.; Kennedy, M.; Kozauer, N.; Margolin, R.A.; Molinuevo, J.L.; et al. The roles of inflammation and immune mechanisms in Alzheimer's disease. *Alzheimer's Dement. Transl. Res. Clin. Interv.* **2016**, *2*, 99–109, doi:10.1016/j.trci.2016.05.001.
66. Illes, P.; Rubini, P.; Ulrich, H.; Zhao, Y.; Tang, Y. Regulation of Microglial Functions by Purinergic Mechanisms in the Healthy and Diseased CNS. *Cells* **2020**, *9*, 1–24, doi:10.3390/cells9051108.
67. Wang, L. xun; Zhang, S. xi; Wu, H. juan; Rong, X. lu; Guo, J. M2b macrophage polarization and its roles in diseases. *J. Leukoc. Biol.* **2019**, *106*, 345–358, doi:10.1002/JLB.3RU1018-378RR.
68. Etemad, S.; Zamin, R.M.; Ruitenberg, M.J.; Filgueira, L. A novel in vitro human microglia model: Characterization of human monocyte-derived microglia. *J. Neurosci. Methods* **2012**, *209*, 79–89, doi:10.1016/j.jneumeth.2012.05.025.
69. Orihuela, R.; McPherson, C.A.; Harry, G.J. Microglial M1/M2 polarization and metabolic states. *Br. J. Pharmacol.* **2016**, 649–665.
70. Helmut Kettenmann; Semtner, M. The VGF-derived peptide TLQP21 impairs purinergic control of chemotaxis and phagocytosis in mouse microglia. *J. Neurosci.* **2020**, *40*, 1458–19.
71. Casella, G.; Garzetti, L.; Gatta, A.T.; Finardi, A.; Maiorino, C.; Ruffini, F.; Martino, G.; Muzio, L.; Furlan, R. IL4 induces IL6-producing M2 macrophages associated to inhibition of neuroinflammation in vitro and in vivo. *J. Neuroinflammation* **2016**, *13*, 1–10, doi:10.1186/s12974-016-0596-5.
72. Rojo, A.I.; McBean, G.; Cindric, M.; Egea, J.; López, M.G.; Rada, P.; Zarkovic, N.;

Cuadrado, A. Redox control of microglial function: Molecular mechanisms and functional significance. *Antioxidants Redox Signal.* **2014**, *21*, 1766–1801, doi:10.1089/ars.2013.5745.

73. Jang, G.Y.; Lee, J. won; Kim, Y.S.; Lee, S.E.; Han, H.D.; Hong, K.J.; Kang, T.H.; Park, Y.M. Interactions between tumor-derived proteins and Toll-like receptors. *Exp. Mol. Med.* **2020**, *52*, 1926–1935, doi:10.1038/s12276-020-00540-4.
74. Chow, A.; Zhou, W.; Liu, L.; Fong, M.Y.; Champer, J.; Van Haute, D.; Chin, A.R.; Ren, X.; Gugiu, B.G.; Meng, Z.; et al. Macrophage immunomodulation by breast cancer-derived exosomes requires Toll-like receptor 2-mediated activation of NF-κB. *Sci. Rep.* **2014**, *4*, doi:10.1038/srep05750.
75. Hu, F.; Dzaye, O.D.A.; Hahn, A.; Yu, Y.; Scavetta, R.J.; Dittmar, G.; Kaczmarek, A.K.; Dunning, K.R.; Ricciardelli, C.; Rinnenthal, J.L.; et al. Glioma-derived versican promotes tumor expansion via glioma-associated microglial/macrophages Toll-like receptor 2 signaling. *Neuro. Oncol.* **2015**, *17*, 200–210, doi:10.1093/neuonc/nou324.
76. Hoelzinger, D.B.; Demuth, T.; Berens, M.E. Autocrine factors that sustain glioma invasion and paracrine biology in the brain microenvironment. *J. Natl. Cancer Inst.* **2007**, *99*, 1583–1593, doi:10.1093/jnci/djm187.
77. Couto, M.; Coelho-Santos, V.; Santos, L.; Fontes-Ribeiro, C.; Silva, A.P.; Gomes, C.M.F. The interplay between glioblastoma and microglia cells leads to endothelial cell monolayer dysfunction via the interleukin-6-induced JAK2/STAT3 pathway. *J. Cell. Physiol.* **2019**, *234*, 19750–19760, doi:10.1002/jcp.28575.
78. Pukrop, T.; Dehghani, F.; Chuang, H.; Lohaus, R.; Bayanga, K.; Heermann, S.; Regen, T.; Rossum, D.V.A.N.; Klemm, F.; Schulz, M. Microglia Promote Colonization of Brain Tissue by Breast Cancer Cells in a Wnt-Dependent Way. **2010**, *1489*, 1477–1489, doi:10.1002/glia.21022.
79. Lorger, M.; Felding-Habermann, B. Capturing changes in the brain microenvironment during initial steps of breast cancer brain metastasis. *Am. J. Pathol.* **2010**, *176*, 2958–2971, doi:10.2353/ajpath.2010.090838.
80. Fitzgerald, D.P.; Palmieri, D.; Hua, E.; Hargrave, E.; Steeg, P.S. Reactive glia are recruited by highly proliferative brain metastases of breast cancer and promote tumor cell colonization. *Clin. Exp. Metastasis* **2008**, 799–810, doi:10.1007/s10585-008-9193-z.
81. Andreou, K.E.; Soto, M.S.; Allen, D.; Economopoulos, V.; de Bernardi, A.; Larkin, J.R.; Sibson, N.R. Anti-inflammatory microglia/macrophages as a potential therapeutic target in brain metastasis. *Front. Oncol.* **2017**, *7*, 1–13, doi:10.3389/fonc.2017.00251.
82. Kielbassa, K.; Vegna, S.; Ramirez, C.; Akkari, L. Understanding the origin and diversity of macrophages to tailor their targeting in solid cancers. *Front. Immunol.* **2019**, *10*, 1–15, doi:10.3389/fimmu.2019.02215.
83. Aires, I.D.; Ribeiro-Rodrigues, T.; Boia, R.; Ferreira-Rodrigues, M.; Girão, H.; Ambrósio, A.F.; Santiago, A.R. Microglial extracellular vesicles as vehicles for neurodegeneration spreading. *Biomolecules* **2021**, *11*, 1–23, doi:10.3390/biom11060770.
84. Giordano, C.; Camera, G. La; Gelsomino, L.; Barone, I.; Bonofiglio, D.; Andò, S.; Catalano, S. The biology of exosomes in breast cancer progression: Dissemination,

immune evasion and metastatic colonization. *Cancers (Basel).* **2020**, *12*, 1–16, doi:10.3390/cancers12082179.

85. Cobley, J.N.; Fiorello, M.L.; Bailey, D.M. 13 Reasons Why the Brain Is Susceptible To Oxidative Stress. *Redox Biol.* **2018**, *15*, 490–503, doi:10.1016/j.redox.2018.01.008.
86. Simpson, D.S.A.; Oliver, P.L. ROS Generation in Microglia: Understanding Oxidative Stress and Inflammation in Neurodegenerative Disease. *Antioxidants* **2020**, *9*, 1–27, doi:10.3390/antiox9080743.
87. Bordt, E.A.; Polster, B.M. NADPH oxidase- and mitochondria-derived reactive oxygen species in proinflammatory microglial activation: A Bipartisan affair? *Free Radic. Biol. Med.* **2014**, *76*, 34–46, doi:10.1016/j.freeradbiomed.2014.07.033.
88. Park, J.; Min, J.S.; Kim, B.; Chae, U. Bin; Yun, J.W.; Choi, M.S.; Kong, I.K.; Chang, K.T.; Lee, D.S. Mitochondrial ROS govern the LPS-induced pro-inflammatory response in microglia cells by regulating MAPK and NF-κB pathways. *Neurosci. Lett.* **2015**, *584*, 191–196, doi:10.1016/j.neulet.2014.10.016.
89. Mander, P.K.; Jekabsone, A.; Brown, G.C. Microglia Proliferation Is Regulated by Hydrogen Peroxide from NADPH Oxidase. *J. Immunol.* **2006**, *176*, 1046–1052, doi:10.4049/jimmunol.176.2.1046.
90. Yan, L.; Liu, S.; Wang, C.; Wang, F.; Song, Y.; Yan, N.; Xi, S.; Liu, Z.; Sun, G. JNK and NADPH oxidase involved in fluoride-induced oxidative stress in BV-2 microglia cells. *Mediators Inflamm.* **2013**, *2013*, 1–11, doi:10.1155/2013/895975.
91. Liu, Z.; Yao, X.; Jiang, W.; Li, W.; Zhu, S.; Liao, C.; Zou, L.; Ding, R.; Chen, J. Advanced oxidation protein products induce microglia-mediated neuroinflammation via MAPKs-NF-κB signaling pathway and pyroptosis after secondary spinal cord injury. *J. Neuroinflammation* **2020**, *17*, 1–21, doi:10.1186/s12974-020-01751-2.
92. Liebert, M.A.; Zago, M.P.; Mackenzie, G.G.; Adamo, A.N.A.M.; Keen, C.L.; Oteiza, P.I. Differential Modulation of MAP Kinases by Zinc Deficiency in IMR-32 Cells: Role of H2O2. *Biotechnology* **2005**, *7*.
93. Akhmetzyanova, E.; Kletenkov, K.; Mukhamedshina, Y.; Rizvanov, A. Different Approaches to Modulation of Microglia Phenotypes After Spinal Cord Injury. *Front. Syst. Neurosci.* **2019**, *13*, 1–12, doi:10.3389/fnsys.2019.00037.
94. Takada, Y.; Mukhopadhyay, A.; Kundu, G.C.; Mahabeleshwar, G.H.; Singh, S.; Aggarwal, B.B. Hydrogen peroxide activates NF-κB through tyrosine phosphorylation of IκBα and serine phosphorylation of p65. Evidence for the involvement of IκBα kinase and Syk protein-tyrosine kinase. *J. Biol. Chem.* **2003**, *278*, 24233–24241, doi:10.1074/jbc.M212389200.
95. Gao, F.; Chen, D.; Hu, Q.; Wang, G. Rotenone Directly Induces BV2 Cell Activation via the p38 MAPK Pathway. *PLoS One* **2013**, *8*, 1–9, doi:10.1371/journal.pone.0072046.
96. Aldieri, E.; Riganti, C.; Polimeni, M.; Gazzano, E.; Lussiana, C.; Campia, I.; Ghigo, D. Classical Inhibitors of NOX NAD(P)H Oxidases Are Not Specific. *Curr. Drug Metab.* **2008**, *9*, 686–696, doi:10.2174/138920008786049285.
97. Wind, S.; Beuerlein, K.; Eucker, T.; Müller, H.; Scheurer, P.; Armitage, M.E.; Ho, H.; Schmidt, H.H.H.W.; Wingler, K. Comparative pharmacology of chemically distinct NADPH oxidase inhibitors. *Br. J. Pharmacol.* **2010**, *161*, 885–898, doi:10.1111/j.1476-5381.2010.00920.x.

98. Qin, L.; Liu, Y.; Wang, T.; Wei, S.J.; Block, M.L.; Wilson, B.; Liu, B.; Hong, J.S. NADPH Oxidase Mediates Lipopolysaccharide-induced Neurotoxicity and Proinflammatory Gene Expression in Activated Microglia. *J. Biol. Chem.* **2004**, *279*, 1415–1421, doi:10.1074/jbc.M307657200.
99. Go, Y.M.; Chandler, J.D.; Jones, D.P. The cysteine proteome. *Free Radic. Biol. Med.* **2015**, *84*, 227–245, doi:10.1016/j.freeradbiomed.2015.03.022.
100. Hübner, C.; Haase, H. Interactions of zinc- and redox-signaling pathways. *Redox Biol.* **2021**, *41*, 101916, doi:10.1016/j.redox.2021.101916.
101. Mailloux, R.J.; Harper, M.E. Uncoupling proteins and the control of mitochondrial reactive oxygen species production. *Free Radic. Biol. Med.* **2011**, *51*, 1106–1115, doi:10.1016/j.freeradbiomed.2011.06.022.
102. Sara, M.; Yaser, K.-B.; Maedeh, A.; Mohamadreza, A.; Beitullah, A. The review of the relationship between UCP2 and obesity: Focusing on inflammatory-obesity. *New Insights Obes. Genet. Beyond* **2021**, *5*, 001–013, doi:10.29328/journal.niogb.1001015.
103. De Bilbao, F.; Arsenijevic, D.; Vallet, P.; Hjelle, O.P.; Ottersen, O.P.; Bouras, C.; Raffin, Y.; Abou, K.; Langhans, W.; Collins, S.; et al. Resistance to cerebral ischemic injury in UCP2 knockout mice: Evidence for a role of UCP2 as a regulator of mitochondrial glutathione levels. *J. Neurochem.* **2004**, *89*, 1283–1292, doi:10.1111/j.1471-4159.2004.02432.x.
104. Kizaki, T.; Suzuki, K.; Hitomi, Y.; Taniguchi, N.; Saitoh, D.; Watanabe, K.; Onoé, K.; Day, N.K.; Good, R.A.; Ohno, H. Uncoupling protein 2 plays an important role in nitric oxide production of lipopolysaccharide-stimulated macrophages. *Proc. Natl. Acad. Sci. U. S. A.* **2002**, *99*, 9392–9397, doi:10.1073/pnas.142206299.
105. Emre, Y.; Hurtaud, C.; Nübel, T.; Criscuolo, F.; Ricquier, D.; Cassard-Doulcier, A.M. Mitochondria contribute to LPS-induced MAPK activation via uncoupling protein UCP2 in macrophages. *Biochem. J.* **2007**, *402*, 271–278, doi:10.1042/BJ20061430.
106. Bai, Y.; Onuma, H.; Bai, X.; Medvedev, A. V; Misukonis, M.; Weinberg, J.B.; Cao, W.; Robidoux, J.; Floering, L.M.; Daniel, K.W.; et al. Persistent Nuclear Factor-κB Activation in Ucp2−/− Mice Leads to Enhanced Nitric Oxide and Inflammatory Cytokine Production. *J Biol Chem.* **2005**, *19*, 19062–19069.
107. Yavuz Cakir, S.W.B. Reactive Species-Mediated Regulation of Cell Signaling and the Cell Cycle: The Role of MAPK. **2005**, *7*, 726–740.
108. Zacherl, J.R.; Tourkova, I.; Croix, C.M.S.; Robinson, L.J.; Palmer, O.M.P.; Mihalik, S.J.; Blair, H.C. Elaidate, an 18-Carbon Trans-monoenoic Fatty Acid, but not Physiological Fatty Acids Increases Intracellular Zn2+ in Human Macrophages. *J Cell Biochem* **2015**, *116*, 524–532, doi:10.1002/jcb.25002.Elaidate.
109. Maret, W. The redox biology of redox-inert zinc ions. *Free Radic. Biol. Med.* **2019**, *134*, 311–326, doi:10.1016/j.freeradbiomed.2019.01.006.
110. Serra, M.; Columbano, A.; Ammarah, U.; Mazzone, M.; Menga, A. Understanding Metal Dynamics Between Cancer Cells and Macrophages: Competition or Synergism? *Front. Oncol.* **2020**, *10*, 1–16, doi:10.3389/fonc.2020.00646.
111. Ueba, Y.; Aratake, T.; Onodera, K. ichi; Higashi, Y.; Hamada, T.; Shimizu, T.; Shimizu, S.; Yawata, T.; Nakamura, R.; Akizawa, T.; et al. Attenuation of zinc-enhanced inflammatory M1 phenotype of microglia by peridinin protects against short-term spatial-memory impairment following cerebral ischemia in mice.

Biochem. Biophys. Res. Commun. **2018**, *507*, 476–483, doi:10.1016/j.bbrc.2018.11.067.

112. Gao, H.; Dai, W.; Zhao, L.; Min, J.; Wang, F. The role of zinc and zinc homeostasis in macrophage function. *J. Immunol. Res.* **2018**, *2018*, doi:10.1155/2018/6872621.
113. Brieger, A.; Rink, L.; Haase, H. Differential Regulation of TLR-Dependent MyD88 and TRIF Signaling Pathways by Free Zinc Ions. *J. Immunol.* **2013**, *191*, 1808–1817, doi:10.4049/jimmunol.1301261.
114. Higashi, Y.; Segawa, S.; Matsuo, T.; Nakamura, S.; Kikkawa, Y.; Nishida, K.; Nagasawa, K. Microglial zinc uptake via zinc transporters induces ATP release and the activation of microglia. *Glia* **2011**, *59*, 1933–1945, doi:10.1002/glia.21235.
115. Higashi, Y.; Aratake, T.; Shimizu, S.; Shimizu, T.; Nakamura, K.; Tsuda, M.; Yawata, T.; Ueba, T.; Saito, M. Influence of extracellular zinc on M1 microglial activation. *Sci. Rep.* **2017**, *7*, 1–13, doi:10.1038/srep43778.
116. Sies, H. Hydrogen peroxide as a central redox signaling molecule in physiological oxidative stress: Oxidative eustress. *Redox Biol.* **2017**, *11*, 613–619, doi:10.1016/j.redox.2016.12.035.
117. Cooney, S.J.; Bermudez-Sabogal, S.L.; Byrnes, K.R. Cellular and temporal expression of NADPH oxidase (NOX) isotypes after brain injury. *J. Neuroinflammation* **2013**, *10*, 1–13, doi:10.1186/1742-2094-10-155.
118. Guo, Z.; Mo, Z. Keap1-Nrf2 signaling pathway in angiogenesis and vascular diseases. *J. Tissue Eng. Regen. Med.* **2020**, *14*, 869–883, doi:10.1002/term.3053.
119. Wang, Z.; Yang, J.; Qi, J.; Jin, Y.; Tong, L. Activation of NADPH/ROS pathway contributes to angiogenesis through JNK signaling in brain endothelial cells. *Microvasc. Res.* **2020**, *131*, 104012, doi:10.1016/j.mvr.2020.104012.
120. Sivandzade, F.; Bhalerao, A.; Cucullo, L. Cerebrovascular and neurological disorders: Protective role of NRF2. *Int. J. Mol. Sci.* **2019**, *20*, 8–12, doi:10.3390/ijms20143433.
121. Vilhardt, F.; Haslund-Vinding, J.; Jaquet, V.; McBean, G. Microglia antioxidant systems and redox signalling. *Br. J. Pharmacol.* **2016**, *174*, 1719–1732, doi:10.1111/bph.13426.
122. Xie, F.; Xiao, P.; Chen, D.; Xu, L.; Zhang, B. miRDeepFinder: A miRNA analysis tool for deep sequencing of plant small RNAs. *Plant Mol. Biol.* **2012**, *80*, 75–84, doi:10.1007/s11103-012-9885-2.
123. Ding, Y.; Zheng, Y.; Huang, J.; Peng, W.; Chen, X.; Kang, X.; Zeng, Q. UCP2 ameliorates mitochondrial dysfunction, inflammation, and oxidative stress in lipopolysaccharide-induced acute kidney injury. *Int. Immunopharmacol.* **2019**, *71*, 336–349, doi:10.1016/j.intimp.2019.03.043.
124. Hingtgen, S.D.; Tian, X.; Yang, J.; Dunlay, S.M.; Peek, A.S.; Wu, Y.; Sharma, R. V.; Engelhardt, J.F.; Davisson, R.L. Nox2-containing NADPH oxidase and Akt activation play a key role in angiotensin II-induced cardiomyocyte hypertrophy. *Physiol. Genomics* **2006**, *26*, 180–191, doi:10.1152/physiolgenomics.00029.2005.
125. Li, B.; Bedard, K.; Sorce, S.; Hinz, B.; Dubois-Dauphin, M.; Krause, K.H. NOX4 expression in human microglia leads to constitutive generation of reactive oxygen species and to constitutive il-6 expression. *J. Innate Immun.* **2009**, *1*, 570–581, doi:10.1159/000235563.

126. Hämälaïnen, M.; Teppo, H.R.; Skarp, S.; Haapasaari, K.M.; Porvari, K.; Vuopala, K.; Kietzmann, T.; Karihtala, P. NRF1 and NRF2 mRNA and Protein Expression Decrease Early during Melanoma Carcinogenesis: An Insight into Survival and MicroRNAs. *Oxid. Med. Cell. Longev.* **2019**, *2019*, doi:10.1155/2019/2647068.
127. Da Silva, L.P.; Neves, B.M.; Moura, L.; Cruz, M.T.; Carvalho, E. Neurotensin decreases the proinflammatory status of human skin fibroblasts and increases epidermal growth factor expression. *Int. J. Inflam.* **2014**, *2014*, doi:10.1155/2014/248240.
128. Leite, D.M.; Zvar Baskovic, B.; Civita, P.; Neto, C.; Gumbleton, M.; Pilkington, G.J. A human co-culture cell model incorporating microglia supports glioblastoma growth and migration, and confers resistance to cytotoxics. *FASEB J.* **2020**, *34*, 1710–1727, doi:10.1096/fj.201901858RR.
129. Gu, Y.; Liu, H.; Kong, F.; Ye, J.; Jia, X.; Zhang, Z.; Li, N.; Yin, J.; Zheng, G.; He, Z. MiR-22/KAT6B axis is a chemotherapeutic determiner via regulation of PI3k-Akt-NF-kB pathway in tongue squamous cell carcinoma. *J. Exp. Clin. Cancer Res.* **2018**, *37*, 1–14, doi:10.1186/s13046-018-0834-z.
130. Li, H.; Zhai, N.; Wang, Z.; Song, H.; Yang, Y.; Cui, A.; Li, T.; Wang, G.; Niu, J.; Crispe, I.N.; et al. Regulatory NK cells mediated between immunosuppressive monocytes and dysfunctional T cells in chronic HBV infection. *Gut* **2018**, *67*, 2035–2044, doi:10.1136/gutjnl-2017-314098.
131. Dello Russo, C.; Cappoli, N.; Coletta, I.; Mezzogori, D.; Paciello, F.; Pozzoli, G.; Navarra, P.; Battaglia, A. The human microglial HMC3 cell line: Where do we stand? A systematic literature review. *J. Neuroinflammation* **2018**, *15*, 1–24, doi:10.1186/s12974-018-1288-0.
132. Suzuki, H.; Isogai, M.; Maeda, R.; Ura, K.; Tamura, T.A. TBP-like protein (TLP) interferes with Taspase1-mediated processing of TFIIA and represses TATA box gene expression. *Nucleic Acids Res.* **2015**, *43*, 6285–6298, doi:10.1093/nar/gkv576.
133. Schindelin, J.; Arganda-Carreras, I.; Frise, E.; Kaynig, V.; Longair, M.; Pietzsch, T.; Preibisch, S.; Rueden, C.; Saalfeld, S.; Schmid, B.; et al. Fiji: An open-source platform for biological-image analysis. *Nat. Methods* **2012**, *9*, 676–682, doi:10.1038/nmeth.2019.
134. de Aquino, C.C.; Leitão, R.A.; Alves, L.A.O.; Coelho-Santos, V.; Guerrant, R.L.; Ribeiro, C.F.; Malva, J.O.; Silva, A.P.; Oriá, R.B. Effect of hypoproteic and high-fat diets on hippocampal blood-brain barrier permeability and oxidative stress. *Front. Nutr.* **2019**, *5*, 1–10, doi:10.3389/fnut.2018.00131.
135. Rock, R.B.; Peterson, P.K. Microglia as a pharmacological target in infectious and inflammatory diseases of the brain. *J. Neuroimmune Pharmacol.* **2006**, *1*, 117–126, doi:10.1007/s11481-006-9012-8.
136. Lepiarz, I.; Olajide, O. The human microglia (HMC-3) as a cellular model of neuroinflammation. *IBRO Reports* **2019**, *6*, S92, doi:10.1016/j.ibror.2019.07.299.
137. Sarkar, S.; Döring, A.; Zemp, F.J.; Silva, C.; Lun, X.; Wang, X.; Kelly, J.; Hader, W.; Hamilton, M.; Mercier, P.; et al. Therapeutic activation of macrophages and microglia to suppress brain tumor-initiating cells. *Nat. Neurosci.* **2014**, *17*, 46–55, doi:10.1038/nn.3597.
138. Bal-Price, A.; Brown, G.C. Inflammatory neurodegeneration mediated by nitric

oxide from activated glia-inhibiting neuronal respiration, causing glutamate release and excitotoxicity. *J. Neurosci.* **2001**, *21*, 6480–6491, doi:10.1523/jneurosci.21-17-06480.2001.

139. Salleles, J. Progressive Neurodegeneration after Experimental Brain Trauma: Association with Chronic Microglial Activation. *Rev. For. Fr.* **2014**, *66*, 14–29, doi:10.4267/2042/56283.
140. Loane, D.J.; Stoica, B.A.; Pajoohesh-Ganji, A.; Byrnes, K.R.; Faden, A.I. Activation of metabotropic glutamate receptor 5 modulates microglial reactivity and neurotoxicity by inhibiting NADPH oxidase. *J. Biol. Chem.* **2009**, *284*, 15629–15639, doi:10.1074/jbc.M806139200.
141. Luna, J.D.; Chan, C.C.; Derevjanik, N.L.; Mahlow, J.; Chiu, C.; Peng, B.; Tobe, T.; Campochiaro, P.A.; Vinores, S.A. Blood-retinal barrier (BRB) breakdown in experimental autoimmune uveoretinitis: Comparison with vascular endothelial growth factor, tumor necrosis factor and interleukin-1β-mediated breakdown. *J. Neurosci. Res.* **1997**, *49*, 268–280, doi:10.1002/(SICI)1097-4547(19970801)49:3<268::AID-JNR2>3.0.CO;2-A.
142. Liu, X.; Quan, N. Microglia and CNS interleukin-1: Beyond immunological concepts. *Front. Neurol.* **2018**, *9*, 1–11, doi:10.3389/fneur.2018.00008.
143. Wesolowska, A.; Kwiatkowska, A.; Slomnicki, L.; Dembinski, M.; Master, A.; Sliwa, M.; Franciszkiewicz, K.; Chouaib, S.; Kaminska, B. Microglia-derived TGF-β as an important regulator of glioblastoma invasion - An inhibition of TGF-β-dependent effects by shRNA against human TGF-β type II receptor. *Oncogene* **2008**, *27*, 918–930, doi:10.1038/sj.onc.1210683.
144. Lee, S.K.; Huang, S.; Lu, W.; Lev, D.C.; Price, J.E. Vascular endothelial growth factor expression promotes the growth of breast cancer brain metastases in nude mice. *Clin. Exp. Metastasis* **2004**, *21*, 107–118, doi:10.1023/B:CLIN.0000024761.00373.55.
145. Treps, L.; Perret, R.; Edmond, S.; Ricard, D.; Gavard, J. Glioblastoma stem-like cells secrete the pro-angiogenic VEGF-A factor in extracellular vesicles. *J. Extracell. Vesicles* **2017**, *6*, doi:10.1080/20013078.2017.1359479.
146. Connelly, L.; Barham, W.; Onishko, H.M.; Chen, L.; Sherrill, T.P.; Zabuawala, T.; Ostrowski, M.C.; Blackwell, T.S.; Yull, F.E. NF-kappaB activation within macrophages leads to an anti-tumor phenotype in a mammary tumor lung metastasis model. *Breast Cancer Res.* **2011**, *13*, doi:10.1186/bcr2935.
147. Shen, S.C.; Wu, M.S.; Lin, H.Y.; Yang, L.Y.; Chen, Y.H.; Chen, Y.C. Reactive oxygen species-dependent nitric oxide production in reciprocal interactions of glioma and microglial cells. *J. Cell. Physiol.* **2014**, *229*, 2015–2026, doi:10.1002/jcp.24659.
148. Xing, F.; Liu, Y.; Wu, S.Y.; Wu, K.; Sharma, S.; Mo, Y.Y.; Feng, J.; Sanders, S.; Jin, G.; Singh, R.; et al. Loss of XIST in breast cancer activates MSN-c-Met and reprograms microglia via exosomal miRNA to promote brain metastasis. *Cancer Res.* **2018**, *78*, 4316–4330, doi:10.1158/0008-5472.CAN-18-1102.
149. Kalyanaraman, B.; Darley-Usmar, V.; Davies, K.J.A.; Dennery, P.A.; Forman, H.J.; Grisham, M.B.; Mann, G.E.; Moore, K.; 2nd, L.J.R.; Ischiropoulos, H. Measuring reactive oxygen and nitrogen species with fluorescent probes: challenges and limitations. *Free Radic Biol Med* **2012**, *23*, 1–6, doi:10.1016/j.freeradbiomed.2011.09.030.

150. Doron, H.; Pukrop, T.; Erez, N. A blazing landscape: Neuroinflammation shapes brain metastasis. *Cancer Res.* **2019**, *79*, 423–436, doi:10.1158/0008-5472.CAN-18-1805.
151. Emre, Y.; Nübel, T. Uncoupling protein UCP2: When mitochondrial activity meets immunity. *FEBS Lett.* **2010**, *584*, 1437–1442, doi:10.1016/j.febslet.2010.03.014.
152. La Marca, J.E.; Richardson, H.E. Two-Faced: Roles of JNK Signalling During Tumourigenesis in the Drosophila Model. *Front. Cell Dev. Biol.* **2020**, *8*, 1–20, doi:10.3389/fcell.2020.00042.
153. Himes, S.R.; Sester, D.P.; Ravasi, T.; Cronau, S.L.; Sasmono, T.; Hume, D.A. The JNK Are Important for Development and Survival of Macrophages. *J. Immunol.* **2006**, *176*, 2219–2228, doi:10.4049/jimmunol.176.4.2219.
154. Dhanasekaran, D.N.; Premkumar Reddy, E. JNK-signaling: A multiplexing hub in programmed cell death. *Genes and Cancer* **2017**, *8*, 682–694, doi:10.18632/genesandcancer.155.
155. Liva, S.M.; Kahn, M.A.; Dopp, J.M.; De Vellis, J. Signal transduction pathways induced by GM-CSF in microglia: Significance in the control of proliferation. *Glia* **1999**, *26*, 344–352, doi:10.1002/(SICI)1098-1136(199906)26:4<344::AID-GLIA8>3.0.CO;2-L.
156. Chen, Y.; Jin, Y.; Wu, N. Role of tumor-derived extracellular vesicles in glioblastoma. *Cells* **2021**, *10*, 1–14, doi:10.3390/cells10030512.
157. Abels, E.R.; Maas, S.L.N.; Nieland, L.; Wei, Z.; Cheah, P.S.; Tai, E.; Kolsteeg, C.J.; Dusoswa, S.A.; Ting, D.T.; Hickman, S.; et al. Glioblastoma-Associated Microglia Reprogramming Is Mediated by Functional Transfer of Extracellular miR-21. *Cell Rep.* **2019**, *28*, 3105-3119.e7, doi:10.1016/j.celrep.2019.08.036.
158. Hollmén, M.; Karaman, S.; Schwager, S.; Lisibach, A.; Christiansen, A.J.; Maksimow, M.; Varga, Z.; Jalkanen, S.; Detmar, M. G-CSF regulates macrophage phenotype and associates with poor overall survival in human triple-negative breast cancer. *Oncoimmunology* **2016**, *5*, doi:10.1080/2162402X.2015.1115177.
159. Zhang, F.; Nance, E.; Alnasser, Y.; Kannan, R.; Kannan, S. Microglial migration and interactions with dendrimer nanoparticles are altered in the presence of neuroinflammation. *J. Neuroinflammation* **2016**, *13*, 1–11, doi:10.1186/s12974-016-0529-3.
160. Lively, S.; Schlichter, L.C. The microglial activation state regulates migration and roles of matrix-dissolving enzymes for invasion. *J. Neuroinflammation* **2013**, *10*, 1–14, doi:10.1186/1742-2094-10-75.
161. Juliano, J.; Gil, O.; Hawkins-Daarud, A.; Noticewala, S.; Rockne, R.C.; Gallaher, J.; Massey, S.C.; Sims, P.A.; Anderson, A.R.A.; Swanson, K.R.; et al. Comparative dynamics of microglial and glioma cell motility at the infiltrative margin of brain tumours. *J. R. Soc. Interface* **2018**, *15*, doi:10.1098/rsif.2017.0582.
162. Lee, C.F.; Ullevig, S.; Kim, H.S.; Asmis, R. Regulation of Monocyte Adhesion and Migration by Nox4. *PLoS One* **2013**, *8*, doi:10.1371/journal.pone.0066964.
163. Cui, K.; Ardell, C.L.; Podolnikova, N.P.; Yakubenko, V.P. Distinct migratory properties of M1, M2, and resident macrophages are regulated by αdβ2and αmβ2integrin-mediated adhesion. *Front. Immunol.* **2018**, *9*, 1–14, doi:10.3389/fimmu.2018.02650.
164. Wang, J.; Zhao, H.; Xu, Z.; Cheng, X. Zinc dysregulation in cancers and its potential

as a therapeutic target. *Cancer Biol. Med.* **2020**, *17*, 612–625, doi:10.20892/j.issn.2095-3941.2020.0106.

165. Slepchenko, K.G.; Lu, Q.; Li, Y. V. Cross talk between increased intracellular zinc (Zn2+) and accumulation of reactive oxygen species in chemical ischemia. *Am. J. Physiol. - Cell Physiol.* **2017**, *313*, C48–C459, doi:10.1152/ajpcell.00048.2017.
166. Segawa, S.; Tatsumi, N.; Ohishi, A.; Nishida, K.; Nagasawa, K. Characterization of zinc uptake by mouse primary cultured astrocytes and microglia. *Metallomics* **2015**, *7*, 1067–1077, doi:10.1039/c5mt00085h.
167. Jouybari, L.; Kiani, F.; Akbari, A.; Sanagoo, A.; Sayehmiri, F.; Aaseth, J.; Chartrand, M.S.; Sayehmiri, K.; Chirumbolo, S.; Bjørklund, G. A meta-analysis of zinc levels in breast cancer. *J. Trace Elem. Med. Biol.* **2019**, *56*, 90–99, doi:10.1016/j.jtemb.2019.06.017.
168. Vogel-González, M.; Musa-Afaneh, D.; Gil, P.R.; Vicente, R. Zinc favors triple-negative breast cancer's microenvironment modulation and cell plasticity. *Int. J. Mol. Sci.* **2021**, *22*, doi:10.3390/ijms22179188.
169. Benderli Cihan, Y.; Sözen, S.; Öztürk Yıldırım, S. Trace elements and heavy metals in hair of stage III breast cancer patients. *Biol. Trace Elem. Res.* **2011**, *144*, 360–379, doi:10.1007/s12011-011-9104-z.
170. Kagara, N.; Tanaka, N.; Noguchi, S.; Hirano, T. Zinc and its transporter ZIP10 are involved in invasive behavior of breast cancer cells. *Cancer Sci.* **2007**, *98*, 692–697, doi:10.1111/j.1349-7006.2007.00446.x.
171. Arts, J.; Bade, S.; Badrinas, M.; Ball, N.; Hindle, S. Should DTPA, an Aminocarboxylic acid (ethylenediamine-based) chelating agent, be considered a developmental toxicant? *Regul. Toxicol. Pharmacol.* **2018**, *97*, 197–208, doi:10.1016/j.yrtph.2018.06.019.
172. Kumari, A.; Singh, K.P.; Mandal, A.; Paswan, R.K.; Sinha, P.; Das, P.; Ali, V.; Bimal, S.; Lal, C.S. Intracellular zinc flux causes reactive oxygen species mediated mitochondrial dysfunction leading to cell death in Leishmania donovani. *PLoS One* **2017**, *12*, 1–25, doi:10.1371/journal.pone.0178800.
173. Liny, C.W.; Shen, S.C.; Ko, C.H.; Lin, H.Y.; Chen, Y.C. Reciprocal activation of macrophages and breast carcinoma cells by nitric oxide and colony-stimulating factor-1. *Carcinogenesis* **2010**, *31*, 2039–2048, doi:10.1093/carcin/bgq172.
174. Sun, Q.; Zhong, W.; Zhang, W.; Li, Q.; Sun, X.; Tan, X.; Sun, X.; Dong, D.; Zhou, Z. Zinc deficiency mediates alcohol-induced apoptotic cell death in the liver of rats through activating ER and mitochondrial cell death pathways. *Am. J. Physiol. - Gastrointest. Liver Physiol.* **2015**, *308*, G757–G766, doi:10.1152/ajpgi.00442.2014.
175. Kido, T.; Ishiwata, K.; Suka, M.; Yanagisawa, H. Inflammatory response under zinc deficiency is exacerbated by dysfunction of the T helper type 2 lymphocyte–M2 macrophage pathway. *Immunology* **2019**, *156*, 356–372, doi:10.1111/imm.13033.
176. Gangoda, L.; Liem, M.; Ang, C.S.; Keerthikumar, S.; Adda, C.G.; Parker, B.S.; Mathivanan, S. Proteomic Profiling of Exosomes Secreted by Breast Cancer Cells with Varying Metastatic Potential. *Proteomics* **2017**, *17*, 1–15, doi:10.1002/pmic.201600370.
177. Gao, H.; Zhao, L.; Wang, H.; Xie, E.; Wang, X.; Wu, Q.; Yu, Y.; He, X.; Ji, H.; Rink, L.;

et al. Metal transporter Slc39a10 regulates susceptibility to inflammatory stimuli by controlling macrophage survival. *Proc. Natl. Acad. Sci. U. S. A.* **2017**, *114*, 12940–12945, doi:10.1073/pnas.1708018114.

178. Adkins, C.E.; Mohammad, A.S.; Terrell-hall, T.; Dolan, E.L.; Shah, N.; Sechrest, E.; Griffith, J.; Lockman, P.R. Characterization of passive permeability at the blood-tumor barrier in five preclinical models of brain metastases of breast cancer. *Clin Exp Metastasis* **2017**, *33*, 373–383, doi:10.1007/s10585-016-9784-z.Characterization.
179. Murrell, D.H.; Hamilton, A.M.; Mallett, C.L.; Gorkum, R. Van; Chambers, A.F.; Foster, P.J. Understanding heterogeneity and permeability of brain metastases in murine models o her2-positive breast cancer through magnetic resonance imaging: Implications for detection and therapy. *Transl. Oncol.* **2015**, *8*, 176–184, doi:10.1016/j.tranon.2015.03.009.
180. Mendes, B.; Marques, C.; Carvalho, I.; Costa, P.; Martins, S.; Ferreira, D.; Sarmento, B. Influence of glioma cells on a new co-culture in vitro blood-brain barrier model for characterization and validation of permeability. *Int. J. Pharm.* **2015**, *490*, 94–101, doi:10.1016/j.ijpharm.2015.05.027.
181. Lee, H. Te; Xue, J.; Chou, P.C.; Zhou, A.; Yang, P.; Conrad, C.A.; Aldape, K.D.; Priebe, W.; Patterson, C.; Sawaya, R.; et al. Stat3 orchestrates interaction between endothelial and tumor cells and inhibition of Stat3 suppresses brain metastasis of breast cancer cells. *Oncotarget* **2015**, *6*, 10016–10029, doi:10.18632/oncotarget.3540.
182. Lee, T.H.; Avraham, H.K.; Jiang, S.; Avraham, S. Vascular endothelial growth factor modulates the transendothelial migration of MDA-MB-231 breast cancer cells through regulation of brain microvascular endothelial cell permeability. *J. Biol. Chem.* **2003**, *278*, 5277–5284, doi:10.1074/jbc.M210063200.